DNP/solid state NMR probehead for the investigation of oriented membranes

Hiba Sarrouj

UNIVERSITÉ DE STRASBOURG

ÉCOLE DOCTORALE DE SCIENCES CHIMIQUES

[UMR 7177 - Institut de chimie]

THÈSE présentée par :

[Hiba SARROUJ]

soutenue le : **09 Janvier 2014**

pour obtenir le grade de : **Docteur de l'Université de Strasbourg**

Discipline/ Spécialité : Biophysique

Sonde DNP/RMN du solide pour l'étude des protéines membranaires

[DNP/ solid state NMR probehead for the investigation of oriented membranes]

THÈSE dirigée par :

[Monsieur BECHINGER Burkhard] Professeur, Université de Strasbourg
[Monsieur ENGELKE Frank] Directeur de Recherche, Bruker Biospin

RAPPORTEURS :

[Monsieur GLAUBITZ Clemens] Professeur, Goethe Universität Frankfurt
[Monsieur PIOTTO Martial] Directeur de recherche, Bruker Biospin SA

AUTRES MEMBRES DU JURY :

[Monsieur KIEFFER Bruno] Professeur, Université de Strasbourg
[Monsieur AUSSENAC Fabien] Docteur, Bruker Biospin SA

Hiba SARROUJ

Sonde DNP/RMN du solide pour l'étude des protéines membranaires

Résumé

Les protéines membranaires en hélices alpha forment le tiers des protéines codées par notre génome. D'autres protéines membranaires sont formées typiquement de feuillets bêta. Leur fonction varie de la formation de pores, la transmission de signaux à l'activité antibiotique. Elles sont aussi capables de transporter de larges cargos comme les protéines ou les acides nucléiques au travers de la membrane. Récemment, les peptides ont émergé comme un moyen prometteur pour le transport de médicaments vers leurs cibles.

Les protéines membranaires peuvent être synthétisées chimiquement ou exprimées et marquées isotopiquement dans les bactéries, isolées, purifiées et reconstituées dans les bicouches lipidiques hydratées. Elles présentent une variété de configurations en interagissant avec ces bicouches lipidiques. Ceci dépend de la composition et de l'épaisseur de ces bicouches. L'orientation des bicouches lipidiques est maintenue mécaniquement en les disposant entre des plaques de verre.

La RMN du solide des échantillons orientés est un des moyens possibles pour accéder à la topologie des peptides associés à des membranes phospholipidiques.

Les échantillons sont difficiles à exprimer dans les bactéries en grande quantités et possède une solubilité réduite en dehors des membranes. En outre leur taille est trop importante pour la RMN du liquide et il est difficile de les cristalliser.

Un des inconvénients majeur de la spectroscopie RMN est sa faible sensibilité. Cela résulte du faible moment magnétique nucléaire qui résulte en un décalage Zeeman faible et donc une polarisation réduite. Par ailleurs, l'intensité du signal RMN dépend de plusieurs facteurs comme la quantité d'échantillon la polarisation et le champ magnétique B_0. Et le temps d'acquisition de certaines expériences peut être très long.

Le but de ce projet est d'obtenir plus de signal des protéines membranaires. Dès lors, nous avons développé une cryosonde DNP (dynamic nuclear polarization) / RMN du solide. La DNP est une technique ingénieuse qui est utilisée pour le transfert de polarisation des noyaux hautement polarisés à des noyaux moins polarisés par irradiation microonde. Les microondes vont exister sélectivement les électrons qui transfèreront leur polarisation à l'ensemble des protons voisins, le signal proton peut ainsi être augmenté de 660 fois.

Pour cela la cryosonde DNP RMN du solide qui opère à 100 K et 9,4 T a été utilisée. Une sonde est la pièce mécanique qui maintient l'échantillon dans le centre magnétique de l'aimant du spectromètre. C'est une antenne modulable qui irradie et détecte des champs radiofréquence. La pièce centrale de la sonde est une bobine solénoïdale ou une bobine en forme de selle enveloppant l'échantillon.

La faisabilité de ces expériences DNP a été validée sur les échantillons orientés en rotation à l'angle magique. Ces expériences ont été menées sur des échantillons enroulés dans un rotor. Même si leur orientation par rapport au champ magnétique B_0 est perdue, une valeur d'augmentation de 17 a été obtenue.

Dans le deuxième chapitre de cette thèse, nous revoyons la théorie et les méthodes utilisées au cours de ce projet de thèse. Premièrement, nous introduisons l'étude des protéines membranaires et leur synthèse en phase solide. Deuxièmement, nous survolons la théorie RMN. La RMN du solide est introduite en tant que méthode de détermination de contraintes de distances et d'orientation. Des expériences comme la 15N CP et PISEMA sont présentées. D'une part, la CP relie les interactions internucléaires comme l'anisotropie de déplacement chimique CSA et les interactions dipolaires à l'orientation des peptides dans les bicouches lipidiques. D'un autre côté, le PISEMA (polarization inversion spin exchange at magic angle) corrèle le déplacement chimique ^{15}N dépendant de l'orientation aux fréquences de couplage dipolaire et ainsi aux contraintes d'orientation. Ensuite, la technologie et l'instrumentation RMN sont explorées. Finalement, nous introduisons la DNP RMN comme technique pionnière pour augmenter le signal RMN. Nous revoyons la théorie et l'instrumentation DNP et introduisons les mécanismes de polarisation DNP dans les solides.

Dans le troisième chapitre, nous décrivons la cryosonde DNP RMN du solide que nous avons conçue et construite. Nous présentons le circuit de la sonde ainsi que les étapes de base de la construction. Ensuite, plusieurs résultats préliminaires sont montrés. En occurrence, le bench test pour raccorder la sonde et le test de puissance pour déterminer quelle puissance la sonde peut supporter.

En outre des spectres ^{15}N CP d'un peptide modèle à température ambiante sont montrés. Plusieurs paramètres ont été optimisés comme le T_1 (de l'ordre de quelques secondes) et l'homogénéité du champ B_1. Des défis techniques comme la configuration de bobines doubles raccordées aux fréquences ^{15} N and ^{1} H ont été surmontés, dans le but d'optimiser l'homogénéité de champs B_1 dans la région active de la bobine RMN. Plusieurs échantillons standards ont été testés comme la glycine et l'histidine. Par la suite, le premier spectre à basse température du peptide transmembranaire standard HΦ19W a été enregistré.

Dans le chapitre 4, des simulations CST ont été effectuées pour optimiser la pénétration des microondes dans l'échantillon entre les plaques de verre. Ensuite, nous présentons les résultats de mesure DNP sur le chlorure d'ammonium hyperpolarisé et nous les comparons aux valeurs d'augmentation obtenues en rotation à l'angle magique.

Notre premier essai sur les échantillons orientés n'a pas abouti. En effet, nous n'avons pas obtenu de signal ^{15}N DNP. Après avoir comparé plusieurs supports d'échantillon, nous avons finalement choisi de travailler avec le HDPE (high density polyethylene) qui a été testé pour les échantillons orientés en rotation à l'angle magique. En outre nous révélons les résultats sur HΦ19W et PGLa sur du HDPE. Nous publions des résultats des expériences DNP ^{1}H-^{15}N CP statique sur des échantillons de polypeptides en première mondiale. Ces résultats montrent une augmentation de 4 entre la configuration microonde éteinte et allumée avec le radical bTbk et une valeur de 4.5 avec AMUPOL. Ceci nous permet de diminuer le temps d'expériences de 16 fois. .

Enfin, nous sommes revenus à la configuration de bobine unique d'une section 4 x 4 (mm^2) pour récupérer l'efficacité RMN de la sonde. L'augmentation DNP est restée la même mais nous avons obtenu une meilleure performance RMN. Nous avons mesuré un signal sur bruit de 32 au lieu de 10 avec la bobine double en 50 minutes. Une augmentation de 7 a été obtenue sur un échantillon non orienté inséré dans un rotor. Ces développements vont nous permettre d'acquérir plus de signal en moins de temps. Des expériences PISEMA ont été optimisées à température ambiante et à 90 K. Dans le futur, nous envisageons d'utiliser des radicaux mieux adaptés aux échantillons orientés.

Résumé en anglais

Helical membrane proteins comprise one third of the expressed proteins encoded in a typical genome. Other membrane proteins are typically beta sheets. Their function varies from pore formation, signaling to antimicrobial activity. They are also capable of transporting large cargo such as proteins or nucleic acids across the cell membrane. Recently, peptides have emerged as promising tools in drug delivery.

Membrane proteins can be synthesized chemically or expressed and isotopically labeled in bacteria, isolated, purified and reconstituted into fully hydrated lipid bilayers. The bilayer orientation is kept mechanically by putting them between glass plates. While interacting with these bilayers they exhibit a variety of configurations depending on the lipids composition and thickness.

Solid-state Nuclear Magnetic Resonance (NMR) on oriented bilayers is one way to access the topology of peptides associated with phospholipid membranes.

Oriented membrane protein are difficult to study with analytical techniques because of their poor solubility outside the lipid membrane, difficulty of expression in bacteria in big quantities, difficulty to crystallize, and they are too large for solution NMR study. The intensity of an NMR signal depends on several factors such as polarization P and magnetic field magnitude B_0.

One of the major drawbacks of NMR spectroscopy is low sensitivity. This is caused by the small magnetic moment of the nuclear spins which results in a modest Zeeman splitting of the nuclear spin energy levels and therefore in a limited Boltzmann Polarization.

The aim of this project is to obtain a better signal from membrane proteins. Thus a Low temperature (LT) solid state NMR with Dynamic Nuclear Polarization (DNP) probe head was created. DNP is an ingenious technique that is used to transfer polarization from highly polarized targets to less polarized nuclei using microwave irradiation. Microwaves will excite selectively the electron spins which will transfer their polarization to the pool of proton nuclei, the proton NMR signal can be enhanced by 660 times.

A probe head for DNP enhanced solid state NMR at 100 K and 9.4 T is described. A probe head includes the mechanical piece that holds the sample in the magnetic center of the NMR magnet. It is a tunable antenna that irradiates and detects the rf fields used in NMR. The centerpiece of the probe is the solenoidal or saddle coil surrounding the sample.

The feasibility of such a DNP experiment is proven on magic angle oriented sample spinning. These experiments are conducted on oriented samples wrapped into a rotor. Through their orientation with regards to B_0 is lost, enhancement values as high as 17 are obtained.

In chapter 2 of this thesis, the theory and methods used in this thesis project are reviewed. First membrane proteins study and synthesis using Solid Phase Peptide Synthesis is presented. Next, NMR spectroscopy theory is overviewed. Solid state NMR is introduced as a method to determine distance and orientational constraints. Experiments such as ^{15}N cross polarization (CP) and polarization inversion spin exchange at magic angle (PISEMA) are discussed. On one hand, CP relates nuclear spin interactions, such as the anisotropic chemical shift CSA and dipolar interactions to the orientation of the peptides within the bilayer membrane. On the other hand PISEMA correlates the orientationally dependent ^{15}N chemical shift and ^{1}H-^{15}N dipolar coupling frequencies to orientational constraints. After that spectrometer technology and instrumentation is explored. Finally, DNP NMR is introduced as a powerful technique to enhance NMR signal. The Dynamic nuclear Polarization theory and hardware are surveyed. DNP mechanisms of polarization transfer in solids are reviewed.

In chapter 3, the Low temperature DNP solid state NMR probe design and construction are described. The probe circuit as well as basic steps of probe construction are presented. Then,

several test results prior to the ultimate spectrometer test are shown. Namely, the bench test to tune and match the probe head and the high power test to determine how much power the probe head withstands.

Moreover, preliminary ^{15}N CP spectra of a model polypeptide at room temperature are obtained. Many parameters are optimized including sample spin lattice relaxation T_1 (in the order of seconds) and B_1 field homogeneity. Technical challenges are overcome to find coil configurations at least doubly tuned to ^{15} N and ^{1} H, leading to optimum B_1 field homogeneity in the active region of the NMR coil. Several standard NMR samples are tested including Glycine and Histidine. After that the first low temperature spectra of HΦ19W, a standard transmembrane helical polypeptide, are obtained.

In chapter 4, CST simulations are conducted to preview the microwave penetration into the glass plates sample. Then, the DNP results on hyperpolarized ammonium chloride and their comparison to the MAS enhancement values are shown.

First shot DNP experiments on glass plates showed an incompatibility of glass plates with microwaves irradiation. After testing several sample supports, high density polyethylene HDPE, which has been proven to work in wrapped oriented membrane sample in a MAS rotor, was chosen. Next, DNP results on HΦ19W and PGLa on HDPE are revealed. DNP enhanced ^{1}H-^{15}N CP static experiments on polypeptide samples are revealed in a world premiere. Results on the DNP enhanced BIO PE NMR static probe show an enhancement of 4 between the microwave off and on configuration using the bTbk biradical and 4.5 using the AMUPOL biradical. This will cut the experiment time by 16.

Lastly, the single coil design with a 4 by 4 mm^2 cross section was chosen to recover NMR efficiency. Although the DNP enhancement wasn't improved, the original NMR performance of the probe was recovered. A signal to noise of 32 was obtained after 50 minutes instead of 10 with the double coil. A DNP enhancement of 7 was measured using an HΦ19W unoriented sample in a sapphire rotor. These developments will allow better signal acquisition in less time.

PISEMA experiments have been optimized at room temperature and at 90 K. In the future free radical dopants will be better adapted to the oriented samples.

Hiba SARROUJ

Sonde DNP/RMN du solide pour l'étude des protéines membranaires

Résumé

Les protéines membranaires en hélices alpha forment le tiers des protéines codées par notre génome, d'autres protéines membranaires sont formées typiquement de feuillets beta. Leur fonction varie de la formation de pores, la transmission de signaux à l'activité antibiotique. Elles sont aussi capables de transporter de larges cargos comme les protéines ou les acides nucléiques au travers de la membrane. Récemment les peptides ont émergé comme un moyen prometteur pour le transport de médicaments vers leurs cibles.

Les protéines membranaires peuvent être synthétisées in vitro ou exprimées et marquées isotopiquement dans les bactéries, isolées, purifiées et reconstituées dans les bicouches lipidiques hydratées. Leur orientation est maintenue mécaniquement en les disposant entre des plaques de verre. Elles présentent une variété de configurations en interagissant avec ces bicouches lipidiques. Ceci dépend de la composition et de l'épaisseur de ces bicouches.

La RMN du solide des échantillons orientés est un des moyens possibles pour accéder à la topologie des peptides associés à des membranes phospholipidiques.

Un des inconvénients majeur de la spectroscopie RMN est sa faible sensibilité. Cela résulte du faible moment magnétique nucléaire qui résulte en un décalage Zeeman faible et donc une polarisation réduite.

L'étude des échantillons orientés souffre encore plus de cette faible sensibilité à cause de leur solubilité réduite en dehors des membranes, leur difficulté d'expression dans les bactéries en grande quantité et leur difficulté à cristalliser. En outre elles sont très larges pour la RMN du liquide. L'intensité du signal RMN dépend de plusieurs facteurs comme la polarisation et le champ magnétique B_0.

Le but de ce projet est d'obtenir plus de signal des protéines membranaires. Dès lors nous avons développé une cryosonde DNP (dynamic nuclear polarization) / RMN du solide. La DNP est une technique ingénieuse qui est utilisée pour le transfert de polarisation des noyaux hautement polarisés à des noyaux moins polarisés par irradiation microonde. Les microondes vont exciter sélectivement les électrons qui transfèreront leur polarisation à l'ensemble des protons voisins, le signal proton peut ainsi être augmenté de 660 fois.

Nous décrivons une cryosonde DNP RMN du solide qui opère à 100 K et 9,4 T. Une sonde est la pièce mécanique qui maintient l'échantillon dans le centre magnétique de l'aimant du spectromètre. C'est une antenne modulable qui irradie et détecte des champs radiofréquence. La pièce centrale de la sonde est une bobine solénoïdale ou une bobine en forme de selle enveloppant l'échantillon.

La faisabilité de ces expériences DNP a été prouvée sur les échantillons orientés en rotation à l'angle magique. Ces expériences sont menées sur des échantillons enroulés dans un rotor. Même si leur orientation par rapport au champ magnétique B_0 est perdue, une valeur d'augmentation de 17 a été obtenue.

Dans le deuxième chapitre de cette thèse, nous revoyons la théorie et les méthodes utilisées au cours de ce projet de thèse. Premièrement, nous introduisons l'étude des protéines membranaires.

Les peptides de défense font partie du système immunitaire. Les organismes multicellulaires secrètent des peptides antimicrobiens cationiques pour se protéger contre les pathogènes. Plusieurs peptides antimicrobiens ont été étudiés au cours de cette thèse. D'habitude ils comportent 20 à 50 acides aminés. Ils possèdent un large spectre d'activités contre les bactéries et les pathogènes. Les cecropines et les magainines détruisent la membrane cellulaire en agissant comme des détergents et forment des pores. Plusieurs de ces peptides comme la magainine et l'histatine ont été modélisés pour être utilisés dans la conception de nouveaux médicaments. Plusieurs développements in silico et in vivo sont nécessaires pour les valider en tant qu'antibiotiques efficaces.
La synthèse des polypeptides en phase solide a été inventée par Robert Bruce Merrifield. Elle est convenable pour les chaines peptidiques de plus de 10 acides aminés. Les chaines peptidiques sont assemblées de la partie C terminale à la partie N terminale. Le peptide synthétique est attaché à son support de manière covalente. Un grand excès de réactants est utilisé pour rendre les réactions complètes et rapides. Finalement le peptide est clivé du support et purifié par HPLC pour éliminer les produits indésirables.
D'un autre côté, les phases lipidiques et les transitions de phases sont présentées. Les lipides sont des molécules amphiphiles. Ils sont constitués d'une tête polaire et de deux chaines hydrophobes qui varient en longueur et en saturation. Les bicouches lipidiques sont très flexibles et ils permettent l'insertion de protéines, peptides et polysaccharides. Ils se forment spontanément en milieu aqueux possédant les propriétés de pH, température et salinité convenables. Ceci résulte en des membranes stables et auto réparatrices avec un grand degré de flexibilité.
Pour préparer un échantillon nous dissolvons des lipides et des polypeptides dans du tetrafluoro ethanol. Pour les tests DNP des radicaux sont rajoutés au mélange. L'alcool est ensuite évaporé et l'échantillon est étalé sur un support de verre ou de polyéthylène. Nous le laissons dans le lyophilisateur pendant toute une nuit. Le lendemain l'échantillon est récupéré et disposé en plusieurs couches. Il est prêt pour être testé en RMN.
La résonnance magnétique nucléaire est une technique de spectroscopie moderne qui a été mise au point par Edward Purcell en 1945. Elle exploite les propriétés magnétiques du noyau atomique. Chaque orientation nucléaire de spin correspond à un niveau d'énergie diffèrent. Les transitions entre différents niveau ont lieu lorsque l'échantillon est exposé à une radio fréquence égale à la différence d'énergie entre deux niveaux. Ce phénomène est appelé résonnance. Les spins précessent et un signal électrique est induit dans la bobine RMN. La RMN enregistre un signal dépendant du temps dont la transformée de Fourrier représente le spectre RMN.
En mécanique quantique la résolution de l'équation de Schrödinger dépendant du temps nous permet d'obtenir le Hamiltonien des interactions de spins. Le Hamiltonien n'est rien d'autre que l'énergie du système. Chaque interaction de spin nous donne accès à une grandeur mesurable comme l'orientation et la distances. Ces quantités sont essentielles pour la détermination de structure 3D.
Plusieurs expériences de RMN du solide nous donnent accès aux contraintes d'orientation. Nous allons nous concentrer sur la polarisation croisée CP et PISEMA qui est littéralement l'inversion de polarisation et échange de spin à l'angle magique. Nous avons utilisés ces expériences pour déterminer l'orientation d'un échantillon synthétique modèle HΦ19W et du peptide antimicrobien PGLa. PGla est un polypeptide de 21 résidus cationiques qui fait partie de la famille des magainines. C'est particulièrement les interactions de déplacement chimique anisotropique et couplage dipolaire qui donnent accès à l'angle de tilt d'un polypeptide en hélice alpha. La résolution du tenseur de déplacement chimique anisotropique ou celui de couplage dipolaire permet de calculer l'angle de tilt en utilisant des logiciels préétablis comme SIMPSON.
Pour la CP : si le déplacement chimique azote 15 est compris entre 50 et 100 ppm nous sommes en présence d'un polypeptide dans le plan et si le déplacement chimique est compris entre 200 et 250 ppm nous avons un polypeptide transmembranaire. PISEMA est une expérience 2D qui donne le couplage dipolaire proton-azote 15 en fonction du déplacement chimique de l'azote 15. Elle nous permet d'obtenir l'angle de tilt d'une hélice alpha avec plus de précision que la CP.

Ensuite la technologie et l'instrumentation RMN sont explorées. Les différentes parties du spectromètre RMN sont présentées. L'envoi et la réception du signal RMN radiofréquence sont décrits en détails. Les différentes séquences de pulses utilisées au cours de ce projet sont introduites : one pulse, hpdec, Hahn echo et CP. En outre, nous présentons deux méthodes de mesure de T1 : le temps de relaxation longitudinal à savoir l'inversion récupération et la saturation récupération.

Finalement, nous introduisons la DNP RMN comme technique pionnière pour augmenter le signal RMN. Nous revoyons l'instrumentation et la théorie DNP. La polarisation haute des électrons libres des radicaux est transférée aux protons moins polarisés par le biais de radiation microonde. Cette radiation correspond à la transition EPR des électrons libres. La génération de rayonnement microonde nécessite un instrument qui provient de la physique des hautes énergies à savoir un gyrotron à 263 GHz. En plus le transfert de ces microondes à moindre coût énergétique dans la sonde RMN nécessite un guide d'onde ondulé. Finalement, les mécanismes de polarisation DNP dans les solides sont introduits. En effet plusieurs mécanismes de transferts sont connus aujourd'hui : l'effet solide (solid effect SE), l'effet de croisement (cross effect CE) et le mélange thermique (thermal mixing TM). Chaque radical possède son propre mécanisme de fonctionnement. Par exemple le mécanisme de transfert des biradicaux comme TOTAPOL, bTbK et AMUPOL est le cross effect. Dans le troisième chapitre, nous décrivons la cryosonde DNP RMN du solide que nous avons conçue et construite. La basse température est nécessaire d'une part pour augmenter le T_1 et permettre la diffusion et spin et d'une autre part pour augmenter le facteur qualité du circuit électronique de la sonde et augmenter la polarisation de Boltzmann.

Nous présentons le circuit de la sonde. En bref, la bobine RMN constitue avec le condensateur de réglage et parfois une ligne de transmission un circuit LC. L'impédance de ce circuit est réglée à 50 Ohm à l'aide d'un analyseur de circuit. Plusieurs éléments inductifs ou capacitifs sont rajoutés au circuit pour ce faire.

Parallèlement, les étapes de base de la construction d'une sonde sont citées. Une fois que le support mécanique est assemblé il ne reste plus qu'à fixer les différents éléments du circuit (condensateur, bobine, ligne de transmission) et les alimenter. En effet chaque chaine est alimentée indépendamment. Pour une sonde en mode triple 1H/13C/15N, trois alimentations (ports) ou câbles coaxiaux sont nécessaires. Chaque chaine est isolée de l'autre par un filtre. Les thermocouples sont fixés. La ligne de transfert interne de gaz froids est insérée dans le tube prévu à cet effet. Pour commencer, plusieurs bobines ont été construites et positionnées de façon à occuper le centre magnétique du spectromètre. Ensuite, plusieurs résultats préliminaires sont montrés. En occurrence le bench test pour raccorder la sonde et le test de puissance pour déterminer quelle puissance la sonde peut supporter.

Le bench test consiste à déterminer les intervalles de fréquences opératoires de chaque chaine ainsi que l'isolation entre deux canaux. Le facteur qualité du circuit et la fréquence de shift lors de l'introduction d'un matériau conducteur dans la bobine. Le test de puissance consiste à envoyer dans la sonde des puissances de plus en plus grandes à la fréquence convenable pour déterminer le maximum qu'elle peut supporter. Ces valeurs devront être respectées lors d'une expérience RMN. Le bench test est réalisé pour une bobine carrée aplatie et une bobine en forme de selle. Un tableau récapitulatif reporte les valeurs des fréquences de réglage, l'isolation entre les canaux, le signal sur bruit lors d'une expérience CP, le facteur de qualité et le shift de fréquence.

A la fin de cette partie technique nous expliquons comment passer d'un mode à l'autre pour la sonde RMN. Plusieurs modes sont possibles : en mode triple 1H/31P/15N et 1H/13C/15N, en mode double toutes les combinaisons sont possibles (1H/31P/ 1H/15N et 1H/13C).

Les premiers résultats RMN sont présentés pour le chlorure d'ammonium pour comparer les deux types de bobine proposés à savoir la bobine aplatie et la bobine en forme de selle. La première simulation de champs magnétique B_1 est réalisé pour la bobine aplatie carrée (section : 3 x 3 mm^2)

avec le logiciel CST (Computer simulation technology). Pour chaque type de bobine le signal sur bruit est mesuré lors d'une expérience hpdec et cp. Par la suite l'homogénéité du champ est vérifiée par une expérience de nutation proton et carbone. Une comparaison entre les deux est résumée dans un tableau récapitulatif.

En outre des spectres ^{31}P one pulse de bicouches POPC et ^{15}N CP d'un peptide modèle, la surfactine, orienté à température ambiante sont montrés. La surfactine est un lipopeptide extrait de Bacillus subtilis. Elle possède deux chaines latérales chargées négativement qui forment une tête polaire, Les autres chaines latérales sont hydrophobes. Ces propriétés sont responsables de son caractère amphiphile et ses propriétés de surfactant. Le spectre phosphore nous permet de vérifier l'orientation des bicouches lipidique et le spectre azote nous permet de cerner si le polypeptide en question est transmembranaire ou dans le plan. Pour ce test une bobine plate 3 x 7 mm^2 est utilisée.

Avant de se lancer dans les expériences à basse température nous avons vérifié le T_1 du chlorure d'ammonium par les deux méthodes de mesures l'inversion récupération d'abord et la saturation récupération ensuite. Les valeurs trouvées concordent bien (0,4 secondes)

Des premiers tests à basse température ont été tentés sur le chlorure d'ammonium en poudre sans succès. Le rajout d'un radical à l'échantillon n'a pas amélioré les choses. En effets le T_1 du chlorure d'ammonium est très long à basse température. Par la suite une simulation AWR microwave nous a permis de déterminer que le champ B_1 était inhomogène dans ce type de bobine pourtant standard pour l'étude des échantillons orientés. Un voltmètre relie à chaque extrémité de la bobine nous a permis de déterminer que le courant n'était pas reparti de façon homogène des deux côtés de la bobine. En effet la sonde est prévue à la base pour une bobine solénoïdale de 3.2 mm pour la rotation à l'angle magique.

Par la suite, plusieurs paramètres sont optimisés comme le T_1 (de l'ordre de quelques secondes) et l'homogénéité du champ B_1.

Des défis techniques comme la configuration de bobines doubles raccordées aux fréquences ^{15} N and ^{1} H ont été surmontés, dans le but d'optimiser l'homogénéité de champs B_1 dans la région active de la bobine RMN.

La simulation AWR nous a poussé à changer le circuit de la sonde et d'isoler le canal proton du canal azote. Un circuit indépendant prévu pour X et Y a été réattribué pour les protons et l'azote. Des simulations de champ magnétique B_1 nous ont prouvé l'homogénéité du champ radiofréquence dans ce type de bobine double. Après ce changement le réglage des pulses proton et azote est devenu à nouveau possible.

Plusieurs échantillons standards ont été testés à basse température comme $^{15}NH_4Cl$, la glycine et l'histidine.

Nous mélangeons du $^{15}NH_4Cl$ dissous dans de l'eau deutérrée de l'eau et du glycerol à du 4 amino TEMPO. A basse température, ils forment un réseau qui permet la distribution homogène des radicaux. Dans une première étape nous avons suivi l'évolution du pic proton avec la température ainsi que le changement de phase de l'échantillon. Ensuite pour rendre notre étude plus systématique nous avons étudié l'évolution du T_1 proton de l'histidine mélangée à de l'eau deutérrée de l'eau et du glycerol à du 4 amino TEMPO. A basse température le T_1 proton est plus court. Le signal sur bruit augmente lorsque la température diminue pour diminuer ensuite lorsque le radical est en excès. Une fois que nous avons déterminé le comportement de l'histidine nous sommes revenus au mélange de chlorure d'ammonium hyperpolarisé. Nous avons tenté avec succès la première expérience CP à basse température. $^{15}NH_4Cl$ sera utilisé par la suite pour la calibrations des expériences sur les échantillons membranaires.

Par la suite le premier spectre à basse température du peptide transmembranaire standard HΦ19W a été enregistré. Enfin des simulations CST sont effectuées pour optimiser la pénétration des

microondes dans l'échantillon entre les plaques de verre. Nous remarquons pertinemment un profil de diffraction causé par la distance entre les deux spires qui est voisine de la longueur d'onde microonde. Le maximum de l'intensité de l'onde n'est pas forcément entre deux plaques de verres et s'éteint carrément à certains endroits.

Dans le chapitre 4, nous présentons les résultats de mesure DNP sur le chlorure d'ammonium hyperpolarisé et nous les comparons aux valeurs d'augmentation obtenues en rotation à l'angle magique. Nous avons mesuré une augmentation de 44 en rotation à l'angle magique à 5 kHz. Lorsqu'on arrête de tourner nous enregistrons une valeur de 20. Lorsque nous plaçons le même échantillon dans la sonde DNP statique nous obtenons une augmentation de 18.

Notre premier essai sur les échantillons de verre n'a pas abouti. En effet, nous ne pouvions pas obtenir de signal ^{15}N DNP. Ensuite une comparaison de support d'échantillon est présentée. Nous voulions trouver un nouveau support d'échantillon qui entraine une bonne orientation de l'échantillon ainsi que de bonnes propriétés diélectriques. Nous avons finalement choisi de travailler avec le HDPE qui a été testé pour les échantillons orientés en rotation à l'angle magique. En outre nous révélons les résultats sur HΦ19W et PGLa sur du HDPE. Nous publions des résultats des expériences DNP ^{1}H-^{15}N CP statique sur des échantillons de polypeptides en première mondiale. Ces résultats montrent une augmentation de 4 entre la configuration microonde éteints et allumés avec le radical bTbk et une valeur de 4.5 avec AMUPOL. Ceci nous permet de diminuer le temps d'expériences de 16 fois.

Enfin nous sommes revenus à la configuration de bobine unique d'une section 4 x 4 (mm^2) pour récupérer l'efficacité RMN de la sonde. L'augmentation DNP est restée la même mais nous avons obtenu une bonne performance RMN. Nous avons mesuré un signal sur bruit de 32 au lieu de 10 avec la bobine double en 50 minutes. Nous avons ainsi comparé la sonde DNP avec la sonde e-free. La première donne deux fois plus de signal. Sachant que le volume interne de la bobine e-free est 2 fois plus grand ça revient au même donc les deux sondes possèdent la même efficacité RMN. Afin de comprendre le comportement DNP de la sonde nous avons effectué des expériences avec des puissances microondes croissantes (correspondant à un courant de collecteur croissant). Les résultats sont différents selon l'échantillon. En effet pour le chlorure d'ammonium l'augmentation est moindre lorsqu'on augmente la puissance. Cela est vrai lorsque le même échantillon est mis dans un rotor en zirconium ou saphir. Par contre l'augmentation augmente pour l'échantillon de HΦ19W placé dans un rotor en saphir. Ceci concorde bien avec les résultats préliminaires obtenus pour le chlorure d'ammonium dans un rotor de saphir.

La calibration du champ B_1 de l'azote 15 est obtenue d'après une nutation (une expérience 1H-15N CP suivie par une nutation sur l'azote 15), nous permet de déterminer la puissance à appliquer sur le canal azote pour obtenir un champ rf donné. En effet, pour atteindre 50 kHz sur le canal azote 100 W sont nécessaires. Nous effectuons la même expérience pour le proton 40 W sont nécessaires pour atteindre 50 kHz sur le canal proton.

Une augmentation de 7 a été obtenue sur un échantillon non orienté inséré dans un rotor. Ces développements vont nous permettre d'acquérir plus de signal en moins de temps. Des expériences PISEMA ont été optimisées à température ambiante et à 90 K. Sur un même graphe, nous reportons La simulation d'une hélice idéale (Φ=65°, ψ= 45°) et un tenseur de déplacement chimique anisotropique CSA de σ_{11}=227ppm; σ_{22}= 83,5ppm; σ_{33}= 70,5ppm. L'ajustement de ces données à la simulation donne un angle de tilt 10° par rapport à la normale membranaire.
Dans le futur, nous envisageons d'utiliser des radicaux mieux adaptés aux échantillons orientés. L'amélioration du couplage échantillon microonde serait d'un très grand avantage. L'utilisation de nouveaux radicaux dont certains peuvent être directement couplés au peptide étudié. Un dispositif d'échange d'échantillon sera aussi d'un très grand avantage pour éviter le réchauffement de la sonde pour chaque nouvel échantillon.

DNP/ solid state NMR probehead for the investigation of oriented membranes

Hiba Sarrouj
Universite de Strasbourg
Bruker Biospin

March 31, 2014

Contents

Abstract

In this project dynamic nuclear polarization DNP ia used as a hyperpolarization method which theoretically induce a ^{1}H-NMR enhancement of 660. This is due to the transfer of the large Boltzmann polarization of paramagnetic species to the nuclei of interest by microwave irradiation of the sample at the electron Larmor frequency. The polarization of the electrons is transmitted to the neighboring protons by spin diffusion. The proton polarization is then transmitted to the dilute nuclei such as ^{15}N. It has been demonstrated that DNP/solid-state NMR is feasible also for oriented membranes . This thesis reports about our work on a DNP/ NMR probe specially designed for the investigation of polypeptides reconstituted in oriented membranes at low temperature. Here, technical challenges that have been overcome to reach optimal B_1 field homogeneity in the active region of the NMR coil as well as first results on oriented membrane samples are presented. CP and PISEMA DNP/solid state NMR experiments have been realized on a model peptide and an antimicrobial peptide PGLa at low temperature (i.e. 95 K). Promising enhancement factors have been measured. Tilt angles with respect to the membrane normal were successfully fitted. Our aim is to acquire 2D and 3D experiments more rapidly. In the future, these results permit structural restraints calculation and the efficient establishment of 3D structures.

Acknowledgments

First of all I would like to thank Burkhard Bechinger and Frank Engelke for giving me the opportunity to work on this challenging project. Our discussions have always been very informative and inspiring. Their keen insight has always helped me surmount obstacles on the way. Then I would like to acknowledge all the people from the probe head department in Rheinstetten. Ernst Neumann who has always been supportive since day 1. Christian Reiter who has taught me everything on probehead construction. Priyanga Bandara for his unconditional support in coil design and for his introduction on computer simulations. Alexander Krahn for being so welcoming when I first joined the group and for the time he has invested in helping me with my project. The people from the application department. Gerhardt Althoff for his great experience in NMR. The people from the production Martin Armbruster for introducing me to probe mechanics, Jutta Czanderle for her help in conference preparation and Uwe Priller for coil winding. Liz Maeir for her support in German and her unconditional friendship. Fabien Aussenac and Jerome Coutant from Bruker Wissembourg. Fabien has always been very patient in introducing NMR. Martial Piotto and Maryse Bourdonneau for their encouragements. Melanie Rosay and Marc Caporini from Bruker Billerica for their support in DNP. I would also like to thank all the colleagues from the Institute of Chemistry in Strasbourg. Evgeniy Salnikov for teaching me sample preparation and test. Christopher Aisenbrey for the time he has invested in testing the probe for PISEMA. Jesus Raya and Jerome Hirsinger for their help in NMR. Omar Rifi for his unconditional support and friendship. Elise Glattard who has always been coaching us. Patricia Kemayo and Nataliia Voievoda for their kind support. Many thanks to the Paul Tordo group from Marseille: Olivier Ouari and Claire Sauvee for bTbK and AMUPOL Special thanks to Geoffrey Bodenhausen and his group in Geneva who gave us access to their spectrometer. AJ Perez Linde and Sami Janin The NMR and DNP community was so enriching and meeting new people in conferences in the last few years was very nice. Many thanks to Jan Henrik Ardenkjaer Larsen and the people form the COST network. I wouldn't have made it without the encouragements of many of my teachers in ENGO-Tripoli and Paris 6 : Gemma Kosta, Patricia Moukaddem, Hala Moufarrej, Marguerite Quilichini and Sophie Cribier to cite some of them.

On a personal level I will be always thankful to my parents who have always been an inspiration to me. My family and friends who have always supported me unconditionally: Tante Jihane, Fida, Bacel, Tania, Jihad, Marie, Marina, Thomas, Rima, Nina, Jorge, Marianne, Lea, Lina, Valerie, Dimitri, Mathilde and Nelli.

Chapter 1

Introduction

Scientists have found a way to mimic [1] the cell membrane by rehydrating specific lipid mixtures. During hydration bilayers (or other membrane phases) spontaneously form. Supported lipid bilayers and uniaxially membranes can be prepared by putting them between glass plates [2]. Lipid bilayers, in the liquid crystalline phase, are soft and flexible and they allow the controlled reconstitution of proteins and peptides [63].

Membrane proteins, many of them exhibiting a high helix content, comprise one third of the expressed proteins encoded in a typical genome. Other membrane proteins are typically beta sheets [9]. Their function varies from pore formation , signaling to antimicrobial activity. Some peptides are also capable of transporting large cargo such as proteins or nucleic acids across the cell membrane [12]. Thereby, peptides have emerged as promising tools in drug delivery [13] .

Membrane polypeptides can be synthesized in vitro or expressed and isotopically labeled in bacteria, isolated, purified and reconstituted into fully hydrated lipid bilayers. While interacting with these bilayers they exhibit a variety of configurations depending on the lipids composition and thickness [3].

Several techniques exist to solve membrane proteins atomic structure: X ray diffraction, electron microscopy, Nuclear magnetic resonance, neutron scattering and molecular modeling.

Two and three dimensional crystallization of membrane proteins is possible but very challenging. Moreover, crystallography places the protein in an artificial environment. Electron microscopy is limited to big protein complexes such as aquaporins with a resolution of 1 to 2 nm. Neutron scattering provides a good resolution close to 1 angstrom. It probes the position and dynamics of deuterated head groups in a protein with regard to the lipid bilayers. The technique use is limited to some membrane proteins such as cytochrome c oxidase. Molecular modeling experiments

in silico still need experimental data to build a proper model.

Nuclear magnetic resonance (NMR) spectroscopy is one of the most important analytical method available today for molecular structure determination. It exploits the magnetic properties of certain atomic nuclei. When a perturbation is provided, here the static magnetic field from the supraconducting magnet at 9.4 Tesla, energy level splitting occurs. The radio frequency (rf) pulse energy ($h\nu$) induced by the NMR coil matches the energy difference ΔE between the freshly split levels. This phenomenon is called resonance.

$$\Delta E = h\nu \tag{1.1}$$

Accordingly the electrons will induce a current in the NMR coil by magnetic induction. In the near field of the coil and the spins, all phenomena are on a distance scale much smaller than the wavelength. In the NMR quantum picture, atoms' nuclei are modeled as spins that turn in a certain direction at a quantified rate. Like every other physical system they have an energy that is called Hamiltonian when they are in a force field (magnetic field in this case). Every spin interaction is represented by its own Hamiltonian. Hamiltonians are represented by second rank cartesian tensors (3x3 matrix). Molecular distances for instance are dependent on by the dipolar spin interaction.

NMR has a wide range of application from gases, liquids, liquid crystals to solids. And it is used in medical imaging as well (MRI, Magnetic Resonance Imaging) [15]. Here are some examples: laser-polarized gases, chocolate, food, drugs, polymers, metals, paint, coal, cement, membranes, peptides, proteins and cells.

In practice, the NMR experiments are managed by a software. An NMR spectrometer sends a rf pulse sequence at a given frequency amplitude and phase into the NMR coil. This frequency is determined by the sample nature (or labeled nuclei) placed in the static magnetic field. At resonance, the sample induces signal into the NMR coil. This signal is detected by measuring the admittance of the transmitting coil [26]. It is then sent back to the amplifiers and is analyzed subsequently. As a result an NMR spectrum is obtained.

Solution NMR and solid state NMR are the two major NMR techniques for structural determination.

In Solution NMR inherent dipolar interactions with neighboring nuclei and chemical shift anisotropy (CSA) are time-averaged due to rapid motional fluctuations and substantially simplified [18, 19]. However membrane protein study by solution NMR is complicated because of the presence of lipids or detergents[25]. Furthermore the solution NMR gives non physiological degrees of freedom and is limited to low molecular weight proteins.

Solid-state NMR on oriented bilayers is one way to access the topology of peptides associated with phospholipid membranes [14]. Molecular structure or specific torsion angles can be measured with errors of only 0.1 angstrom and 5-10 ° respectively [67].

Nowadays, solid state NMR is divided into two branches: magic angle spinning and static solid state NMR.

Magic-angle spinning was first described in 1958 by E. Raymond Andrew et al [16]and independently in 1959 by I. J. Lowe[17]. In MAS NMR, the broadening effects, caused by dipolar coupling and chemical shift anisotropy, can be averaged out by spinning the sample about an axis that is tilted by 54.7° with respect to the static magnetic field. This angle is usually referred to as magic angle and is calculated from the detailed form of the interaction Hamiltonians [26]. The measurement of internuclear distances is still possible by several different methods.

As implied previously, spectral lines are broad in static solid state NMR. However in the particular case of oriented biomembranes studies, the uniaxial orientation provides a mechanism for line-narrowing. Thus, the ^{15}N resonance linewidths are narrower than 3 ppm.

Bilayer environments typically immobilize proteins on the millisecond timescale which corresponds to the operative nuclear spin interactions [9]. So the relevant dipolar coupling and chemical shift interactions present in backbone sites don't go through motional averaging. These interactions retain both the distance and the angular information inherent to oriented sample studies [57].

Consequently, a wide variety of solid-state NMR experiments are highly effective and can be used for structure determination [47, 44]. Starting with ^{15}N Cross Polarization (CP) spectra that give information on the polypeptide alignment with the membrane normal necessary to the determination of angular constraints in structure analysis. These constraints will consist the first elements for 3D molecular structure determination at a resolution close to angstroms [45]. Therefore helical peptides can be classified with the help of their amide ^{15}N chemical shifts into in-plane and transmembrane [8] or in more detail from PISA wheels and dipolar waves [9]

One of the major drawbacks of NMR spectroscopy is low sensitivity. This is caused by the small magnetic moment of the nuclear spins which results in a modest Zeeman splitting of the nuclear spin energy levels and therefore in a limited Boltzmann polarization [11]. Oriented membrane protein studies suffer more from this lack of sensitivity because of their poor solubility outside the lipid membrane, difficulty of expression in bacteria in big quantities, difficulty to crystallize, and they are too large for solution NMR study.

The intensity of an NMR signal depends on several factors such as polarization P and magnetic field magnitude B_0.

$$Intensity \propto PB_0 \tag{1.2}$$

where

$$P \approx \frac{N\gamma\hbar B_0}{2kT} \tag{1.3}$$

N is the total number of spins ($N = N_\alpha + N_\beta$), γ the gyromagnetic ratio. $\hbar$ is the reduced Planck constant i.e. 1.05 x 10^{-34} J.s and k the Boltzman constant 1.38 x $10^{-23} J.\mathrm{K}^{-1}$. It follows that the NMR signal can be enhanced significantly by increasing the strength of the applied magnetic field. Plus decreasing the temperature increases the intensity by increasing the population difference.

Much effort has been done to reach magnetic fields as high as 1 GHz. A cryoprobe on the other hand is a probehead technology that enables having better resolved signal with less noise and more sensitivity. Cooling down the sample to 100 K increases the spin polarization by a factor of 3 and therefore the NMR signal. In more ingenious techniques, polarization can be transfered from highly polarized targets to less polarized nuclei. These techniques ensemble is referred to as hyperpolarization.

Hyperpolarization methods have a great range of application in NMR spectroscopy, imaging and microscopy. These methods have been discovered and consequently applied throughout the years. Starting with dynamic nuclear polarization (DNP) in 1953, chemically induced DNP (CIDNP) in 1967, para hydrogen induced polarization (PHIP) in 1986 and laser polarized noble gases in 1994.

DNP combines solid state NMR and Electron Paramagnetic Resonance (EPR). EPR is the study of unpaired electrons by observing the magnetic fields at which they come into resonance with a monochromatic microwave radiation. Microwaves will excite selectively the electrons which will transfer their polarization to the pool of proton nuclei, enhancing the proton NMR signal by 660 times [56]. Several mechanisms can explain DNP in theory. They will be discussed in this thesis dissertation.

Bruker Biospin has produced the first commercial DNP/ssNMR MAS spectrometer at 400 MHz. A 600 MHz and 800 MHz spectrometer have followed. A commercial static probe for oriented samples still doesn't exist. In this thesis, the first static DNP/ss NMR probehead was built, making this fundamentally different approach available to DNP/ssNMR .

Having established proof-of-concept that DNP can be applied to oriented membrane systems, a static flat-coil NMR probe for samples supported mechanically between ultra-thin glass plates or high density polyethylene (HDPE) films was developed [82]. The probe is required to work at cryogenic temperatures as low as 100 K. A Low Temperature (LT) DNP NMR static probe was built. It comprises three channels: A proton channel, an X channel that can be tuned to carbon, phosphorous

or nitrogen in a double mode. In triple mode the Y channel is reserved for nitrogen. Phosphorous is naturally abundant in membranes. Therefore phosphorous spectra are acquired to asses membrane orientation. 15 nitrogen or 13 carbon are used for proteins' labeling to be able to probe the proteins topology.

Many electronic parameters were tested before accessing the NMR spectrometer like the tuning range the channels' isolations, the signal to noise, the quality factor and the ball shift. Afterwards high power decoupling and cross polarization experiments were realized.

Several conditions are essential for NMR experiments' parameter optimization: field homogeneity, a short spin-lattice relaxation time T_1 (in the order of seconds) and peak width (less than 50 ppm).

Figure 1.1: The different coil types that were tested. These labels will be displayed in the margin every time a new coil design is tested.

Three coil types were wound and built into the probehead's top plate: the solenoidal flat coil with different dimensions, the saddle coil and the double coil. The saddle coil is suitable for inserting the sample mechanically, it produces a homogeneous field but is less sensitive. The square flat coil (4 x 4 mm^2) is more sensitive and produces a less homogeneous field. As the allover results were satisfactory the first experiments on biological samples were attempted.

However the 4 x 4 mm^2 coil is merely accessible for inserting a sample, therefore a 7 x 3 mm^2 inner dimensions coil was tested. Using this 7 x 3 mm^2 flat coil, the first ^{15}N CP spectrum of a model polypeptide were obtained at room temperature.

For setting up this experiment ammonium chloride powder is used as a calibrating sample then the spectra are acquired by increasing the number of scans.

Although it was efficient for CP on a model peptide, the 7 mm x 3 mm flat coil couldn't assess a proper nutation curve for ammonium chloride powder. First the sample T_1 was suspected. As a matter of fact, at low temperature the relaxation time of ammonium chloride powder is long [83].

Afterwards this coil was proven to generate an inhomogeneous B_1 field. Technical challenges have been overcome to find coil configurations at least doubly tuned to ^{15}N and ^{1}H and leading to optimum B_1 field homogeneity in the active region of the NMR coil.

However in the beginning no CP signal could be obtained on hyperpolarized ammonium chloride at low temperature. Therefore a new calibrating sample had to be found. Several standard NMR samples were tested including glycine and histidine.

By adding a hyperpolarizing agent 4 amino TEMPO in addition to deuterated water and glycerol, the histidine its T_1 was shortened (3.5 seconds). Because of the large ^{1}H peak width at low temperature ^{15}N signal was directly acquired using the Cross Polarization(CP) pulse sequence.

After establishing this new efficient strategy on histidine. Hyperpolarized ammonium chloride and HΦ19W experiments were successful at low temperature. And first DNP experiments were attempted.

To manipulate the electron spin, a 263 GHz gyrotron is needed. In order to transfer microwaves into the NMR probe a waveguide is required into the setup. A straight waveguide, that replaces the miter bent waveguide in MAS DNP probes was used.

In a first DNP test, the MAS DNP probe was compared to the static probe, using ^{15}N labeled ammonium chloride.

The first shot DNP experiments on glass plates didn't succeed. As a matter of fact no ^{15}N DNP signal could be obtained. That is why a new sample support with good sample orientation and dielectric properties had to be found. Polyether ether ketone (PEEK) was used in a second set of experiments that were not successful as well. Finally HDPE, which has been proven to work in wrapped oriented membrane sample in a MAS rotor, was utilized.

Fortunately, DNP enhanced ^{1} H-^{15}N cross-polarization (CP) static experiments on polypeptide samples are shown in this thesis in a world premier. Results on the DNP enhanced BIO PE NMR static probe have shown an enhancement of 4 between the microwave off and on configuration using bTbk and 4.5 using AMUPOL. There is a big advantage, it will cut the experiment time by 16.
At the end the single initial square shaped flat coil with a 4 by 4 cross section. This

didn't improve the DNP enhancement however the original NMR performance of the probe was recovered. A signal to noise of 32 after 50 minutes instead of 10 with the double coil was obtained.

With such an NMR probe head, the investigation of oriented samples using DNP solid-state NMR will become more feasible and in particular introduce improved sensitivity to some of the well-established multidimensional experiments used in oriented solid-state NMR [85].

In chapter 2 the materials and methods' theory used in this thesis project are reviewed. First membrane proteins study is presented. Next, NMR spectroscopy theory, instrumentation, application in molecular structure determination of antimicrobial peptides are reviewed. Finally, DNP NMR is introduced as a powerful technique to enhance NMR signal. The DNP theory and hardware is surveyed.

In chapter 3, the LT DNP NMR probe design and construction are described. Then several test results prior to the ultimate spectrometer test are shown. Many parameters are optimized including sample T_1 and B_1 field homogeneity. After that the first low temperature spectra of $H\Phi 19W$, a standard transmembrane helical polypeptide, are obtained.

In Chapter 4, the DNP results on hyperpolarized ammonium chloride and their comparison to the MAS enhancement values are ahown. Next DNP results on $H\Phi 19W$ and PGLa on HDPE are revealed. Lastly, it is shown how the single coil design recovered NMR efficiency. These developments will cut the experimental time by 10.

Chapter 2

Theory and Methods

2.1 Membrane polypetide study

Host defense peptides are part of the innate immune system. Multicellular organisms secrete cationic anti-microbial peptides to protect themselves against pathogens. This discovery has initiated much effort in the detailed study of peptide-membrane interaction. Antimicrobial peptides usually comprise 20 to 50 amino acids. They have a broad spectrum of activity against bacterial, fungal and viral pathogens. Cecropins and magainins disrupt the cellular membrane by acting as a detergent and forming pores. Several of these peptides like magainin and histatin have been modeled to be used in drug design especially for localized infections cf. figure 2.1. A more detailed potential mechanism of membrane disruption and/or translocation by antimicrobial peptides is illustrated in figure 2.2. Finally figure 2.3 shows alamethicin one example of antimicrobial peptides. Further developments in silico and in vivo are needed to validate them as efficient antibiotics [81].

This image was taken from : *http* : *//www.naturereviews.com/*

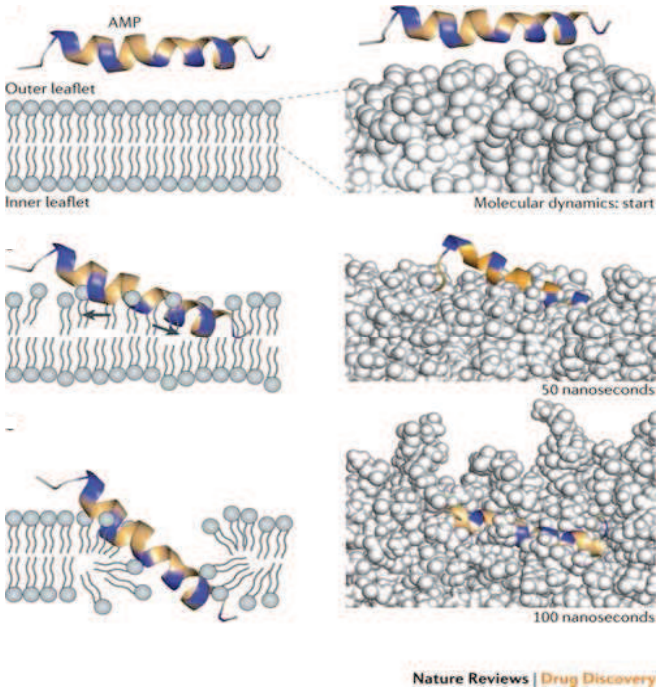

Figure 2.1: Potential mechanism of membrane disruption and/or translocation by antimicrobial peptides. The antimicrobial peptide (AMP) is represented as a ribbon diagram, with positively charged residues indicated in blue (other residues are shown in yellow). The initial stages include membrane attachment (top) and insertion into the outer leaflet (center). Not all AMPs actually insert into and disrupt the membrane (bottom) or form pores. Some peptides are too short to span the bilayer (for example, the cyclic decapeptide gramicidin S). A high peptide concentration leads to increased membrane curvature and facilitates pore formation or translocation across the membrane. A suggested feature of the mode of action of AMP is to stretch, disorder and thin the outer leaflet of the membrane (center). The panels on the right illustrate hypothetical mechanisms of the AMP-membrane interaction that can be studied by molecular dynamics simulations. Here, spinigerin (Protein Data BankID: 1ZRV) was simulated in explicit water with a POPE (1-palmitoyl-2-oleoyl-phosphaethanolamine) membrane bilayer model using the NAMD v2.7b2 software and the CHARMM22 force field. Fjell et al Nature reviews Drug Discovery 2012

2.2 Antimicrobial-peptide-induced mechanisms of cell killing

To better understand the process of antimicrobial-peptide-induced mechanisms of cell killing, the concept of a characteristic lipid composition for a given cell membrane is introduced. It stipulates that the different physicochemical properties of the lipids found in biological membranes allow host defense peptides to discriminate between bacterial, cancer and non-cancer cell membranes. In a simplified view, these cationic amphipathic peptides will exhibit a higher affinity to cell membranes that expose negatively charged lipids on their outer membrane leaflet. The molecular mechanism(s) of membrane destruction depends on both the nature of both peptides and membrane lipids.

In figure 2.2 several models are suggested to explain antimicrobial peptides biological activity. The most common modes of action are the toroidal pores formation and the carpet model. In the toroidal pore model, peptides assemble with the lipid to form a supra-molecular arrangement of high curvature consisting of a water-filled pore. There is not much evidence that the majority of these peptides act in vivo via transmembrane pores, even if a number of molecules including α-helical and β-sheet type peptides adopt such a pore configuration under the given experimental conditions. The carpet model is the most recognized for explaining the membrane disintegration process. In this model, the amphipathic peptides accumulate at the membrane surface. Membrane permeabilization occurs once the peptide concentration is high enough, consequently the membrane bilayer is disrupted. Thereby, at the molecular level different cases may apply. In brief, membrane permeabilization can be due to (a) peptide induced clustering or phase separation of lipids creating defects at the peptide-rich and peptide-poor domains , (b) the sinking raft model, which allows a formal thermodynamic analysis to predict membrane perturbation, (c) disruption of the strict segregation of polar and non-polar groups of the lipids driven by the partitioning of an imperfectly amphipathic peptide into the bilayer interface or (d) a detergent-like action in particular at high peptide concentration. Furthermore, to explain in a more general sense the mode of action of these cationic amphipathic peptides a phase diagram has been developed. It associates the membrane interactions of cationic amphipathic peptides to their molecular shape. Several properties are known to play a significant role in the aggregation state of lipids and affect their interactions with membrane-active peptides: electrostatic interactions, molecular properties such as their shape and spontaneous curvature. In fact the insertion of antimicrobial peptide molecules, promotes the formation of inverted hexagonal or bi-continuous cubic phases in membrane mimetic systems [34].

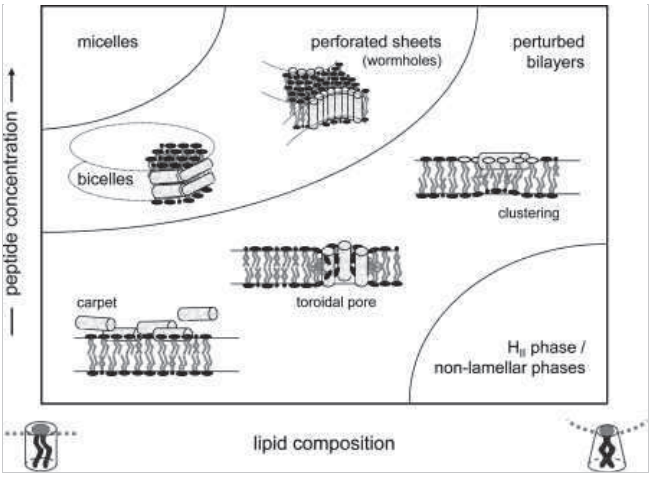

Figure 2.2: Mode of action of membrane-active host defense peptides: boundaries of the schematic phase diagram of amphipathic peptide/phospholipid aggregates are given as a function of the concentration of membrane-associated peptide and the composition of the membrane from mixtures of cylindrical (phosphatidylserine, phosphatidylcholine) and truncated inverted cone lipids (cardiolipin, phosphatidylethanolamine). Membrane association of the cationic peptides is strongly increased in the presence of anionic phospholipids such as PS or cardiolipin. In the presence of cholesterol, an abundant membrane component in mammalian cells, the bilayer will be stabilized, i.e. the phase region of stable bilayers will be enhanced. Some molecular mechanisms of bilayer perturbation are schematically shown (taken from Lohner et al. 2011)

This image was taken from : *http* : *//people.ucalgary.ca/ tieleman/*

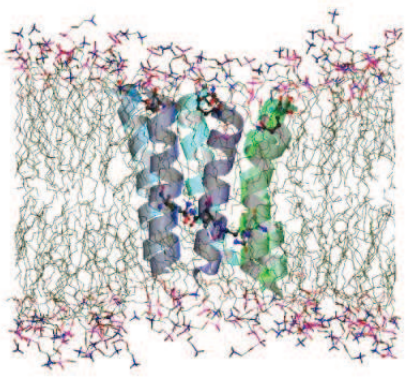

Figure 2.3: An example of antimicrobial peptides: Alamethicin is a peptaibol peptide that is produced by the fungus Trichoderma viride. In its sequence, it contains Aib (2-aminoisobutyric acid) amino acid residue which induces the formation of this alpha-helical secondary structure

2.3 Solid Phase Peptide Synthesis

Solid Phase Peptide Synthesis (SPPS) was pioneered by Robert Bruce Merrifield who was attributed the Nobel prize in chemistry in 1984. It is convenient for peptide chains that have more than 10 aminoacids. Peptide chains are assembled from the carboxy terminus to the amino terminus. The growing peptide chain is attached covalently on an insoluble support. A big excess of reactants is used to render the reactions complete and quick. Finally, the peptide is cleaved from the support and purified by reversed phase HPLC to eliminate products. Mostly deletions of amino acids or incomplete peptide fragments. There are two "chemistries" for peptide synthesis: Fmoc and Boc synthesis. For this thesis project Fmoc synthesis is used. Here are the detailed steps of peptide synthesis that are used to prepare the Hϕ19W

and PGLa peptides using the Millipore 9050 synthesizer [36]:

- Deblocking : 9-fluorenylmethyxycarbonyl (Fmoc) group protects alpha amino groups temporarily. They are rapidly removed by using 1,8-diasabicyclo [5.4.0] undec-7-ene (DBU) or beta elimination (piperidine). These products are flushed through the column.
- washing: to eliminate excess of deblock reagent
- Activation: of aminoacids by dissolving them in activating solution. HBTU (2-(1H-Benzotriazole-1-yl)-1,1,3,3-tetramethyluronium hexafluorophosphate) is used to form active esters in situ.
- Coupling: Amino acids are delivered to the support bound peptide which has a fully deprotected amine and mixed to achieve peptide bond formation
- Washing: The excess of aminoacid. The next cycle begins with deblocking the alpha amino group of the N terminal aminoacid. The deblocking and coupling cycles are repeated
- Capping: to remove the sequence easily while purifying. If the coupling step didn't work the capping will stop the synthesis. So instead of deletions small fragments are obtained.
- Cleavage from the support and deprotection of the side chains

  Some more steps are essential to obtain the final pure product:

- Precipitation in ether (to remove the protection groups which are cleaved but still present in the sample)
- Purification using high-pressure liquid chromatography HPLC is an chromatographic technique of analytical chemistry. It is utilized to isolate components in a mixture. Afterwards, each component can be identified and quantified. In general, the method involves a liquid sample being passed over a solid adsorbent material packed into a column using a flow of liquid solvent.

This image was taken from : *http : //www.sigmaaldrich.com/*

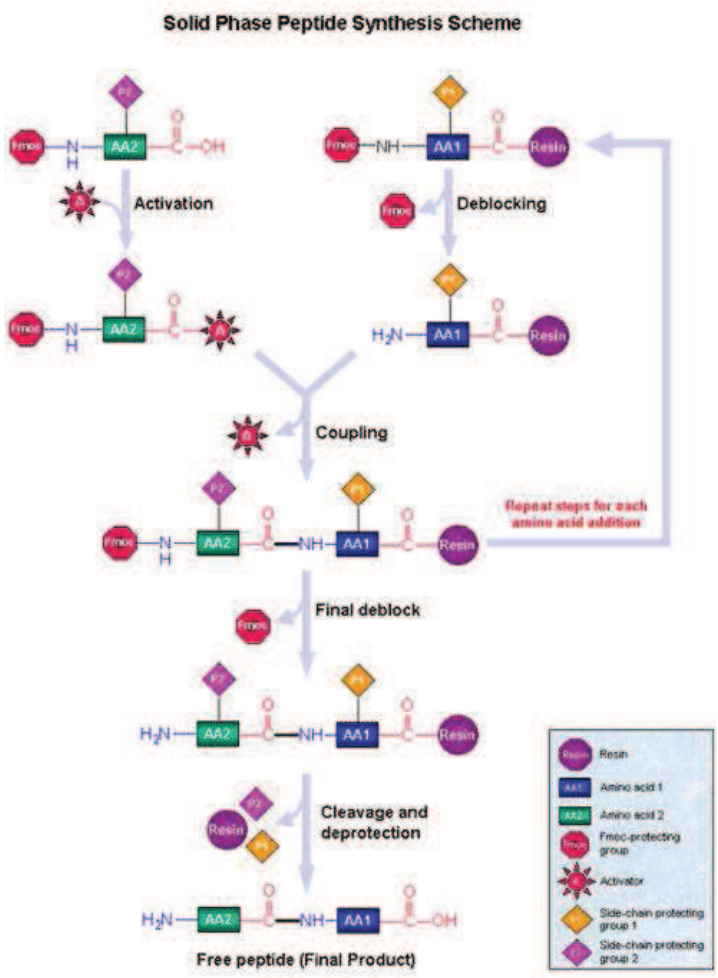

Figure 2.4: Steps of Solid Phase Peptide Synthesis including deblocking of the Fmoc group, activation of amino-acids, coupling of the deblocked and activated residues, cleavage and deprotection to obtain the final product

2.4 Lipid phases and phase transitions

Lipid bilayers (in the liquid crystalline phase) are very flexible. They allow the controlled insertion of proteins, peptides and polysaccharides. Lipid bilayers spontaneously form in an aqueous environment with the right chemical properties (pH,

temperature, salinity etc...). The resulting membranes possess self-healing properties and a high degree of flexibility.

Lipids are amphiphilic molecules, consisting of a polar head-group and two hydrophobic hydrocarbonhydrate chains linked by a glycerol group. The hydrophobic hydrocarbon sidechains can vary in length and in saturation. The headgroup consists mostly of a phosphate group linked to a polar group (i.e.: Choline, Serine, Ethanolamine).

For example, the 1-palmitoyl-2-oleoyl-sn-glycero-3-phosphocholine (POPC) headgroup is zwitterionic. It consists of a negatively charged phosphate group and a positively charged choline cf. figure 2.5. These chemical properties generate lipid bilayers with a negative surface charge. This correlates perfectly with the fact that many proteins need a negative surface charge to interact with the membrane. The glycerol group links the headgroup with the fatty acid chains. The fatty acids consist of palmitoyl (hexadecanoic) with 16 carbons at the glycerol position 1 and of oleoyl (9-cisoctadecenoic) with 18 carbons and an unsaturated bond between the 9 and 10 position. With this chain length the hydrophobic thickness of the bilayers is in the range of about 27 Å[63].

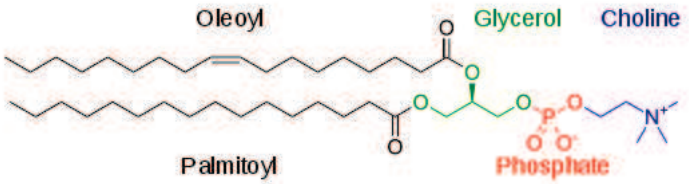

Figure 2.5: 1-palmitoyl-2-oleoyl-sn-glycero-3-phosphocholine. The choline headgroup is linked by a phosphate to the glycerol group. The hydrocarbonate chains are attached to the 1- and 2- position of the glycerol group

Lipids have different geometrical properties [63]. An important factor is the relationship between the cross-sectional area of the hydrocarbon portion A to the optimal surface area required by the polar headgroup (S_0)

- If A/S_0 is between 0.5 and 1 (i.e. phosphatidylcholine, phosphatidylserine) the shape of the lipid is cylindrical and lipid bilayers are formed.
- If $A/S_0 > 1$ (i.e. phosphatidylethanomine, phosphatic acid) the lipids are considered to have a cone shape and an inverted hexagonal phase is formed .
- If $0.5 > A/S_0$ (i.e. lysophospholipids or detergents) the lipids have the shape of an inverted cone and form either rods which can arrange in a hexagonal shape (HI phase)

- If $0.5 > A/S_0 > 0.3$ or $0.3 > A/S_0$ they form micelles. However it has to be noted that the most lipids for micelles formation have only one hydrocarbonate chain.

Lipids can be found in 3 phases

- lamellar gel (L_β) and lamellar liquid crystalline (L_α) phases
- hexagonal HI (cylinders packed in the shape of a hexagon with polar heads facing out into water
- hexagonal HII (cylinders packed in a hexagonal arrangement with the acyl chains pointing out as in reverse micelles, and micellar (M) etc...

Due to their diamagnetic anisotropy lipids, like bicelles, align in a magnetic field. Additionally, the temperature plays an important role for the macroscopic structure of lipid bilayers. At low temperatures frozen samples are always in the gel phase (L_β or $L_{\beta'}$). In absence of any lateral diffusion the lipids are arranged in a hexagonal lattice . At high temperatures the lipids become liquid crystalline (L_α)[63].

2.5 Preparation of oriented membrane samples

When proteins are dissolved in a diluted lipid solution, an oriented and anisotropic sample is obtained. At room temperature the liquid crystalline state provides the membrane proteins and polypeptides the mobility they need to fulfill their functions. The membrane allows mobility in two dimensions (in-planar) and blocks effectively all uncontrolled exchange in the third dimension (flip-flop across the membrane).

The use of glass plates for orienting bilayers depends on the ability of the glass surface to interact with the lipid molecules so that a lipid bilayer will form at the surface. Freshly cleaved borosilicate sheets have also been used as a support for orientation. The orientation is due to the "Helfrich" interaction. The method began in the early 1960s when the first pulsed field gradient NMR diffusion measurements were performed [2].

Since then, the method has been improved. During the sample preparation process, the lipids and the polypeptides are co-dissolved in suitable organic solvents (Tetra Fluoro ethanol) in order to mix properly all components. It is also possible to work with vesicles and buffer systems. The solvent is then quickly evaporated in a first step by using a nitrogen gas flow. Accordingly the sample volume is reduced. The solution must wet the sample support. It is then spread onto ultra-thin cover glasses (9 x 22 mm, Marienfeld, Lauda-Konigshofen, Germany) or carefully cut high

density polyethylene sheets (HDPE: 6 mm x 5 cm). All organic solvents are removed by exposure to a high vacuum overnight and the membranes are equilibrated at 93 % relative humidity. Before the slides are stacked on top of each other, a second hydration is performed for one hour at room temperature for POPC and for 15 minutes at 310 K for DMPC membranes to transform them into the fluid phase. The exposure time is limited for DMPC samples to avoid biradical degradation as much as possible. The subsequent hydration softens the membrane paste, helps in the annealing of defects and a more homogeneous spread and thereby a high degree of orientation. This produces a thin film of lipids on the glass plates or between the HDPE sheets [27].

2.6 Nuclear magnetic resonance

In 1945, Felix Bloch and Edward Mills Purcell discovered NMR. A discovery for which they were awarded the Nobel prize in Physics in 1952.

NMR is a spectroscopy method that exploits the magnetic properties of atomic nuclei. In quantum mechanics, each nuclear spin orientation corresponds to a different energy level.

The spins make a transition between the levels when the sample is exposed to a radio frequency which frequency matches exactly the energy difference. This is called resonance. At resonance, the spins flip and an electric signal is induced into the NMR coil. NMR records a time-domain signal whose Fourier transform represents the NMR spectrum. Around 1950, it was discovered that the nuclear resonance frequencies depended not only on the nature of the atomic nuclei, but also on their chemical environment. After that, the utility of NMR in chemistry became obvious: The signals could be used to determine the number and type of chemical groups in a compound. However, a difficulty in the early days was the relatively low sensitivity of the NMR method.

Electrons and nuclei behave like small bar magnets. They possess intrinsically magnetic moments. These magnetic moments are induced by orbital and spin angular momenta. In addition to a magnetic moment μ, nuclear spins are characterized with a spin I [26]. In the classical model and in the absence of a magnetic field, the individual nuclear magnetic moments are oriented randomly so that there is no net magnetization. When a sample is placed in a magnetic field, however, the nuclear magnetic moments are aligned preferentially with the applied field. According to Boltzmann's law, thermal effects cause a distribution of orientations rather than perfect alignment. Nevertheless, a net nuclear magnetization can be measured [67].

Scientists use NMR to derive molecular structure and function. Making of it the most important method in analytical chemistry.

NMR has been further developed to conceive magnetic resonance imaging scanners used in medicine to visualize the internal body tissues in detail.

2.7 Quantum mechanical approach

Every spin interaction is represented by its own Hamiltonian. A Hamiltonian is a quantum mechanical operator that represents energy. Spin interactions can be represented by second-rank Cartesian tensors (like, e.g., the dipole coupling tensor) [18].

For the purposes of NMR, a simplified time-dependent Schroedinger equation is used according to the spin Hamiltonian hypothesis. This Equation of motion of the wave function, contains only the nuclear spin states.

$$i\frac{d}{dt}|\Psi_{spin}(t)>=\hat{H}|\Psi_{spin}(t)> \tag{2.1}$$

The Hamiltonian eigenvalues are called the energy levels of the quantum system, and the Hamiltonian eigenstates are called the stationary states of the system or, equivalently, the energy eigenstates.

In particular, a nuclei population of spin I placed in a static field B_0 experience interactions that can be described by the Hamiltonian spin interaction concept that was explored by Abragam [42].

This Hamiltonian can be written as the sum of the external spin interactions (coupling between the magnetic moment and the applied field) and the internal spin interactions (internal field in the sample). The spin Hamiltonian operator for a nucleus is [40]:

$$H = H_{int} + H_{ext} \tag{2.2}$$

For spin -1/2 nuclei, the electric interactions vanish.

During an NMR experiment the spin system experiences two types of external spin interactions: One with the static field B_0 and the other with the rf field B_{rf} that is generated by the NMR coil for signal acquisition. The external Hamiltonian or the Zeeman Hamiltonian describes the coupling between the magnetic moment μ and the total magnetic field B which is the sum of the static field B_0 and the applied radio frequency field B_{rf}.

$$H_{ext} = H_Z = -\hat{\mu}\hat{B} = -\hat{\mu}(\hat{B_0} + \hat{B_{rf}}) = H_0 + H_{rf} \tag{2.3}$$

with:

$$\hat{\mu} = \gamma \hbar \hat{I} \tag{2.4}$$

γ is the gyromagnetic ratio.

$$\hbar = \frac{h}{2\pi} \tag{2.5}$$

where h is the Plank constant i.e. 6,6 . $10^{-34} m^2 kg/s$

The Hamiltonian H_0 describes the interaction between the nuclear spins and the static field B_0

$$\hat{H}_0 = -\gamma \hbar \hat{I}_z B_0 \tag{2.6}$$

I_0 represents the spin operator in the direction z parallel to B_0.

The internal Hamiltonian describes the interactions between the magnetic moment μ and the local fields in the sample [18] :

$$\hat{H_{int}} = \hat{H}_J + \hat{H}_D + \hat{H_{CSA}} + \hat{H}_Q \tag{2.7}$$

The J coupling Hamiltonian H_J reflects the indirect spin-spin interactions between two nuclei's magnetic moment in the same molecule through the chemical bond. The J coupling can be homonuclear (between the same nuclei) or heteronuclear (two different nuclei).
The dipolar coupling Hamiltonian H_D is associated with the direct interaction between two magnetic dipoles μ_A and μ_B of two nuclei A and B. It can also be homo or heteronuclear.
The chemical shift anisotropy Hamiltonian H_{CSA} is due to the coupling between the magnetic moment of the nuclei and the local magnetic field induced by the electrons that surround the nuclei under the influence of B_0. The density distribution of the electrons around the nuclei and its anisotropy induces the displacement of the resonance frequency. The chemical shift of the peak depends then on the orientation of the molecule with respect to the static magnetic field.
The quadrupolar interaction H_Q is for nuclei with a spin bigger than 1/2 which possess a quadrupolar moment. It is the coupling between the quadrupolar moment of a nuclei and the gradient of the local electric field gradient. It is given by a second rank tensor (3x3 matrix) and is generated by surrounding nuclei and electrons.

2.8 The energies of nuclei in magnetic fields

To every operator corresponds an observable (eigenvalue) that can be physically measured. In the case of the Hamiltonian it is energy. Classically, the energy of a magnetic moment μ in a magnetic field B is equal to the scalar product [39]:

$$E = -\vec{\mu} \cdot \vec{B} \tag{2.8}$$

The spin quantum number, I, of a nucleus is a fixed characteristic property of a nucleus and is either an integer or a half-integer. A nucleus with spin quantum number I has the following properties:

- A component of angular momentum $m_I\hbar$ on a specified axis (the z-axis),where m_I = I,I-1,...,-I.
- If I $>$ 0, a magnetic moment with a constant magnitude and an orientation that is determined by the value of m_I.

According to the first property, the spin, and therefore the magnetic moment, of the nucleus may lie in 2I + 1 different orientations relative to an axis. In the static field B_0, an energy level splinting occurs: That's the Zeeman effect. One resonance peak is observed at the Larmor frequency.

The energy of the Zeeman Hamiltonian resulting from the interaction between a nucleus with a magnetic moment μ and an external magnetic field B is:

$$E_m = -\gamma\hbar m B_0 \tag{2.9}$$

The corresponding energies are

$$E_{m_I} = \mu_z \cdot B_0 = \gamma\hbar B_0 m_I \tag{2.10}$$

The energy separation between the m_I = +1/2 (up or α) and the m_I = -1/2 (down or beta) states of spin -1/2 nuclei, for nuclei with I = 1/2 , is:

$$\Delta E = E_\beta - E_\alpha = \frac{1}{2}\gamma\hbar B_0 - (-\frac{1}{2}\gamma\hbar B_0) = \gamma\hbar B_0 \tag{2.11}$$

and resonant absorption occurs when the resonance condition is fulfilled:

$$h\nu = \gamma\hbar B_0 \tag{2.12}$$

A spectrometer's characteristic field is usually referred to by the proton resonance frequency. For a 9.4 T magnet ω_{1_H} is 400.1 MHz .

2.9 The Maxwell equations and the NMR signal

A rotating magnetic moment generates a rotating magnetic field. Through the Maxwell equations, a time-varying magnetic field is associated with an electric field and vice versa [26].

$$\nabla.D = \rho \tag{2.14}$$

$$\frac{\partial}{\partial t}\Psi\nabla \times H = J + \frac{\partial D}{\partial t} \tag{2.15}$$

$$\nabla.B = 0 \tag{2.16}$$

$$\nabla \times E = -\frac{\partial B}{\partial t} \tag{2.17}$$

(2.17)

The time-varying magnetization of the sample (precession of the magnetization in the xy plane) induces a voltage in the nearby NMR detection coil (Faraday induction). If this coil is connected to a circuit (and this circuit to the preamplifier, and the preamplifier to the main receiver), a current can flow through the coil caused by the voltage induced by the nuclear magnetization. This current is what is usually called the time-domain NMR signal (free induction decay, FID).

The signal in NMR spectroscopy results from the difference between the energy absorbed by the spins which make a transition from the lower energy state to the higher energy state, and the energy emitted by the spins which simultaneously make a transition from the higher energy state to the lower energy state. Thus, the signal is proportional to the small population difference between the states.

Nowadays the rf electronics is quite advanced to detect the weak NMR signal with good S/N, as compared to earlier times.

$$S_{NMR} \propto \gamma^2 P B_0 \tag{2.18}$$

γ is the gyromagnetic ratio, P is the polarization (see definition below) and B_0 is the applied static field.

The intensity of absorption, is proportional to the product of the rate of absorption and the energy of each photon, and the latter is proportional to the frequency

ν of the incident radiation (through E = h ν). At resonance, this frequency is proportional to the applied magnetic field [39]:

$$S_{NMR} \propto (N_\alpha - N_\beta)B_0 \tag{2.19}$$

As mentioned above, when a group of spins is placed in a magnetic field, each spin aligns in one of the two possible orientations. At room temperature, the number of spins in the lower energy level, N_α, slightly outnumbers the number in the upper level, N_β. It can be deduced from Boltzmann statistics that:

$$\frac{N_\beta}{N_\alpha} = e^{\frac{-\Delta E}{kT}} = 1 - \frac{\Delta E}{kT} = 1 - \frac{\gamma\hbar B_0}{kT}$$

(2.20)

is the energy difference between the spin states, k is Boltzmann's constant, $1,3805.10^{-23}$ J/Kelvin and T is the temperature in Kelvin. The expansion of the exponential term is appropriate for much smaller than kT, a condition usually met for nuclear spins.

$$P = \frac{N_\alpha - N_\beta}{N_\alpha + N_\beta} = \frac{N_\alpha(1 - \frac{N_\beta}{N_\alpha})}{N_\alpha(1 + \frac{N_\beta}{N_\alpha})} = \frac{1 - \frac{N_\beta}{N_\alpha}}{1 + \frac{N_\beta}{N_\alpha}} = \frac{1 - (1 - \frac{\gamma\hbar B_0}{kT})}{1 + (1 - \frac{\gamma\hbar B_0}{kT})} = \frac{\gamma\hbar B_0}{2kT} \tag{2.21}$$

$\mathrm{N}_\alpha - N_\beta = \frac{N\gamma\hbar B_0}{2kT}$(2.22)
N= $\mathrm{N}_\alpha + N_\beta$

It follows that decreasing the temperature increases the intensity by increasing the population difference. By combining these two equations, it can be deduced that the intensity is proportional to ${B_0}^2$, so the NMR signal can be better enhanced and resolved by increasing the strength of the applied magnetic field. It can also be concluded that spectra of nuclei with large gyromagnetic ratios like protons are more intense than those with small gyromagnetic ratios (^{15}N, for instance)

2.10 Bloch equations and relaxation times

When a B_{rf} rotating field is applied in the xy plane, then the nuclear spins are driven by this field into the xy plane. For example if a 90° pulse is applied the spins

reach the xy plane and rotate in it. When the pulse is stopped the spins align again along the z axis. The magnetization time evolution depends on the B_0 and B_1 fields and is described by the Bloch equations. NMR pulses will be discussed into more details in the next sections.

$$\frac{d}{dt}M_x = \gamma M_y(B_0 - \frac{\omega}{\gamma}) - \frac{M_x}{T_2} \tag{2.23}$$

$$\frac{d}{dt}M_y = \gamma M_x B_1 - \gamma M_x(B_0 - \frac{\omega}{\gamma}) - \frac{M_y}{T_2} \tag{2.24}$$

$$\frac{d}{dt}M_z = -\gamma M_y B_1 - \frac{M_x - M_0}{T_1} \tag{2.25}$$

More information about pulse programming can be found in Appendix A.

Mathematically, T_1 spin-lattice (or longitudinal) relaxation time is the time it takes for the magnetization to recover 63% of its equilibrium value [88]. When the differential equation is solved, the following expression for the magnetization is obtained:

$$M_z = M_0(1 - e^{\frac{-t}{T_1}}) \tag{2.26}$$

$$M_0 = \frac{N\gamma^2\hbar^2 I(I+1))}{3kT}B_0 \tag{2.27}$$

When molecular motions are very fast, as in non viscous liquids, T_1 equals T_2 for most interactions and T_2 offers no additional information. However, in solids typically T_2 is much smaller than T_1 and then T_2 does offer additional information.

T_2 spin-spin (or transverse) relaxation time is the time constant for the decay of the precessing xy component of the magnetization following an rf pulse.

T_{2*} is the decay time of the FID, i.e., the NMR detectable signal. T_{2*} is always smaller than or equal to T_2. After a 90° pulse, the magnetization in the xy plane will induce a decaying sinusoidal voltage in the pickup coil. For a single Lorentzian line the decay of the magnetization in the xy plane will be exponential with the time constant T_2* and the output of the pickup coil will be a sinusoidal wave whose amplitude is decaying at the rate exp (-t/T_{2*}).

Other relaxation processes that will just be mentioned are those characterized by $T_{1\rho}$ and T_{1D}. The former is called spin lattice relaxation in the rotating frame while the latter is called dipolar spin lattice relaxation.

2.11 Solid state NMR

Solid-state NMR is the study of solid samples using NMR. Solid state NMR experiments measure the magnitudes and orientations of the chemical shift anisotropy CSA and heteronuclear dipolar coupling tensors. They provide very powerful information for characterizing rapid, large-amplitude motions in solids [20, 21]. First the spin interactions involved in solids are briefly presented:

The chemical shift interaction: When an atom is put in a magnetic field, the electrons interact with it, generating an electron current. This electron current will induce a shielding magnetic field that will affect the atom nucleus. This shielding interaction will cause a shift in the resonance frequency of the nuclei. This frequency shift is referred to as the chemical shift. Here is the expression of the chemical shift interaction for a spin I in a static magnetic field $\mathrm{B}_0 \hat{H}_{CS} = -\gamma\hbar\hat{I}.\sigma.B_0 (2.28)$

σ is the chemical shift shielding second rank tensor. In most solids, the molecules are lined up on a rigid lattice. On the one hand, in a *crystal*, all molecules have the same orientation. In this case, all principle values of the chemical shift are equal and the chemical shift tensor is called isotropic. The chemical shift can be measured in NMR:

$$\delta_{ppm} = \frac{\nu_{sample} - \nu_{standard}}{\nu_{spectrometer}} 10^6 \tag{2.29}$$

where the resonance frequency for the reference compound TMS $\nu_{standard}$ is set to 0.

In this particular case, the chemically shifted Larmor frequency of ^{15}N and the internal molecular Hamiltonian term depend on the orientation θ of the atomic framework of the sample with respect to the magnetic field [43].

$$\omega_j^0 = -\gamma_j B_0 (1 + \delta_{zz}^j(\theta)) \tag{2.30}$$

On the other hand, in a *powder* the molecules have all possible orientations. Moreover, because the chemical shift of each crystallite is different, the solid-state NMR spectrum of a powder has a typical broad shape with sharp corners. It is called a powder pattern cf. appendix B. The broad pattern comes from the superposition of many sharp peaks with different frequencies, each one coming from a crystallite with a different orientation. When two or more of the principle values are unequal, the chemical shift tensor is said to be anisotropic. The CSA causes the broadening of the powder NMR spectra. CSA is the largest deviation in chemical shift from the isotropic value.

The sharp features of a chemical shift powder pattern coincide with the principal values of the chemical shift tensor $(\delta_j^{xx}, \delta_j^{yy}, \delta_j^{zz})$.

And a Hamiltonian:

$$H_j^0 = H^{static} + H_j^{CS} = \omega_j^0 \hat{I}_{jz} \tag{2.31}$$

Dipolar coupling: As mentioned before, every nuclear spin is a dipole. It generates a magnetic field which field line loop around , according to the direction of the spin magnetic moment. This magnetic field is sensed by other neighboring spins and vice versa. The interaction between the spins is mutual. The first nuclear spin also experiences the field generated by the second nuclear spin.

This interaction is called the through-space dipole-dipole coupling, or direct dipole-dipole coupling, because the fields between the nuclear spins propagate through space without involving anything else.

The full form of the direct dipole-dipole interaction between spins I_j and I_k is represented in the spin Hamiltonian by the following term [43]:

In the homonuclear case:

$$H_{jk}^{DD} = -\frac{\mu_0 \gamma_j \gamma_k \hbar}{4\pi r_{jk}^3} \frac{3\cos^2(\theta_{jk}) - 1}{2} (3\hat{I}_{jz}\hat{I}_{kz} - \hat{I}_j.\hat{I}_z) \tag{2.32}$$

In the heteronuclear case:

$$H_{jk}^{DD} = -\frac{\mu_0 \gamma_j \gamma_k \hbar}{4\pi r_{jk}^3} \frac{3\cos^2(\theta_{jk}) - 1}{2} (2\hat{I}_{jz}\hat{I}_{kz}) \tag{2.33}$$

These are the secular parts of the direct dipolar coupling, i.e., those parts that commute with the nuclear Zeeman Hamiltonian. In practice the ^{15}N-^{1}H dipolar coupling is measured.

As shown previously, the molecular spatial and angular information are given by the dipole-dipole interaction. When two nuclei are linked covalently the distance between them (r) is known. Therefore, the angle θ between the chemical bond and the applied magnetic field can be easily measured given the frequency splitting between the Nitrogen and proton peaks.

$$\nu_n(^1\mathrm{H} -^{15}\mathrm{N}) = \pm\frac{\mu_0 \gamma_H \gamma_N \hbar}{4\pi r_{N-H}^3} \frac{3\cos\theta^2 - 1}{2} \tag{2.34}$$

2.12 Magic angle spinning

To eliminate the chemical shift anisotropy and to help abstract the heteronuclear dipolar coupling interactions magic angle spinning is used in solid state NMR experiments. Fast spinning MAS removes the effect of homonuclear dipolar coupling[67].

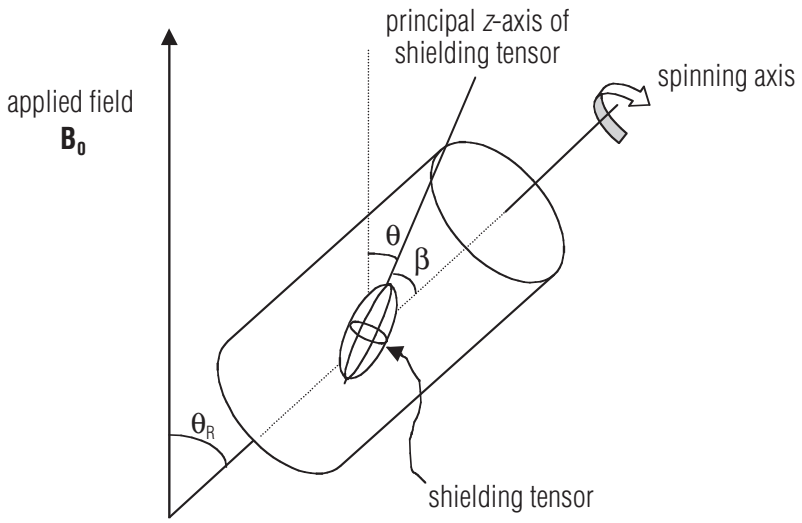

Figure 2.6: The magic-angle spinning experiment. The sample is spun rapidly in a cylindrical rotor about a spinning axis oriented at the magic angle ($\theta_R = 54.74°$) with respect to the applied magnetic field B_0. Magic-angle spinning removes the effects of chemical shielding anisotropy and heteronuclear dipolar coupling. The chemical shielding tensor is represented here by an ellipsoid; it is fixed in the molecule to which it applies and so rotates with the sample. The angle θ is the angle between the principal z-axis of the interaction tensor and the applied field B_0. The angle β is fixed for a given nucleus in a rigid solid, but like θ it takes on all possible values in a powder sample. Duer, Solid-State NMR Spectroscopy Principles and Applications

When the sample is spun about an axis inclined at an angle θ_R with respect to the applied field, then θ, the angle describing the orientation of the interaction tensor fixed in a molecule within the sample, varies with time as the molecule rotates with the sample. To average the anisotropy associated with any interaction which causes a shift in the energies of the Zeeman spin functions, such as chemical shift anisotropy, heteronuclear dipolar coupling θ_R is fixed to the magic angle. As seen in the previous section the heteronuclear dipolar coupling depends on $(3cos^2\theta - 1)$ factor. When the sample is spun, this factor is averaged to zero, as shown in equation 2.35.

$< 3\ \cos^2\theta - 1 >= \frac{1}{2}(3cos^2\theta_R - 1)(3cos^2\beta - 1)(2.35)$

θ_R is the angle between B_0 and the spinning axis. The angle θ is the angle between the principal z-axis of the interaction tensor and the applied field B_0. The angle β is fixed for a given nucleus in a rigid solid, but like θ it takes on all possible values in a powder sample.

Obviously $3\ \cos^2\theta_R - 1 = 0.\beta$ can take all possible values in a powder sample but it is fixed for a given nuclei. And at fast spinning speeds $< 3cos^2\beta - 1 >$ averages to zero.

2.13 Solid state NMR study of biological solids

Solid-state NMR spectroscopy has been used since the 1960s for the investigation of lyotropic liquid crystalline phases to obtain information about, e.g. phase structures, solubilization, extent of hydration, dynamics and orientation of biological molecules [27].

The characterization of CSA tensors in peptide bonds is essential for structural studies of membrane-associated proteins [22]. The ^{15}N CSA tensor depends on the type of amino acid residue, the secondary structure, the dynamics, and the hydrogen bonding [23]

In 1993, the first high resolution structure by solid state NMR of a membrane-bound polypeptide gramicidin A was presented [4]. At that time home made programs were used to calculate diplane coordinates by using the diplane direction cosine solutions along with the (Φ, Ψ) solutions. At the same time, in 1994, a new experiment called PISEMA was developed by Opella, Ramamoorthy and co-workers [52]. PISEMA improves the spectral resolution for ^{15}N-^{1}H dipolar observation by an order of magnitude. By 1999, molecular dynamics was introduced to refine conformational energy calculations [51]. In 2010, ^{13}C - ^{2}H REDOR spectra were used successfully in the structure determination of Influenza M2 proton channel [54]. By all means structural constraints need to be determined in order to establish a protein 3D structure.

Two types of structural constraints can be determined by solid-state NMR of biological samples [67]:

- Distance constraints between specifically labeled homonuclear and/or heteronuclear spins, using rotational resonance [6], multiple-pulse recoupling, double-quantum spectroscopy or Rotational Echo Double Resonance (REDOR) [5]

- Orientational constraints determination of torsion angles in various specifically labeled fragments of biopolymers by chemical shift-chemical shift tensor correlation experiments, dipolar-chemical shift tensor correlation experiments and experiments correlating two dipole-dipole coupling tensors, CP [4],Separated local field spectra (SLF) [49, 50], PISEMA [58] , SAMMY [10] etc...

The orientational constraints approach permits the determination of helices tilt angles with respect to the bilayer normal.

First, one-dimensional solid-state ^{15}N chemical-shift NMR spectra of ^{15}N-labeled mechanically or spontaneously, magnetically oriented systems with respect to B_0, membrane peptides are acquired. In these spectra, each ^{15}N resonance arises from a single nitrogen atom in the protein, and has a frequency that reflects the orientation of the corresponding NH bond in the lipid bilayer membrane [48]. Second, these interactions are represented in the molecular frame of the molecule by a coordinate system or tensor that is fixed with respect to the covalent bonds of the molecular frame. Consequently, by observing the orientation-dependent nuclear spin interactions, such as the anisotropic chemical shift CSA and dipolar and quadrupolar interactions, the nuclear spin tensor and the molecular frame are constrained with respect to B_0 [25].

- 1 D solid state NMR orientational constraints determination: In the case of membrane polypeptides, the sample orientation is verified using solid state ^{31}P and ^{15}N CP NMR .The orientation dependence of chemical shift and dipolar or quadrupolar interactions are used to obtain dynamic as well as angular information from polypeptides that strongly interact with phospholipid bilayers. In practice, it is the anisotropic ^{15}N or ^{31}P chemical shift interactions that allow one to obtain information on the alignment of helical polypeptides or of phospholipid head groups with respect to the membrane normal. The anisotropic chemical shift interaction is mathematically described by second-rank tensors that can be written as a diagonal matrix in the principal axis system (PAS):

$$\begin{pmatrix} \sigma_{11} & 0 & 0 \\ 0 & \sigma_{22} & 0 \\ 0 & 0 & \sigma_{33} \end{pmatrix}$$

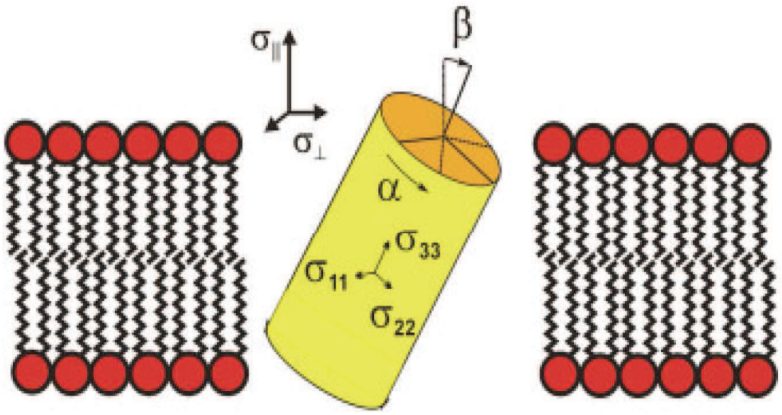

Figure 2.7: Helical peptide orientation into the lipid bilayer using the anisotropic chemical shift tensor. Bechinger et al Concepts in Magnetic Resonance 2003

Helical peptides uniaxially oriented along the membrane normal, which is parallel to the magnetic field, exhibit ^{15}N resonances superior to 200 ppm. In contrast, they resonate in the σ_{11}-σ_{22} range (i.e., resonance peak inferior to 100 ppm) when aligned parallel to the membrane surface (c.f. figure 2.9).

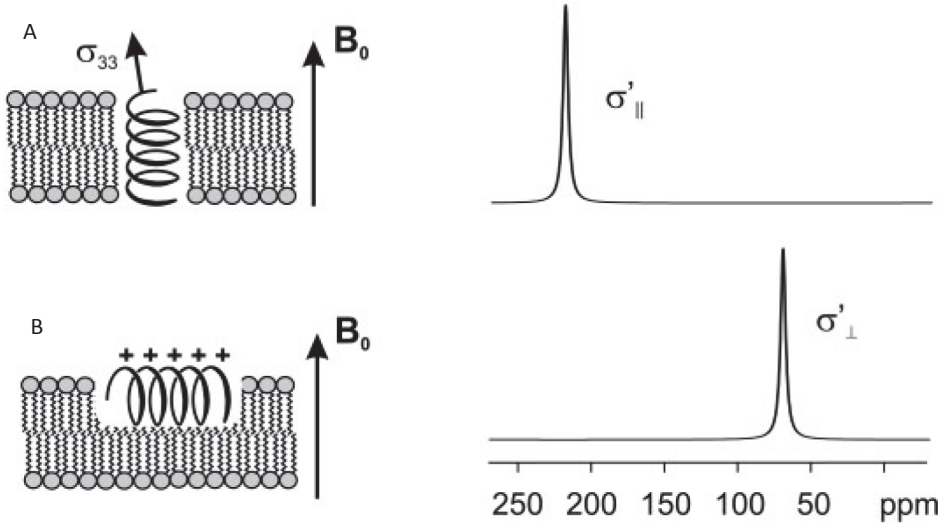

Figure 2.8: Proton-decoupled ^{15}N ssNMR spectrum to determine alpha helix protein orientation with respect to the magnetic field. If ^{15}N resonances are superior to 200 ppm, the helical peptides are uniaxially oriented along the membrane normal, which is parallel to the magnetic field . In contrast, if the resonance peak is inferior to 100 ppm then the alpha helix is aligned parallel to the membrane surface. Bechinger et al Concepts in Magnetic Resonance 2003

- 2 D solid state NMR orientational constraints determination: As mentioned above, solid state NMR spectroscopy can be used independently to determine the three-dimensional structures of small and medium sized uniformly labeled polypeptides in bilayers [25]. Additionally, the orientationally dependent ^{15}N chemical shift and ^{1}H-^{15}N dipolar coupling frequencies provide orientational constraints for structure determination of ^{15}N-labeled peptides in lipid bilayer membranes. These constraints can be measured directly from the highly resolved two-dimensional solid-state polarization inversion spin exchange at the magic angle PISEMA or SAMMY spectrum of polypeptides[51] In fact, every labeled site gives rise to a resonance peak due to the chemical shift anisotropy and dipolar spin interaction described above. These resonance frequencies retain information about the protein's orientation in the phospholipid bilayer.

The analysis of these frequencies is done through the representations of the PISA (polarity index slant angle) wheels and dipolar waves, structural fitting of spectra, and the calculation of the structure from orientation-dependent frequencies [9]. PISA wheels and dipolar waves involve the analysis of the periodic patterns observed in spectral data.

Dipolar waves provide a measure of the regularity of alpha-helices. A periodic function is obtained by using a simple distribution on a cone assuming a constant angle between the N-H bond and the helix axis. As a result the dipolar couplings (or chemical shifts) of the helices exhibit wavelike helices as a function of residue number.

The two-dimensional ^{1}H-^{15}N dipolar coupling/^{15}N chemical shift PISEMA spectra of oriented proteins display distinctive resonance patterns that are a consequence of the direct mapping of protein structure onto NMR frequencies. These wheel-like patterns, called Pisa (polarity index slant angle) wheels, are sensitive indications of secondary structure and topology, and reflect the helical wheel projections of residues in both alpha helices (trans-membrane and in-plane) [59] and beta strands [60]. The tilt of a helix can be determined by interpreting a Pisa wheel without resonance assignments. The sequential assignment of one or the identification of a few residues by type and their position on the PISA wheel determines the rotation angle (polarity index) of the helix along its long axis, for example, one sequential assignment or the pattern from one selectively labeled sample [62]. An example of helix tilt angle determination using PISEMA is shown in section 4.12.

Structural fitting is a recently developed complementary approach to complete structure determination. It has been shown to identify subtle deviations from ideal helical structure and also other features. This is accomplished by the fitting of the spectrum to a model structure assuming a constant peptide plane geometry. In the case where the resonances have been assigned, the Ramachandran angles Φ and Ψ are considered to be the only degrees of freedom. The whole structure is assembled by the sequential walking from one residue to the next calculating the angles Φ and Ψ directly from two orientation-dependent frequencies for these residues. In principle, it provides an assignment-free approach to structure determination. In practice, at its present stage of development, it can use partial assignment information to determine protein structures in the absence of complete sequential assignments [10]

2.14 Spectrometer technology

In 1952, HR-30, the first commercial spectrometer was manufactured by Varian Associates benefiting from an earlier collaboration with William Hansen and Felix Bloch from Stanford university [64]. In 1967 Bruker-Spectrospin launched HFX 90 the first commercially available spectrometer to offer three independent channels (detection, decoupling, lock) taking advantage of the close cooperation with Richard Ernst from the ETH Zurich [65].

In most current NMR spectrometers the magnetic field is generated by a superconducting magnet [66]. The first stage in reaching the very low temperature needed is an outer stainless steel or aluminum dewar which contains liquid nitrogen. An inner dewar contains the superconducting coil immersed in liquid helium. A room-temperature bore is fitted with the shim coils, providing a room-temperature homogeneity adjustment, and a spinner assembly, which contains the turbine system for spinning the NMR sample tube. The probe-head is usually introduced into the magnet from the bottom and is connected to at least three rf cables providing ^{1}H frequency, X and Y-nuclei frequencies. Additional devices to control temperature (heater, thermoelement, air) are needed.

The spectrometer cabinet in many modern spectrometers typically provides three radio frequency channels. Usually these frequencies are derived from digital frequency synthesizers which are phase-locked to a central quartz oscillator. These frequencies are controlled, amplified, pulsed, and transmitted to the probehead. The various NMR signals are preamplified, then mixed with the local oscillator frequency to yield the intermediate frequency (i.f.). The i.f. signal is further amplified, then in a second mixing stage the NMR audio signal is obtained after quadrature phase detection. The two signal components are digitized in the analog-to digital converter (ADC) and fed into the computer memory or, in the case of the lock signal, used for field/frequency regulation [66]

The rf pulse is synthesized in the synthesizer then phase shifted. This process is modulated by the pulse gate that is controlled by the pulse programmer. It is then amplified and transfered to the probehead by the Duplexer. It is then coupled to the probehead's resonant circuit (NMR coil, tunning capacitor). The NMR signal that is generated is amplified then digitized. It then reaches the computer after a last phase shift.

A simple NMR experiment consists of a single rf pulse on a single rf channel, followed by signal detection. The sequence of events is as follows [43]:

1. Initialization: Before the experiment starts, the computer downloads instructions to the pulse programmer and to other pieces of hardware, such as the synthesizer and the ADCs, setting up the carrier frequency, the sampling frequency and the

number of sampled points, etc.

2. Excitation: On initiation, the pulse programmer executes a timed sequence of instructions to set the phase of the rf synthesizer and opens the pulse gate. An rf pulse travels into the probe from the amplifier, via the duplexer. This rf pulse sets up resonant oscillations in the tuned circuit of the probe, irradiating the sample with an rf field close to the Larmor frequency of the chosen nuclear isotope. This rf pulse disturbs the equilibrium of the nuclear spin system and creates transverse nuclear magnetization.

3. Detection: The pulse is switched off. After some microseconds, the pulse energy in the tuned circuit dissipates. The precession of the transverse nuclear spin magnetization sets up oscillations in the tuned circuit, which gives rise to an rf oscillating electric current. This is called the NMR signal or free-induction decay (FID). The NMR signal travels back down the cable from the probe to the duplexer. This signal is amplified by the signal preamplifier and converted down in frequency by the quadrature receiver. The pulse programmer issues an instruction to the ADCs, which proceed to digitize the two quadrature receiver outputs. The digitized complex signal s(t) is stored in the computer memory.

4. Processing and display. The digital complex signal is subjected to various mathematical operations, including the numerical calculation called Fourier transformation (FT). FT converts the NMR signal, which is a function of time, into an NMR spectrum, which is a function of frequency. The NMR spectrum may be processed, displayed on the computer screen, printed or plotted on a sheet of paper.

Here is a list of the used NMR pulse sequences:

1. The 90° pulse, one pulse: The 90° pulse is important for routine operations. It is usually used to calibrate the proton 90° pulse duration to approximately 5 μs. This is equivalent to a 50 KHz B_1 field which is essential for protein CP experiments. In practice, it consists of sending pulse such as the magnetization is turned by 90° and observing the power level at which maximum signal is obtained.

2. hpdec: The signal is acquired on the X Channel with high power proton decoupling. This pulse sequence is suitable for various types of decoupling. By previously doing a "one pulse" pulse sequence the topspin parameter pl12 ,the power level for standard proton decoupling, is calibrated. Then a parameter optimization is run for p1 the pulse duration for X pulse at a fixed pl1 (X power level for excitation pulse). A short pulse duration is usually needed: 5 μs for example.

3. Hahn echo: Spin echo techniques have been designed to remove the effect of applied field inhomogeneity. First a 90 ° pulse is applied, followed by a 180 ° pulse after a period τ of dephasing. The 180° is used for refocusing the spin magnetization

[88].
More precisely, the spins precess in the xy plane after the first 90 ° pulse. However, the NMR signal decays with time because of spin relaxation and local magnetic field inhomogeneities in the sample. Some spin isochromats slow down due to a lower local field strength and other go faster due to stronger local field. The 180° pulse makes the pack of slower spin isochromats lead ahead and the faster spin isochromats trail behind. Progressively they both rephase with the main magnetic moment. The magnetization will refocus along -y axis at 2τ and it will cause an inverted spin echo. The spin echo consists of two FID back to back.

4. Cross polarization(CP): Due to the poor sensitivity of low gyromagnetic ratio nuclei (e.g. γ_{15_N} i.e. -27.1157 MHz/T) and long T_1, relaxation times experiments like a Hahn-echo don't give signal in a reasonable time. Therefore the signal has to be somehow enhanced. This is possible by Hartmann-Hahn Cross-Polarization under certain conditions. For that,the fact that in solids, abundant spins are close to rare spins and are coupled by dipolar interaction is used. So the basic idea of cross-polarization is the induction of transversal magnetization to protons (by a 90° pulse, for a duration p3 at power level pl12) and the transfer of this transversal magnetization to the nitrogen nuclei. This transfer of magnetization can be achieved during a contact time p15 by locking both the proton and the nitrogen nuclear spin by irradiation with an electromagnetic field, which satisfies the Hartmann-Hahn condition.

$$\gamma_H B_1^H = \gamma_N B_1^N \tag{2.36}$$

In this condition, the precession velocities of both proton and nitrogen are the same.

When using the cross polarization experiment the critical factor for the relaxation of the system to the thermal equilibrium is T_1 of protons rather than the one of nitrogen-15. Protons in oriented lipid samples have a T_1 of 1 sec whereas nitrogen have a T_1 of 10 sec. Therefore cross polarization experiments can be performed with a much shorter repetition time than NMR-experiments using direct observation on the ^{15}N channel[63].

CP usually gives access to nuclear mobility and X-H distances [55].

5. The PISEMA pulse sequence

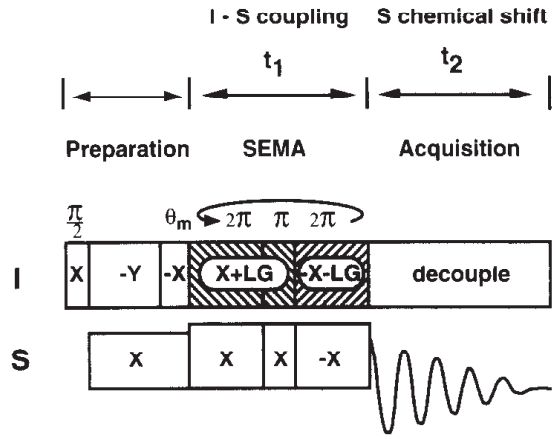

Figure 2.9: PISEMA pulse sequence diagram taken from A. Ramamoorthy and S.J. Opella (1995)

During the preparation period a conventional spin-lock cross polarization the abundant I spin magnetization is transferred to the dilute S spins. It is then followed by polarization inversion that brings the abundant I spins to negative spin temperature. The θ_m, pulse induces a 54.7 ° nutation of the I spin magnetization so that it can be spin-locked at the magic angle by flip-flop Lee-Goldburg (FFLG-2), phase and frequency-switched irradiation, which eliminates the I-I dipolar couplings and I spin chemical shifts, while being phase alternated synchronously with the spin-locking S spin irradiation, which removes S spin chemical shifts, to allow the transverse magnetization of the S nuclei to evolve coherently under the unique influence of the I-S dipolar coupling. Each t_1, increment corresponds to one complete flip-flop Lee-Goldburg cycle, as defined by X + LG in the first part and - X - LG in the second part of each cycle in the diagram. X + LG indicates that the I spin rf irradiation has X phase and a positive frequency offset that satisfies the Lee-Goldburg off-resonance condition and -X - LG has -X phase and a negative frequency offset. During t_2, the acquisition time, high-resolution S spin spectra are acquired , in the presence of continuous I spin irradiation. This pulse sequence suppresses the homonuclear ^{1}H-^{1}H dipolar couplings and gives linewidths of less than 180 Hz in single-crystal samples and less than 400 Hz in stationary powder samples. [53]

2.15 T_1 measurement

The longitudinal (or spin-lattice) relaxation time T_1 is the decay constant for the recovery of the z component of the nuclear spin magnetization, M_z, towards its

thermal equilibrium value, $M_{z,eq}$ (c.f. the Bloch equations section). It is inherently important for integration accuracy to set the recycle delay D1 superior to $5T_1$ (It is 1.3 for DNP measurements) . Therefore if T_1 is too long no NMR data can be acquired, because it takes too long for spins to recover (go back to the parallel position) after one pulse. Nutation curves are somehow distorted and no 180° spin flip can be obtained (c.f. Appendix C)

Generally, the T_1 drops with the temperature but goes up again in the range of liquid nitrogen temperature [83]. When T_1 is long at low temperature as it is the case of ammonium chloride, the spins take a long time to come back to their initial state, as mentioned previously. Therefore they cannot be freely turned and parameter optimization is not possible.

There are two major methods for measuring T_1 in NMR: inversion recovery and saturation recovery.

There is a simple way to do so by hand using a 1D experiment called T_1 inversion recovery. It consists of a 180° pulse followed by a 90 ° pulse. The delay in between these two pulses is varied in such a way that the spins are at 180 ° when the delay is too short and at 90° when the delay is too long. This evolution is exponential. And if the intensity or the area of the peaks are taken into consideration then this exponential crosses the time axis at t = T_1 ln 2.

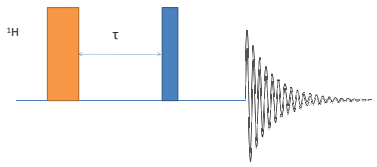

Figure 2.10: Inversion recovery pulse sequence consisting of a 180° pulse followed by a 90 ° pulse. The delay in between these two pulses is varied

Saturation recovery consists of applying several 90° pulses separated by a variable delay list vd. The first delay is too short so the two pulses add up to flip the spin to 180°. For the last pulse the delay is too long that the spins have the time to come back to their equilibrium position before responding to a second 90° pulse. The spectrum area measure corresponds to a maximum peak and therefore a maximum peak area. The variation of the peak area versus the time gives an estimation of the sample T_1.

T_1 can be extracted from the following formula:

$$M_z = M_{z0}(1 - exp^{\frac{-t}{T_1}}) \tag{2.37}$$

Here is the pulse sequence

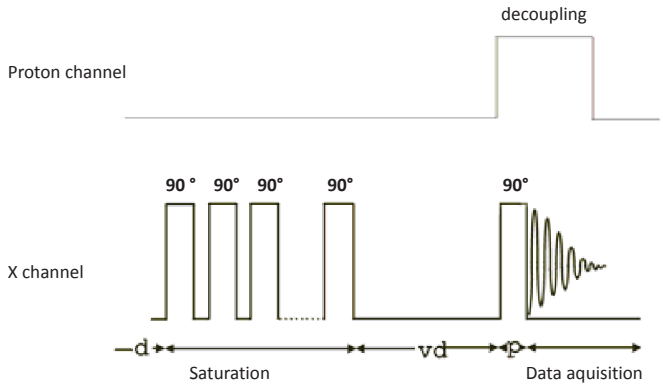

Figure 2.11: Saturation recovery sequence. d is a fixed waiting time and can be set to 1 s. vd is the variable delay list. p is the 90 ° pulse duration

2.16 Dynamic nuclear polarization

NMR is an important method for structure determination in solids and liquids. However its major drawback is its poor signal to noise ratio due to the low magnetic moment of the observed nuclei (^{1}H, ^{13}C, ^{15}N etc). Dynamic nuclear polarization DNP is a signal enhancing method that permits the transfer of the large Boltzmann polarization of a paramagnetic species (stable organic free radicals) to the nuclei of interest by microwave irradiation of the sample (near or at the electronic paramagnetic resonance EPR transition).The maximal theoretical enhancement value is equal to the ratio of the gyromagnetic ratios of electron and the nuclei of interest. It is 660 for protons and 2600 for carbon.

2.17 Polarization transfer in electron-nuclear spin systems

DNP involves polarization transfer processes between the electron and nuclear spin systems that are in contact with a lattice and are governed by the following generalized Hamiltonian:

$$H = H_S + H_I + H_{SS} + H_{IS} + H_{II} + H_M + H_{SL} + H_{IL} + H_L \tag{2.38}$$

where H_S and H_I are the Zeeman Hamiltonians of the electron spins S and nuclear spins I, H_{SS}, H_{IS}, and H_{II} describe the electron-electron, the electron-nuclear, and nuclear-nuclear couplings, H_M is for the microwave excitation, H_{SL} and H_{IL} are the spin-lattice interactions, and H_L is a generalized lattice interaction. H_S, H_I, H_{SS} and H_{IS} are the most important terms in the Hamiltonian for DNP. Further, in situations with diluted electron concentrations, H_{II} mediates the propagation of enhanced nuclear polarization throughout the bulk nuclei. Concurrently, the coupling of the electron and nuclear relaxation due to H_{SL} , H_{IL} and H_L regulates the efficiency of polarization transfer in DNP.

In a CW microwave irradiation experiment, the high polarization of the electrons is transferred to the protons which then transfer their polarization by spin diffusion to the lattice.

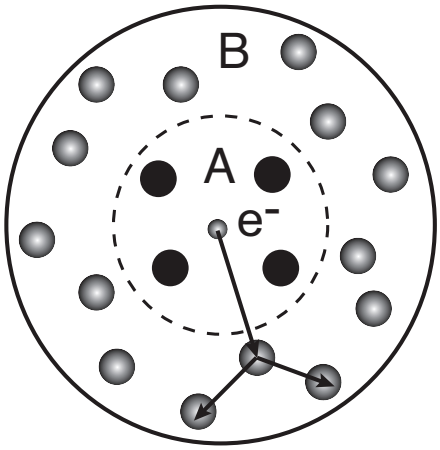

Figure 2.12: A schematic representation of polarization transfer in DNP experiments. Region B represents the observable bulk nuclei. Region A represents the paramagnetic center and nuclei within the diffusion barrier. The electron polarization is transferred to a nuclear spin with a strong hyperfine interaction but residing outside region A. The enhanced polarization then propagates throughout the bulk nuclei via homonuclear spin diffusion. Taken from Hu et al 2011

This spin diffusion process is somewhat complex and is still being discussed. Figure 2.12 represents the polarization transfer in a DNP experiment. The electron spin polarization initially propagates through homonuclear spin diffusion to coupled nuclei outside a "diffusion barrier" (Region A) and subsequently throughout the bulk nuclei (Region B) . It has to be noted that nuclear spins inside the barrier are isolated from the bulk nuclear spin diffusion by the strong electron-nuclear coupling. Experiments suggest a diffusion radius ≤ 3 Å for a paramagnetic metal ions. Particularly, the neighboring nuclei interact weakly with the bulk because the electron-nuclear couplings shift their resonances. Thus, the DNP process involves electron spins and nuclear spins immediately outside Region A. However, in the case of bulky organic radicals, commonly used in DNP experiments nowadays, such as TOTAPOL, bTbk or trityl, the spin density is distributed over part or the whole molecule. Therefore, the barrier between regions A and B is probably less clear, and, accordingly, the polarization and spin diffusion steps can be more complicated than the simplified depicted picture [71].

2.18 DNP mechanisms

The DNP phenomenon is an evolution of the electron Zeeman order to nuclear Zeeman order [71]. The DNP mechanism known for liquid state NMR is the Overhauser effect [74]. As for solids, it is the solid effect SE, thermal mixing TM or cross effect CE.

The energy level diagrams appropriate for the $S_i = I = 1/2$ basis functions $|\alpha_{S_i}>$, $|\beta_{S_i}>$,$|\alpha_I>$, $|\alpha_I>$ are illustrated in figure 2.13

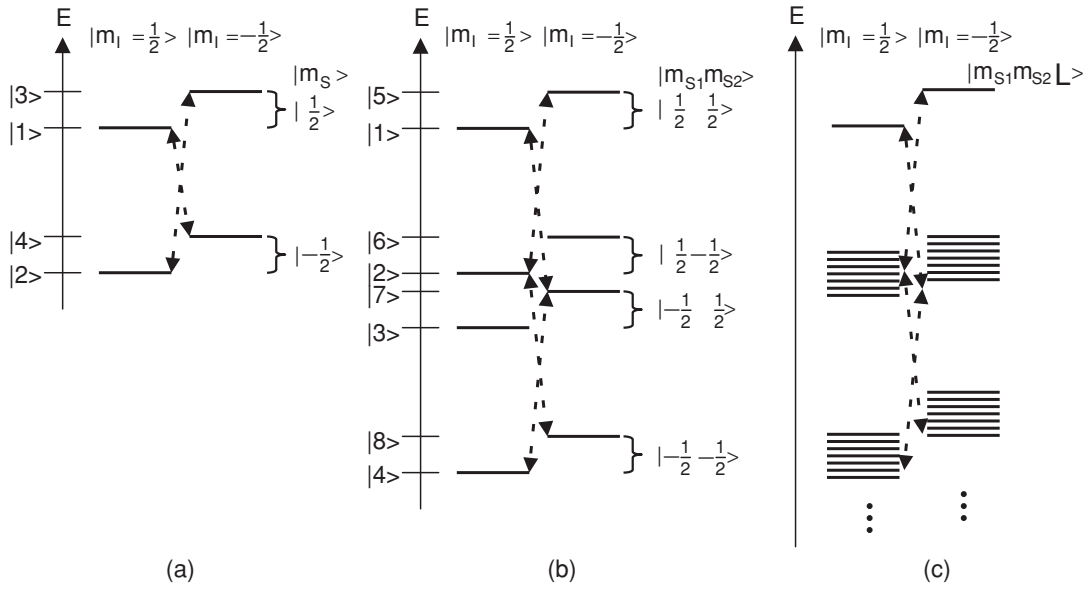

Figure 2.13: Quantum mechanical picture of the electron-nuclear transitions (dashed arrows) in (a) the SE, (b) the CE and (c) TM mechanisms, which involve one, two or multiple electron spins, respectively. Note that the probabilities of electron-nuclear transitions are always small in the SE but could be large in the CE and TM when degeneracy exists between the states with alternating nuclear spin quantum numbers. Taken from Hu et al (2011)

At high magnetic fields the two polarizing phenomenons that are involved in DNP are the cross effect CE and thermal mixing TM.

The SE occurs when using single-electron polarizing agents. In this case, a single electron-nuclear spin pair is sufficient to explain the polarization mechanism. In particular, if $\delta, \Delta < \omega_{0I}$, where δ and Δ are the homogeneous linewidth and inhomogeneous breadth of the EPR spectrum, respectively. The SE occurs when $\omega_M = \omega_{0S} \pm \omega_{0I}$, where ω_M, ω_{0S} and ω_{0I} are, respectively, the microwave, and the EPR and NMR frequencies [71]. The SE arises from a single electron-nuclear interaction, and the DNP and electron-nuclear double resonance transitions excited by the microwave field (indicated as dashed arrows in figure 2.13(a)) are partially allowed due to the mixing of states $|1>$ and $|3>$ and the mixing of states $|2>$ and $|4>$ by terms in the electron-nuclear dipole Hamiltonian of the form $S_z I_{\pm}$. Note that double-quantum (flip-flip) and zero-quantum (flip-flop) transitions occur between states $|1>$ and $|4>$, and $|2>$ and $|3>$. Applying first order perturbation theory leads to a mixing coefficient that governs the probabilities of the above transitions and is proportional to ω_{0I}^{-2}. Therefore, the efficiency of the SE scales with ω_{0I}^{-2} , where ω_{0I} is the nuclear Larmor frequency.

The cross effect is the dominant continuous wave mechanism (cw) at high magnetic field and can be used to understand the improved DNP enhancements observed using biradical polarizing agents [71]. The CE is a three spin process which involves a nuclear spin and two dipolar coupled electrons with EPR frequencies ω_{0S1} (electro spin 1) and ω_{0S2} (electron spin 2) that satisfy the following relation.

$$\omega_{0S2} - \omega_{0S1} = \omega_{0I} \tag{2.39}$$

CE is operative when the polarizing agent has an inhomogeneous broadened EPR spectrum whose breadth Δ is larger than the nuclear Larmor frequency ω_{0I} and concurrently the homogeneous line-width delta remains small ($\delta < \omega_{0I} < \Delta$). This latter condition implies the use of biradicals as polarizing agents where the presence of dipolar coupling between the two electrons improves DNP efficiency [56]. Two dipole coupled electrons, separated by $\omega_{0I}/2\pi$ in the EPR spectrum,execute a three-spin electron-electron-nucleus process involving the mutual flip of an electron and a second electron separated by $\omega_{0I}/2\pi$ and a nuclear spin. The energy difference matches the nuclear Larmor frequency and results in nuclear spin flips that generate the enhanced nuclear polarization[73].

As mentioned earlier, in the case of the CE, there are two participating electrons S_1 and S_2 and a single nuclear spin I. As it is shown in figure 2.13(b), there are eight energy levels to consider. Microwave transitions occur between the levels connected with the dashed lines and result from the mixing of states $|2>$ and $|7>$, or the mixing of states $|3>$ and $|6>$ if $\gamma_I < 0$. The mixing results from electron-electron and electron-nuclear interactions and becomes important when the degeneracy is provided by the frequency matching condition $|\omega_{0S1} - \omega_{0S2}| = \omega_{0I}$.

The frequency matching mentioned here implies electron-electron dipole couplings (approximately 25 MHz) that are smaller than the EPR frequency separation arising from inhomogeneous interactions such as g- and hyperfine anisotropies ($\geq$ 600 MHz at 5 T). However, stronger electron-electron interactions are possible and lead to a different regime of frequency matching, in which the dipolar or hyperfine couplings approximate ω_{0I}[71].

In contrast the thermal mixing polarizing mechanism involves a homogeneously broadened EPR line arising from multiple dipolar coupled electrons. Here the condition $\omega_{0I} < \delta_{min}$ is satisfied when the concentration of polarizing agents is high. This multiple electron spin bath that can be viewed as an extension of the energy conserving three-spin system. For the case of non equilibrium polarization among electrons the following relaxation mode occurs: An allowed electron electron mutual spin flip accompanied by a nuclear spin flip. This leads to the generation of enhanced nuclear polarization. Wind et al [76] have established the following relationship:

$$\varepsilon \propto \frac{\gamma_e}{\gamma_n} \frac{N_e^2}{\delta^2} \frac{B_{1e}^2}{B_0} T_{1n} T_{1e} \tag{2.40}$$

Here B_{1e} is the microwave field strength, B_0 is the static magnetic field strength, N_e is the concentration of electrons, δ is the homogeneous EPR linewidth, and T_{1n} and T_{1e} are the nuclear and electron spin-lattice relaxation times.

TM shares many features with the CE but is due to the coupling of multiple, rather than two, electrons in the paramagnetic center. Weak couplings among those electrons produce the manifolds of states illustrated in 2.13(c). Similar to the frequency matching condition in the CE, the energy overlap between manifolds is required for maximizing the probabilities of electron-nuclear transitions[71].

2.19 DNP hardware and applications

High field DNP was developed in MIT by Robert Griffin and coworkers in the nineties. The 263 GHz spectrometer enables extended DNP solid-state NMR experiments. In parallel, dissolution DNP was pioneered by Jan H. Ardenkjaer-Larsen et al in 2003. They have reported an increase of more than 10 000 in the signal-to-noise ratio in liquid-state NMR. This method can be used generally for signal enhancement and reduction of measurement time in NMR and opens up for a variety of in vitro and in vivo applications of DNP-enhanced NMR[72].

A Solid State DNP NMR spectrometer consists of a 263 GHz gyrotron coupled to a 400 MHz NMR magnet through a corrugated microwaveguide. As the NMR magnet has been previously described, the gyrotron and the waveguide are depicted in this section.

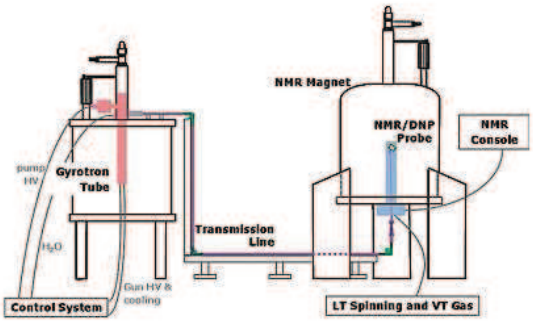

Figure 2.14: Solid State DNP NMR spectrometer consisting of a 263 GHz gyrotron and a 400 MHz NMR magnet. The gyrotron generates microwaves which are then guided through a transmission line to the DNP NMR probe

High power (10 W) high frequency (140-600 GHz) microwave sources such as gyrotrons are needed to drive the continuous-wave (CW) DNP transitions associated with the second-order electron-nuclear dipolar interactions [73].

The 263 GHz gyrotron design is shown in figure 2.14. Gyrotrons are cyclotron resonance masers and a special form of vacuum electronic device (VED) relying on the interaction between an electron beam and a resonant cavity condition to generate microwaves. A gyrotron is composed of the following basic components. First, an electron gun contains a cathode and heater for electron emission. The electron beam is initially accelerated when a high voltage (cathode voltage) is applied across the cathode to ground or an anode. A magnetic field further accelerates and focuses the electron beam through the electron tube. The electron beam energy is then converted into radiation in the interaction cavity. After the cavity, the electron beam continues to the collector and the microwave beam exits the gyrotron through an output window. Gyrotron cavities are cylindrical and can be overmoded. Therefore, the cavity dimensions are not limited by the wavelength and gyrotrons can produce high output power even at frequencies above 30 GHz. Output powers of 20W to 90 W and efficiencies up to 10 % were measured for beam currents from 25 mA to 75 mA. [70].

Low loss microwaveguide transmission lines such as corrugated waveguide are crucial for an efficient delivery of the microwave irradiation. Compared to standard

rectangular waveguides, they have almost negligible ohmic losses: for example, a 250 GHz DNP spectrometer has an overall loss 0.7 dB [56].

In this context a 263 GHz transmission line is utilized. The microwave beam is directed from the gyrotron to the DNP NMR probe into a 19.3 mm inner diameter corrugated transmission line. The distance between the two magnet bores is 2.9 meters. The transmission line is precision machined in 25 cm long aluminium segments that are joined together by coupling clamps and held on an extruded aluminum support rail. Individual corrugations are cut with a period of 1/3 wavelength and 1/4 wavelength depth and length (figure 2.15). The microwave beam travels across the gyrotron magnet top plate, down to a horizontal support rail, across to the NMR magnet, and up to the NMR probe base. At the probe base, the transmission line is coupled to the 7.6 mm probe waveguide. The latter is machined from phosphor bronze and helically tapped. In the case of the static DNP probe, a straight waveguide that will irradiate the sample efficiently is needed. The NMR coil is spaced out for improved microwave penetration. Compared to a regular NMR coil, a 25-30 % increase in DNP efficiency is observed with the wider coil spacings [70].

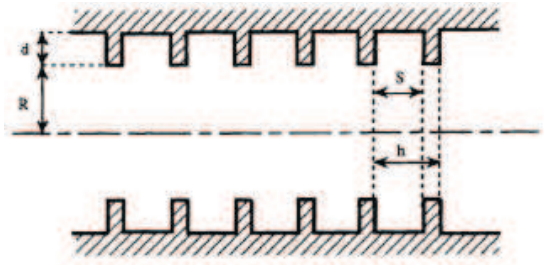

Figure 2.15: Corrugated waveguide. Individual corrugations are cut into the inner surface of the waveguide with a period of 1/3 wavelength and 1/4 wavelength. d and S are the depth the width of the groove respectively. R is the inner radius of the waveguide. h is the period of corrugation. Taken from Rosay et al 2010.

Figure 2.16: Photograph of the Bruker Biospin 263 GHz gyrotron showing from left to right: microwave transmission line, gyrotron magnet with tube installed, gyrotron control system console, and two chiller units. Taken from Rosay et al 2010

Experimentally, significant signal enhancements are acquired (currently in the range of 50 to 300) . Many biological systems are being investigated including membranes and membrane proteins, amyloid fibrils, nanocrystals, phage particles, and more recently chemical systems such as quadrupolar nuclei and surface catalysis [71]. DNP can reduce the experiment time from 3.5 days to 45 minutes.

DNP efficiency depends on the magnetic field, temperature and microwave power [70]. Spin lattice relaxation processes compete with DNP mechanisms and compromise the polarization transfer efficiency [75] That is why DNP experiments are conducted at low temperature (4 to 100 K). At low temperature the spin lattice relaxation times are longer and the spin diffusion is better [71]. Therefore, the lower the temperature the better the enhancement factor cf. figure 2.17.

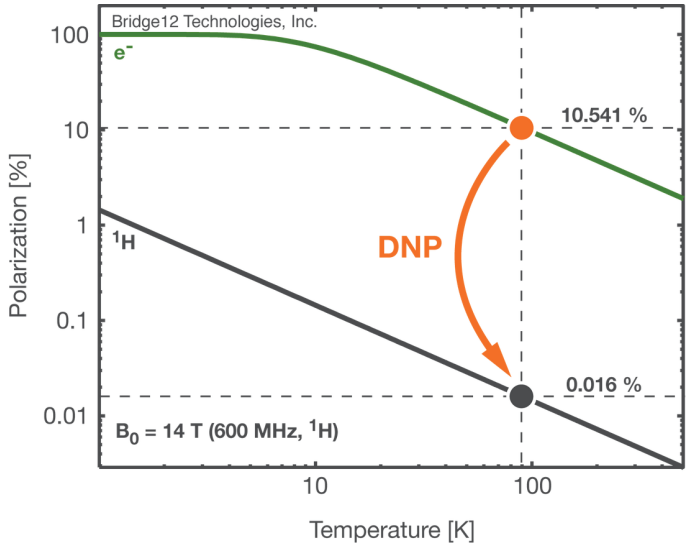

Figure 2.17: Simulation of the temperature dependence of the electron and proton spin polarization between 1 and 450 K. Taken from Bridge 12 Technologies Inc. website

Polarizing agents can be endogenous (stable radical present in a protein) or exogenous paramagnetic system (a mono or a bi radical or metal ion added to the system (TOTAPOL, btbk)

TEMPO is a nitroxide based radical which facilitates the TM polarization at sufficiently high concentrations. It has an electron-electron dipolar coupling of 0.3 MHz in a 10 mM solution.

Biradicals improve the DNP enhancements by a factor of 3 to 4. The large electron-electron dipolar coupling in these molecules (approximately 20-30 MHz in the case of the biradicals TOTAPOL and bTbk) facilitates the cross effect CE polarization mechanism.

TOTAPOL i.e. 1-(TEMPO-4-oxy)-3-(TEMPO-4-amino)-propan-2-ol formed by two TEMPO molecules tethered by a short molecular linker induces the CE mechanism. It is soluble in glycerol/water solutions and is currently the polarizing agent of choice for experiments involving proteins [56].

Chapter 3

Probe design, construction and test

The used DNP spectrometer consists of a 400 MHz NMR spectrometer and a 263 GHz gyrotron coupled to each-other by a corrugated microwave guide. For DNP experiments the DNP probe head is linked to a cooling unit that cools down the probe and sample to temperatures as low as 95 K.

A probe head refers to the mechanical piece that holds the sample in the magnetic center of the NMR magnet. It is a tunable antenna that irradiates and detects the rf fields used in NMR. The centerpiece of the probe is the solenoidal or saddle coil surrounding the sample. Together with a tuning capacitor and sometimes a transmission line, this coil forms an LC oscillator that is matched to the impedance of the transmitter and receiver network via additional inductive or capacitive elements.

The frequency of the LC oscillator, in radians per second is given approximately by:

$$\omega = \frac{1}{\sqrt{LC_T}} \tag{3.1}$$

The coil has two functions: First, during the rf pulse, electrical currents in the coil generate an oscillating magnetic field in the sample area. Second, when the rf pulse stops, the precessing nuclear magnetization generates electrical currents in the coil that give rise to a detectable NMR signal (electromotive force caused by Faraday induction) traveling back down the cable again to be analyzed [43].

Generally speaking, the rf portion of the probe includes two rf observe channels X and Y (^{31}P and ^{15}N) optimized for highest signal to noise ratio and a less efficient rf channel for heteronuclear decoupling (^{1}H). In the case of inverse probes and most MAS probes, especially the double coil design that was used for some of the experiments, the proton channel is the most efficient channel.

Several controls are added to the sample environment such as temperature and orientation detectors. Variable temperature VT control is achieved with heaters in the gas transfer line and thermocouple for the feedback.

Cryoprobes employ cooling of the electronic circuits (not the sample) to cryogenic temperatures (typically around 20 K) in order to improve the signal detection efficiency[43]. In the DNP NMR probe both the sample and the electronics are cooled down to 100 K. When the probe circuit is cooled, the conductivity is increased and subsequently the quality factor Q becomes higher. Furthermore the noise generated in the probe is slightly reduced. As mentioned above, the reason for the necessity of cooling the sample is the relaxation time of the electron spins that is too short at room temperature and transfer of polarization needs time preferably. Another advantage of low temperature is the temperature dependence of the Boltzmann factor.

Construction of an NMR probe with high sensitivity, high resolution, large spectral bandwidth, low background signals and a wide VT range requires competence in material sciences, physics, electrical engineering and mechanical engineering.

3.1 Basic Electronics

An electric resonator stores electric and magnetic energy. In a perfect resonator, the energy is stored consecutively in the magnetic and electric field. The oscillation frequency of this phenomenon is given by the capacitance and inductance. Many types of resonators exist including LC resonators, cavity resonators and transmission lines [78].
In a narrow frequency range, the performance of a real (lossy) resonator is described by a lumped RLC circuit.

In electronics, the lumped element model assumes that the attributes of the circuit, resistance, capacitance, inductance, are concentrated into idealized electrical components; resistors with a resistance R that sums all the circuit losses, capacitors, and inductors, etc. connected through perfectly conducting wires.

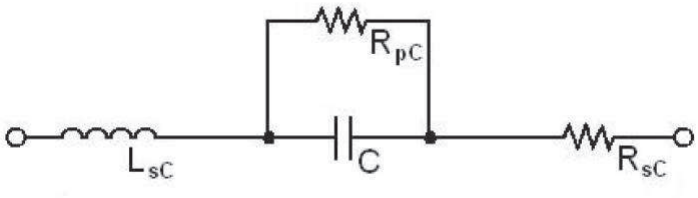

Figure 3.1: First order equivalent circuit for a capacitor taking into account the inductance due to the leads and the geometry of the capacitor plates and the resistances due to conductive and dielectric losses. $R_{pC}$is the parallel equivalent resistance. R_{sC} is the serial resistance. L_{sc} is the serial inductance

Actually components exhibit non-ideal characteristics that are taken into account with an equivalent circuit. For example, a first-order approximation of a non-ideal capacitor consists of a capacitor in parallel to a resistance (representing dielectric losses) and a resistance and inductance in series. In fact the leakage is distributed throughout the dielectric. The inductance is caused by the capacitor leads and the geometry of the capacitor plates. Similarly, the resistance takes into account the conductivity of the leads.

Here is an exemplary electronic circuit of a probe head tuned to three resonances. It is the same as for the corresponding commercial MAS probe except for the coil geometry. It has several components:

- The NMR coil L1
- H tuning and matching capacitors C1 and C2
- A coaxial line COAX (also referred to as lambda half line)
- A proton stop circuit LC1
- A X stop circuit LC2
- The X and Y tuning capacitors C4 and C5
- The X and Y matching inductances L 2 and L3

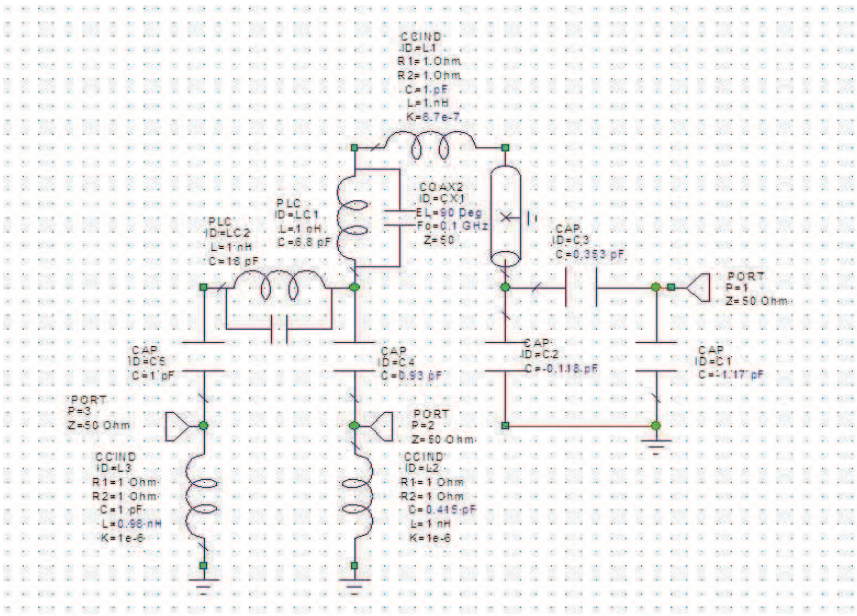

Figure 3.2: ^{1}H/X/Y resonance electronic rf circuit used for the DNP probe with a single coil. The proton channel contains two capacitors C1 and C2. The tuning capacitor is linked to a coaxial line COAX . C 3 represents the capacitors C1 and C2 coupling to C1 and transmission line. The X channel consists of a tuning capacitor C4 and a matching inductances L 2. The Y channel consists of a tuning capacitor C5 and a matching inductances L 3. The X channel is isolated from the proton channel with a proton stop LC1. The Y channel is equally isolated from the X channel with a X stop LC2. P1 is the port for ^{1}H, P2 for X and P3 for Y.

For efficient coupling to the transmitter and preamplifier, the probes channels (resonant circuits), transmission line, the preamplifier and the transmitters must all be matched to the same impedance of 50 Ohms (international standard). Following that a high power test is necessary to check if the probe can handle the rf power without arcing. A first testing of the probe was done in the application department in Bruker Rheinstetten.

3.2 Probe assembly

Probe design and construction demands basics in 3D modeling and mechanics. Designing is a wonderful tool and a basic asset in today's product development. Solid edge, the CAD software developed by Siemens was used to model practically every probe part, print drawings and modify the design of existing parts.

The MAS solid state NMR probe model was already finalized by Bruker engineers. The sample rotating system on the top plate was removed and the tube that crosses the probe's frame was enlarged. As for probe assembly, it is a common technical process that requires some soldering skills, fastening and wiring know-how.

A DNP probehead consists of electrical components (capacitors and coils) structured in a probe frame, and additional vespel (high-performance polyimide-based plastics manufactured by DuPont) part is essential to isolate the probe top from the probe base. The probe base must be heated to avoid icing while the upper part must be kept at 100 K with an ITL fed with cold nitrogen from a heat exchanger. Therefore, several qualities are essential for delivering high quality results: Good thermal isolation, good soldering, accurate placement of probe parts and good grounding.

Here is a step by step description of probe assembly:

- Bore hole widening from 6 mm to 7,1 mm at the workshop in order to accommodate the new insert device.
- Frame soldering: Soldering the frame plates to the ITL internal transfer line tube and the sample insert pipe line. This was done in the Bruker workshop in Rheinstetten using an existing gauge from the production department. The plates and the pipe lines have to be soldered at a fixed length . The overall frame length is nearly the same as for the MAS probe ,i.e., 395 mm.
- the logistics department have sent the frame to be coated in an external workshop in Pforzheim. The coating consisted of 20 μm of Cu and 2-3 μm of CuSnZn
- Groundings soldering: first the groundings have to be cut to the exact perimeter of the plates. Then some soldering is put on the frame and the groundings. Then they are soldered together by heating up the soldering in between. This was done in the workshop with a special soldering tip. One has to be careful that no soldering gets in between the groundings. The groundings have a special direction with the tip pointing to the inside of the probe. (The smoother part to the exterior)

- Soldering the tube for the thermocouple: first, the nut is soldered to the ITL tube with the big soldering cartridge. Then the nut is soldered to the tube with the smaller cartridge. Because the hole for the thermocouple in the vespel part doesn't point exactly in the direction of the tube. The tube must be fixed at a higher level than the bottom plate.

- Fastening the heating foil to the foot-case. There is a cutout in the fixing metal plate where the wire for the heating resistance fits.

- Fastening the vespel plate to the frame with the 6 radial screws. One has to turn the screws from the bottom while fixing the nod from the top in a special position where they fit with the Teflon ring. This can be done with pliers that have an angled pointed tip.

- Fastening the vespel plate to the foot case with the four rectangular holes on the outside. A ring is added in the bore hole that is previewed for this screw so that it doesn't surpass the upper surface of the foot case.

- Fastening the X and Y tuning capacitors. First, the capacitors are fastened to the lower plastic part. Then they are fixed to the upper plastic part. Then that assembly is screwed to the last upper plates. There is a third part that should be screwed to the intermediate bottom plate in order to guide the tuning rods . Once the probe is ready a stop circuit is fixed on top of the assembly. It must be tuned to 100 MHz (96 MHz before the final tuning of the probe) in order to stop the Carbon frequency.

- Fastening the cold gases exhaust tube to the vespel part.

- Fixing the fastening for the waveguide on the ITL tube. Or to preview enough space to do this.

- Fixing the lambda half line to the proton tuning capacitor.

- Cutting the matching and tuning rods to the wanted length and cutting a hole so that they fit the little rod on the bottom capacitor. This rod is cut to the wanted length and pinned to the sleave on the bottom of the cap.

- Fitting the rods with the vespel part in the bottom of the probe

- Wiring the heaters

- Wiring the coaxial lines from the bottom case to the tuning X and Y tuning rings plus the matching coils on one hand and the proton capacitor on the other hand. Before soldering the coaxial wire, it has to be cut to the wanted length

(test before cutting) remove the plastic part at the end plus the shielding. This must be done properly. But in any case the wires have to be handled carefully. An extra length has to be kept in case something goes wrong.

Afterwards, the flat coil was wound and adapted. The coil has two leads soldered to a ring that can be easily mounted to the existing part (top of the lambda half line and the proton stop circuit cf figure 3.3). The coil leads length and bending should be adjusted so that it occupies the Magnetic center.

If the phosphorous or carbon stop circuits are not needed, in a double mode, the proton stop circuit is mounted on an adapter part that has approximately the same length as the X stop circuit. It consists of a 6.8 pF in parallel with a three turns coil. The resonance frequency of a stop circuit is measured by a pick up coil. Stop circuits are used so that no signal from one channel can get to the other.

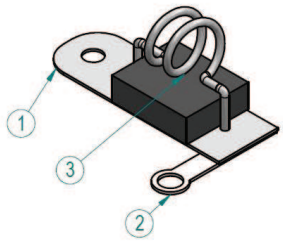

Figure 3.3: Proton stop circuit consisting of a capacitor with a coil. Usually the resonance frequency of this circuit must be tuned to the proton frequency

N.B. The closer the coil is positioned relative to the capacitor in the stop circuit the more the resonance frequency increases ($\omega_R = 400$ MHz). The final adjustments can be done by reducing or increasing the coil's pitch. In this case the tuning of the proton channel didn't work with a stop circuit tuned exactly to 400 MHz but to 402 MHz. This is regularly observed for 400 MHz probes.

First, the proton channel is in a lambda half mode. Then, a grounding clamp is fastened in order to get into the $\lambda/4$ mode. Theoretically the $\lambda/4$ clamp should be put in the cold point where the resonance frequency of the proton channel is not affected. However this view doesn't take into consideration the sensitivity of the proton channel which should be optimized. In fact there is an ultimate position around 400 MHz (plus or minus 3 MHz) for which the sensitivity is maximum. Afterwards the proton stop circuit can be adjusted to match the 400 MHz in the $\lambda/4$ mode. Moreover the lower electrode of the proton tuning capacitor moves which changes the overall length of the transmission line changing with that the position of the cold point.

For the sake of having a broader tuning range and a better sensitivity, the probe circuit was continuously improved . Especially with the saddle coil. In order to reach the ^{15}N resonant frequency, the capacitance of the channel's tuning capacitor had to be increased by putting a 30 pF capacitor in parallel.The value is found experimentally. The circuit comports a shortened lambda half line (approximately 202 mm long). Finally, the parallel capacitance was kept low (i.e. 30 pF) in order to have a wider ^{15}N tuning range in all cases.

Once the probe electronic components are mounted the channels' resonant frequencies have to be tested. This sort of preliminary test is called a bench test.

3.3 Bench test

The NMR probes are designed to resonate at nuclei's Larmor frequency so that the signal they send and receive is maximized at their spin frequency. Tuning and matching the probe to that resonance frequency is an essential part of the bench test. A bench test consists of finding the right resonance frequency of a certain circuit with a network analyzer, as well as the isolation between channels.

The probe circuit has been designed to be a triple MAS probe with an NMR coil of 3.2 mm diameter made of compensated wire. Plus it is made for standard nuclei ^{1}H/^{13}C/^{15}N. So it is not a plug and play system. But it has to be carefully adjusted to the new coil.

As there are two operating modes: $\lambda/2$ (without a grounding clamp at the cold point) and $\lambda/4$ (with grounding clamp on the cold point of the $\lambda/2$ line) the bench tests have to be repeated two times. With and without the grounding clamp. The nitrogen frequency is only reached in the $\lambda/4$ mode. Since this nuclei is the most important in peptide study, the probe was kept in the $\lambda/4$ mode.

First of all, one has to check if all the connections are well made. For every nuclei, the S parameters are measured. They give direct access to the tuning range i.e. frequency interval where the probehead can be tuned and matched efficiently, the quality factor and the ball shift. The product of these two last quantities is the sensitivity (Bruker definition). Old measurements are available for commercial 400 MHz probes, so that the obtained values can be verified. Before giving the results, transmission line theory is quickly overviewed.

When an electric signal propagates through media, a portion of it is reflected [80]. The reflected signal locates and measures discontinuities in a transmission line. In transmission line theory waves traveling from a source to a load have a voltage and a current that are dependent on the longitudinal coordinate (z) [78].

A transmission line is characterized with an impedance of Z_0. Z_0 is defined by

the incident voltage current ratio[78].The transmission line is terminated with a load of impedance Z_L. The normalized impedance is defined as $z = Z_L/Z_0$.

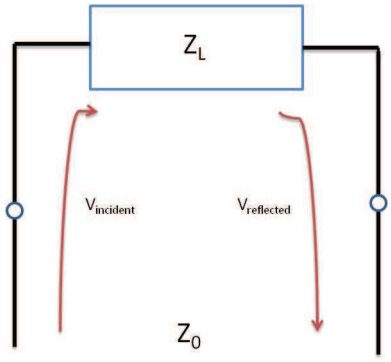

Figure 3.4: Reflection of the incident voltage by a load with an impedance Z_L

Therefore at every point along the transmission line there is a sum waves traveling forward and backward. The signal is reflected with a coefficient Γ. Γ is the ratio between the reflected and the incident voltage

$$\Gamma = \frac{V_{reflected}}{V_{incident}} \tag{3.2}$$

The smith chart, invented by Phillip H. Smith, is graphical chart used for representing complex impedances and scattering parameters. Each point on the Smith chart represents simultaneously both a value of z (bottom left), and the corresponding value of Γ (bottom right), related by

$$Z = \frac{1+\Gamma}{1-\Gamma} \tag{3.3}$$

An impedance Smith chart for channel is used for channel matching. When z = 1 then the impedance is matched.

The scattering parameters are defined in terms of wave amplitude. They relate the amplitudes of the waves pointing inward and outwards.

The relationship between the scattering parameters is given by the scattering matrix S [77].

$\begin{pmatrix} B_1 \\ B_2 \end{pmatrix} = \begin{pmatrix} S_{11} & S_{12} \\ S_{22} & S_{22} \end{pmatrix} \begin{pmatrix} A_1 \\ A_2 \end{pmatrix}$

When the incident and outwards waves are matched $A_2 = 0$

$$B_1 = S_{11}A_1 \; B_2 = S_{21}A_1 \tag{3.4}$$

In practice, scattering parameters can be assessed by a refractometer or a network analyzer [78]. 3 curves are assessed: S_{11} in a log Mag scale (tuning), S_{11} (matching) in a smith chart Z+Rj and S_{21} (to check stop circuits and isolation).

The quality factor can be given automatically by the network analyzer. On the other hand it is defined as follow:

$$Q = \frac{f_L}{f_2 - f_1} \tag{3.5}$$

Where f_L is the resonating frequency. f_2 is the right resonance at -3 dB and f_1 the left resonance at -3 dB

The ball shift method is a perturbative measurement technique that uses a test body cavity perturbation to the field of the cavity in order to determine the rf magnetic field distribution in NMR probes.

This measurement of the perturbation caused by a metallic body was introduced by Slater et al in 1952. In the presence of an electric field, the dielectric body diverts the field lines and reduces the inductance of the coil (figure 3.5 on page 56)

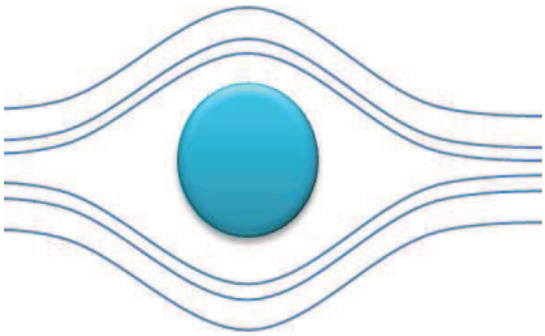

Figure 3.5: Field distortion from a metal sphere placed parallel to the electric lines of force. The arrows represent the field lines.

The frequency shift depends on the local electric and magnetic field at the position of the object. When the perturbing sphere is placed parallel to the electric lines of force the difference between the perturbed frequency and the unperturbed frequency is given by:

$$\frac{f_0^2 - f_p^2}{f_0^2} = -2\pi B_0^2 r_0^3 \tag{3.6}$$

f_0 is the unperturbed resonance frequency , f_p the perturbed frequency

r_0 is the sphere radius

The application of the perturbation formula to a metallic sphere in the magnetic field gives the following formula for the B_1 field:

$$\mathrm{B}_1 \propto \sqrt{\frac{f_0}{f_0+\Delta f}} \quad (3.7)$$

Δf is the ball shift i.e. the resonance frequency difference due to the presence of the metal sphere[26].
In practice, for evaluating the ball shift, the resonance frequencies of the NMR coil is measured with an teflon filled 3,2 mm zirconia rotor and the same rotor with a brass sphere, which dimensions (2 mm) are small compared to the wavelength [79], centered inside to avoid inaccurate frequency shifts due to the presence of the MAS rotor.

$$\Delta f = f_p - f_0 \quad (3.8)$$

f_p center frequency with a metallic ball held in the center of the rotor and f_0 is the center frequency with a Teflon filled rotor

Moreover, the channels' isolation S_{12} is determined in decibels. It is the power transmission from port 1 to 2.

Since the stop circuit had to be detuned from 400 MHz in order to be able to tune the proton channel to its resonance frequency this stop circuit cannot isolate properly the X and Y channels. Therefore a trap circuit is soldered to the X and Y channels to the coaxial line and then to grounding. This trap circuit consists of a coil or simply a wire in series with the capacitor. The thinner the wire is, the more its inductance. The wire length as well as its bending radius have to be optimized in order to have the maximum isolation. On the phosphorous channel a 25 mm bent wire of 1 mm was soldered in series with a 6.7 pF capacitor. For the isolation on the nitrogen 15 channel a 22 mm long wire of 0.7 mm diameter was soldered in series with a 6.7 pF capacitor. Since there is not much space available and components mustn't touch each other, one has to be particularly careful and adroit to insert these short circuits.

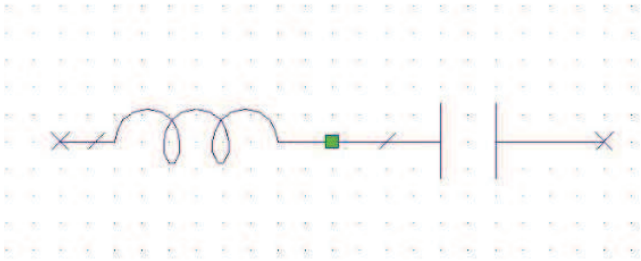

Figure 3.6: Trap circuit consisting of a coil in series with the capacitor to isolate the X and Y channels

The position where the coil or simply a wire is soldered to the capacitor affects the isolation as well as the bending of this trap circuit.

Finally, parallel matching is utilized to reduce the resistance of the circuit. It had to be used on the ^{15}N channel to increase its quality factor. The inductance of the circuit is dominated by the NMR coil.

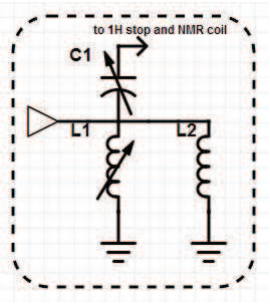

Figure 3.7: Parallel matching to reduce the resistance of the circuit and increase its quality factor

When a 8 turns, 0.7 mm and 3.2 mm diameter coil is inserted in parallel, the quality factor is increased .

Now that the theory was discussed, the bench test results are shown. These measurements were done using a E5061/62A ENA series rf network analyzer from Agilent technologies. As previously mentioned, when a channel is tuned and matched(proton, nitrogen or phosphorous) the logarithmic magnitude of S_{11} is measured in decibels with respect to the resonating frequency. The frequency is read by a trigger. It is 400 MHz for the ^{1}H. The channel matching is verified on the impedance smith chart and the isolation between channels S_{21} measured in decibels. The minimum isolation to avoid any signal to get from one channel to the other is -20 dB. In figures 3.8 3.9 and 3.10 the triple channel bench test is shown.

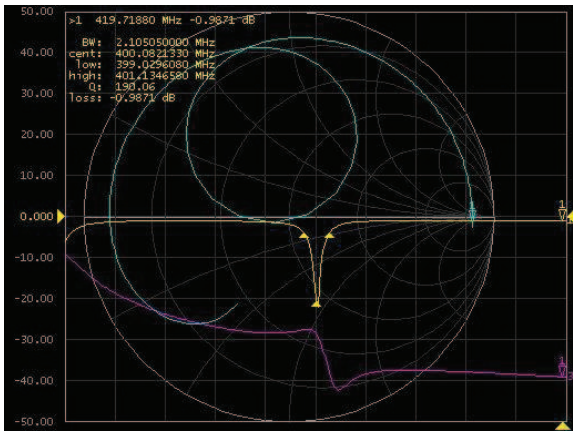

Figure 3.8: Proton channel: In yellow, the proton frequency tuning using the logarithmic magnitude of S_{11} in decibels, in blue: the proton frequency matching is verified and in violet: the channels' isolation S_{12} in decibels.

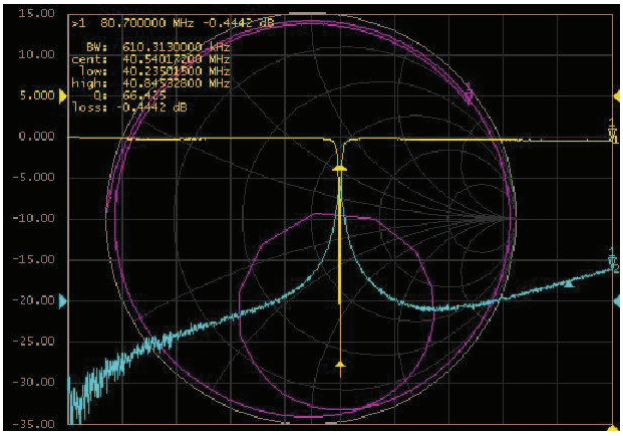

Figure 3.9: Nitrogen channel: In yellow, the nitrogen frequency tuning using the logarithmic magnitude of S_{11} in decibels, in blue: the nitrogen frequency matching is verified and in violet: the channels' isolation S_{12} in decibels.

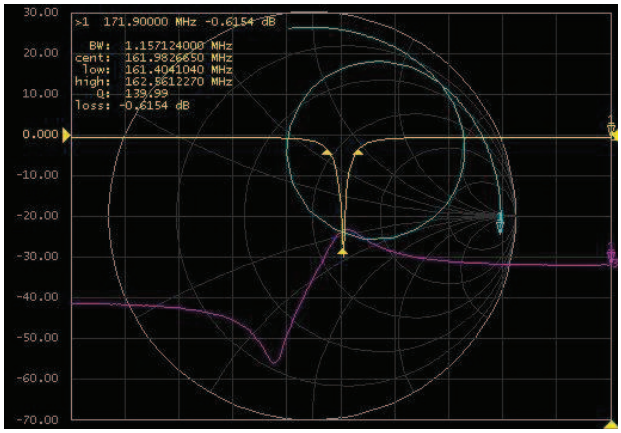

Figure 3.10: Phosphorous channel: In yellow, the phosphorous frequency tuning using the logarithmic magnitude of S_{11} in decibels, in blue: the phosphorous frequency matching is verified and in violet: the channels' isolation S_{12} in decibels.

The following results shown in table 3.1 where obtained in a double mode probe with a 3.7 mm x 3.7 mm cross section flat coil with a length of 11.6 mm and a saddle coil with a 8.8 mm x 4.6 mm x 4.6 mm window with 3 turns.
The sample consists of fully ^{15}N labeled ammonium chloride from the laboratory in Strasbourg. Here are the dimensions of the coils, the results of the bench test as well as the signal to noise obtained at the spectrometer at the end of this section. The ball shift was measured in two different manners due to the difference coil dimensions, therefore the comparison cannot be based on the respective values.

	Solenoidal Flat coil (3,7*3,7mm² cross section 11,6 mm lenght)		Saddle coil(3 turns and a 8,8*4,6*4,5 mm3 window)	
	1H Channel	15N Channel (Cp =27pF)	1H Channel	15N Channel (Cp = 30,7pF)
f_L(MHz)	399,5	37,7	396	38,9
f_H (MHz)	441	42	442	44,7
HX isolation (dB)	-20	-50	-20	-50
S/N (CP experiment)		1672		538
Q	196	65	294	95
Ball shift	1,7 MHz (measured with a 3,2 mm rotor)	1 MHz (measured with a 3,2 mm rotor)	4,1 MHz (measured with empty and silver piece)	2,9MHz (measured with empty and silver piece)

Table 3.1: Comparison of the flat and the saddle coil performances. The tuning range in MHz, the isolation in dB: The isolation between the H and X circuits at the proton frequency is -20 dB , the signal to noise, the quality factor and the ball shift in MHz are shown

3.4 High power test

Power tests are conducted with a high power transmitter using a power meter in order to verify how much power the circuit can withstand without arcing. Wobble curves are measured on every channel, to tune it and match it properly. Otherwise the reflection curve won't be optimal (too much reflected signal). Afterwards a high power pulse is sent into the tested channel (H/F, X1 or X2).
An increasing power is applied up to several hundreds Watts for every channel . The pulse width is set to 5000 μs and the pulse interval to 500 ms (always a factor of 10 between these two quantities). The pulse number can vary (10-100). A value of 10 is usually used for the first power application then 100 for the highest applied power. To make sure the channel withstands hight power for a long time. An Anritsu ML2437A power meter is utilized. It is monitored by a high power test software: HPPH test.

If the probe can't handle the power, it can be identified in the reflected power

that increases stepwise. An arcing sound can also be heard. Sharp edges in the circuit can usually cause arcing in a probe. However, a more serious cause is the Teflon itself because it is a very sensitive dielectric. In addition to this any dirt, including particles of metal (from the scratching of the shield) cause arcing. The arcing occurs at high power, typically 200 W. However these high power levels are necessary for attaining the 50 kHz B_1 on low sensitivity channels (X and Y).

In this case the capacitor arced at 300W on the phosphorous tuning capacitor. The damaged material was removed from the middle of the capacitor. In addition to that, the proton stop circuit position close to the coil of the phosphorous stop circuit was also problematic. Once the edges were rounded and the stop circuit was moved further away from the coil everything went fine.

3.5 Probe modes change

The probe is designed to operate in a triple mode with a proton channel, phosphorous on the X channel and nitrogen on the Y channel. The ^{13}C can also be tuned on the X channel. Any of these 3 nuclei can be measured in a double mode. By connecting the right electronic components (capacitors, coil).
In a triple mode the convenient stop circuit has to be inserted between the X and Y tuning capacitor. A phosphorous stop (161.9 MHz) circuit in the case of ^{1}H/^{31}P/^{15}N mode and a carbon stop (100.6 MHz) in the ^{1}H/^{13}C/^{15}N mode.

It is only possible to reach the nitrogen frequency in a $\lambda/4$ mode (with a clamp). As it was already shown, the Y channel capacitor operates for a capacitance ranging from 2 to 12 pF. In order to reach the nitrogen 15 frequency a capacitor is soldered to the Y tuning capacitor.

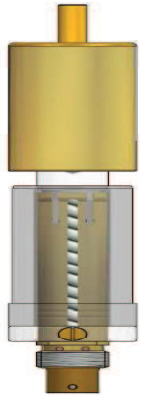

Figure 3.11: Teflon capacitor ranging from 2 to 12 pF

Its capacitance depends on the probe configuration:

- Double mode 27 pF
- Triple mode with ^{13}C 22 pF
- Triple mode with ^{31}P 75 pF

It is typical of this channel to have a small tuning range due to the adding of this capacitor. For instance currently (with $^{15}NH_4Cl$ sample in) the probe can be tuned from 39.4 MHz to 41.7 MHz.

Finally, in a $\lambda/4$ mode with a 68 pF capacitor in series with the X tuning capacitor,the ^{13}C frequency can be reached.

It is easier to reach the phosphorous resonance frequency in a $\lambda/2$ mode. However the nitrogen frequency must be reached in the same probe configuration. Therefore a capacitor C_2 is added in series with the X tuning capacitor C_1. If the two capacitors are put in series the allover capacitance C_{total} diminishes:

$$\frac{1}{C_{total}} = \frac{1}{C_1} + \frac{1}{C_2} \tag{3.9}$$

So in this case, a fixed capacitor is put in serial with the variable 2-12 pF capacitor. When the fixed capacitance decreases and the resonance frequency increases. This is meant to be because the circuit is designed to resonate at 100 MHz (^{13}C). The capacitance choice is made by building in several capacitors at different values and seeing how they affect the channel's resonance frequency. A 27 pF capacitor was

utilized(with the saddle coil). The carbon frequency can still be reached if the range coil is removed. This series capacitor has to be associated with the usual range coil that is used to reach that frequency and they both have to be optimized in order to have the maximum sensitivity.
By putting a grounded range coil on top of the stop circuit, in parallel to the NMR coil the resonance frequency increases consequently (see figure 3.12). In this circuit the same current I will flow through the range coil instead of through the NMR coil where it could contribute to the desired B_1 field. At a given frequency a reduced inductance yields a lower resistance and a higher current I_r this means that I_{NMR} will get smaller. The number of windings and coil diameter and wire diameter should be optimized. A 7 windings coil of 6 mm with a 1 mm wire was utilized.

In order to reach phosphorous in a double mode the clamp has to be removed and a range coil with more than 10 turns has to be soldered.

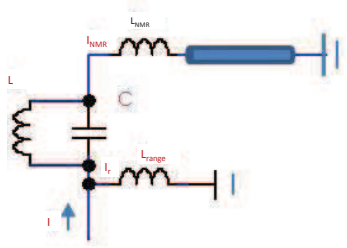

Figure 3.12: A grounded range coil on top of the stop circuit, in parallel to the NMR coil increases the X channel resonance frequency The circuit is considered at the X frequency. The LC in parallel is the proton stop circuit, it lets the X current through. The range coil is short circuited. L_{range} and L_{NMR} are in parallel and give a smaller inductance

3.6 Spectrometer test

Now that the probe head was ready, its NMR efficiency had to be verified. In the following sections probe optimization for peptide study is presented in details, In the beginning of this project the main concern was to find the coil configuration that suits the sample insertion of the sample. The use of a saddle coil was advocated because it was directly accessible from the bottom. In a first series of tests, a 3 turns saddle coil with a 1 mm wire and an 11 turns solenoidal flat coil with a 0.7 mm wire are tested. These combinations permit the use of similar inductance for both types of coils. The same amount of ammonium chloride powder was used to make an accurate comparison between both types of coils. The NMR performances of these

two coils were tested and compared. However their sample volume is relatively small so they can only accommodate flexible samples like ammonium chloride in an adapted plastic bag or oriented samples on high density polyethylene.

More extensive studies allow the determination of the B_1 field intensity and homogeneity in the flat coil. To further evaluate accurately the probe performances the DNP probe with a square flat coil a comparative study with the e-free probe was accomplished. A test PISEMA experiment was conducted on Ac-Leu. To accommodate better the inner coil volume to the glass plates sample a 7 mm x 3 mm rectangular flat coil was wound. AWR microwaves simulations revealed B_1 field inhomogeneity in this type of coil. To remedy this problem, a double coil with two independent circuits for protons and nitrogen was designed. The field homogeneity was simulated. A simulation including the glass plates was realized and test results were compared.

Unless mentioned otherwise all the test in this chapter were conducted at room temperature.

A 90 ° pulse duration of 5 μs is used in order to determine the radio frequency power to field conversion of the circuit. This is achieved experimentally by varying the pulse width p1 in order to determine the 180° pulse width (and therefore the 90° pulse width). The increment is determined by a first parameter optimization experiment with a few number of scans (power of 2 i.e. 2, 4, 8 etc) in order to have an idea of the sought value. Once an approximate value of p1 is found (corresponding to a 90° pulse) the increment can be calculated in order to obtain a peak every 10 °. An actual optimization experiment popt inquires these values: parameter choice p1, a start value, an end value and an increment. A good nutation experiment which is a result of these parameters optimization inquires the 90° pulse duration of the decoupling pulse to be calculated. This is done prior to the hpdec (c.f. section 2.14) sequence by calibrating the proton peak with a simple 90° pulse "one pulse" sequence. The nitrogen 90° pulse is optimized to 5 μs as well.

$$RF(kHz) = \frac{1000}{4p_{90}}$$

(3.10)

p_{90} is in μs.

In the same manner the homogeneity of the rf field inside the NMR coil is obtained. While the homogeneity of the B_0 field is maintained by the probe shimming, the homogeneity of the B_1 field over the active volume of the rf coil should also be considered for multiplepulse experiments. Ideally, each individual nuclear

spin should be affected equally by the rf pulse. To measure the rf homogeneity the intensity of the signals after 90°, 450° and 810° pulses has to be compared. In addition to that, the field to power efficiency conversion can be calculated:

$\eta_P = \frac{B_1}{\sqrt{Pl}}$(3.11)

B_1 is in kHz. Pl is the power level in Watts.

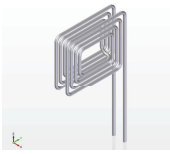

3.7 Saddle coil

The saddle coil has 4 windings, a quality factor Q of 262 on the proton channel and a Q of 97 on the nitrogen channel.

In the case of the saddle coil, the 90° pulse was more difficult to reach using the hpdec pulse sequence. Indeed the ^{1}H tuning capacitor has been damaged and values bigger than 300 W couldn't be attained on the proton channel. During the power test arcing occurred when 485 W were applied on the ^{15}N channel, so that was a limit to respect as well.The proton 90°pulse of a duration of 5 microseconds was reached when applying a power level of 270 W. However a pulse duration of 5.5 microseconds was only attained with a 480 W power level on the ^{15}N channel. The resulting peak has a width at half maximum of 241 Hz or 5.9 ppm and the S/N is 38 (c.f. figure 3.13).

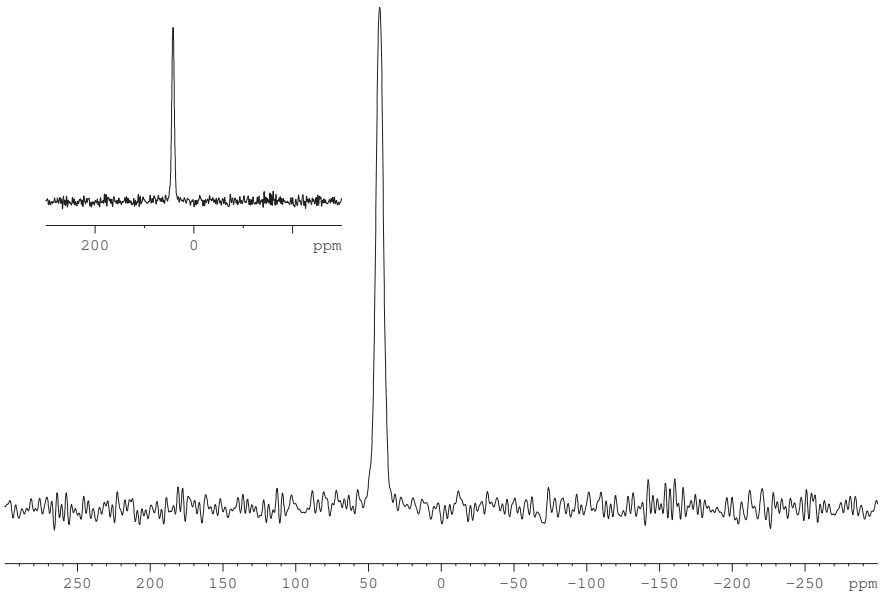

Figure 3.13: ^{15}N hpdec spectrum of 0.1 mg of $^{15}NH_4Cl$ powder in a plastic bag using a saddle coil at room temperature. The acquisition time is 0.01 s, the pulse length is 6.5 μs, decoupling proton power is 270 W. The signal to noise is 38 after 1 scan.

Furthermore, the obtained signal can still be enhanced with this coil type by applying a CP pulse sequence. A 125 W pulse is needed to reach the 5 microseconds peak. The peak width at half maximum is 240 Hz. The signal to noise calculated by the sinocal function (topspin) is 538. This means that this coil type can be used for signal acquisition (c.f. figure 3.14)

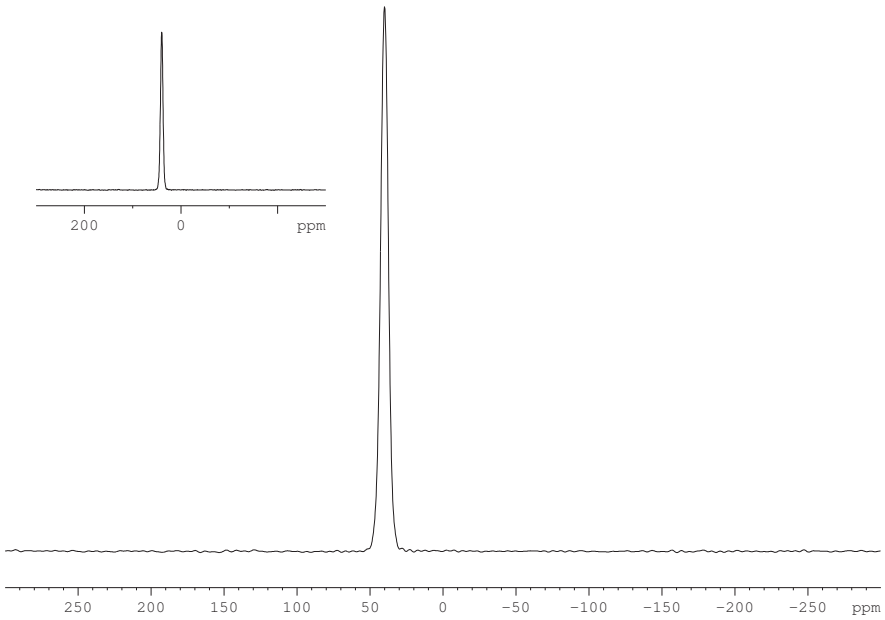

Figure 3.14: ^{15}N proton decoupled CP spectrum of 0.1 mg of $^{15}NH_4Cl$ powder in a plastic bag using the saddle coil (recycle delay 3 seconds) at room temperature. The acquisition time is 0.005 s, the pulse length is 5 μs, contact time 2840 μs, nitrogen power level 125 W, decoupling proton power is 270 W, the number of scans 6. Signal to noise is 538

In the following step, the nutation curve is analyzed. The signal drops to 42 % at 450° and 28 % at 810°. This indicates an inhomogeneous distribution of the B_1 field for this type of coil configuration.

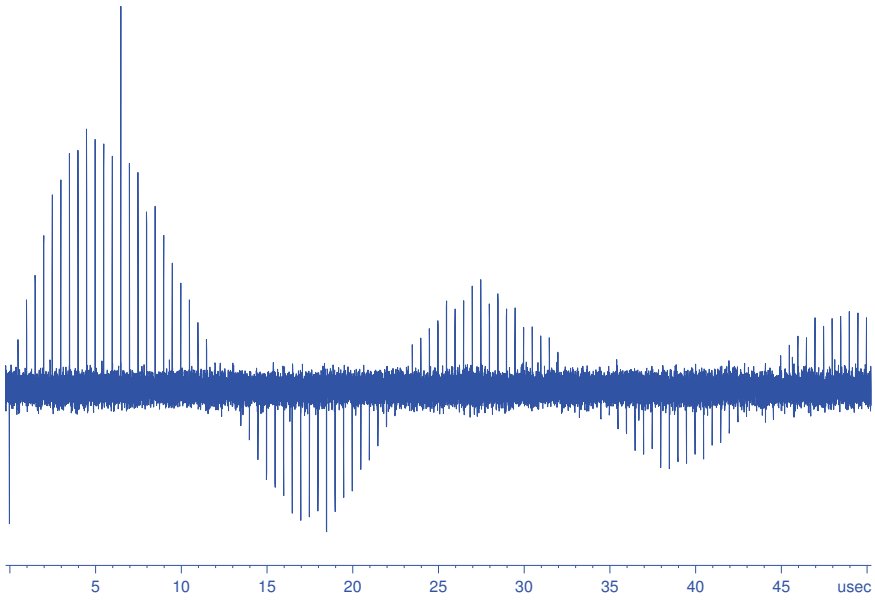

Figure 3.15: Nutation curve to test the saddle coil field homogeneity. The signal drops to 42% at 450° and 28% at 810°

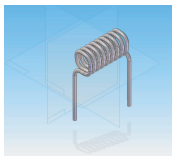

3.8 Flat coil

4x4 mm^2

The same sort of tests were conducted with the flat coil. The solenoidal flat coil has a length of l = 10.6 mm a cross section of 3 x 3 mm^2. It has 8 turns.

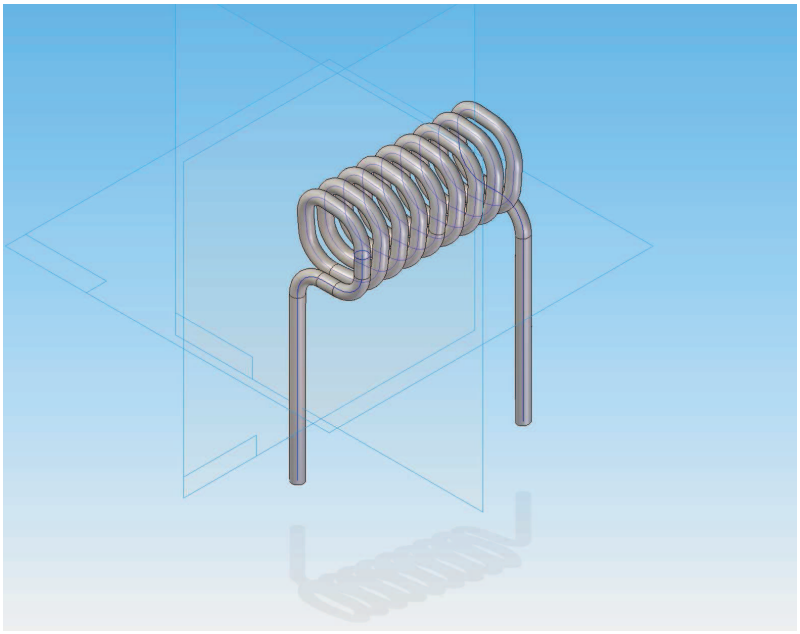

Figure 3.16: Flat square coil 3D design in Solid edge

$$L(nH) = \frac{21.8n^2D(cm)}{1 + 2.2\frac{l}{D}} \tag{3.12}$$

This formula is to estimate the inductance of a round solenoid. Therefore to find out the inductance of the square coil with a side "a" it has to be compared to a round coil with the same area (radius r and diameter D) [78].

$$\pi r^2 = a^2 = 9 \Rightarrow r = 1.7 \tag{3.13}$$

Therefore when D has a value of 3.4 cm then L, i.e., 60 nH.

The quality factors Q of the proton and the X channels (Nitrogen) are 257 and 61 respectively. A 50 kHz pulse has to be insured on the nitrogen channel which is the less sensitive.

In general, the hpdec pulse sequence is used in order to determine the 90° peak. The proton decoupling power of 30 Watts was obtained after a parameter optimization with a simple "one pulse" pulse sequence. The ^{15}N pulse duration of 5 μs is obtained after a nutation curve see figure 3.19 . The pulse power level is adjusted such as there is no peak at 10 μs (nuclear spins parallel to the B_0 field). A value of

165 Watts was determined. The resulting peak has a peak width at half maximum of 242 Hz (i.e. 5.9 ppm) and a signal to noise of 168 after one scan.

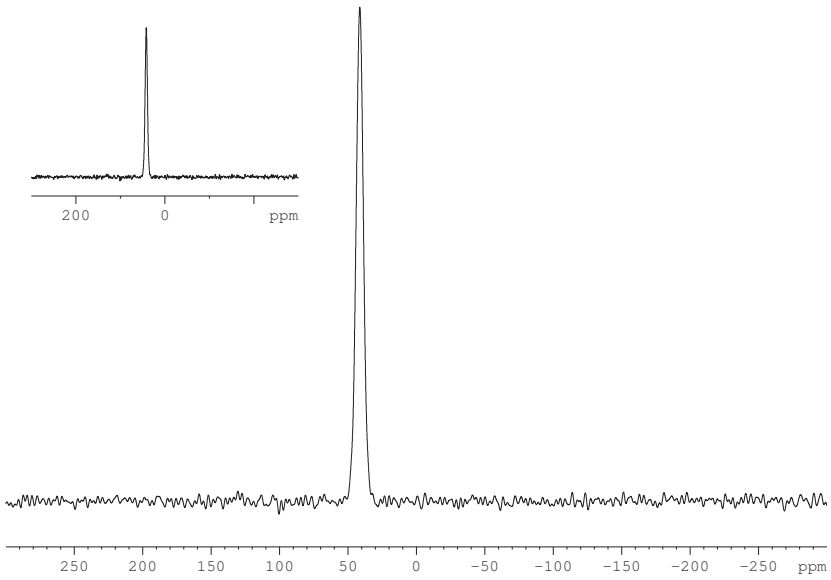

Figure 3.17: ^{15}N High power decoupling spectrum of 0.1 mg of ammonium chloride powder in a plastic bag at room temperature. The acquisition time is 0.01 s. The pulse duration is 4 μs. The signal to noise is 168 after 1 scan, the power level is 165 W, the decoupling power 30 W

The CP pulse sequence is usually used for protein structure determination. It has the effect of increasing the signal by a factor of 9.97 approximately equal to the γ_H/γ_{15N} ratio, in the case where the proton and nitrogen spins are in contact (where γ is the gyromagnetic ratio). To obtain a better signal several parameters are optimized: the nitrogen channel power level ,i.e., 230 W, contact time ,i.e., 2600 microseconds etc. The signal to noise is significantly higher i.e. 1672 and the peak width at half maximum is 221 Hz or 5.4 ppm (c.f. figure 3.18 on page 72).

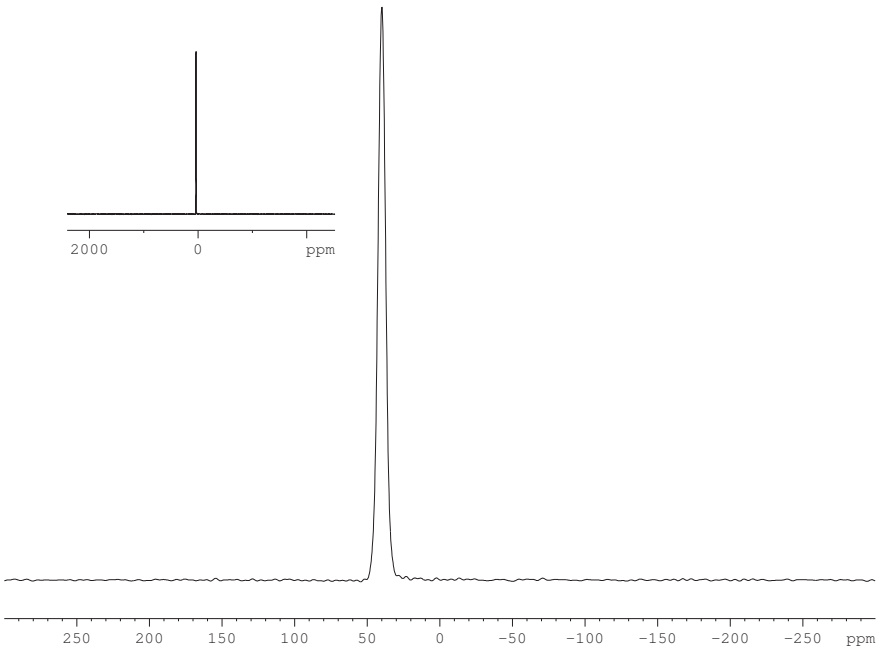

Figure 3.18: Room temperature ^{15}N proton decoupled CP spectrum of 0.1 mg of ammonium chloride powder in a plastic bag after one scan (3 seconds of recycle delay). The acquisition time is 0.005 seconds. The pulse length is 5 μs. The power level on the nitrogen channel is 230 W, the contact time is 2840 mus, the decoupling power on the proton channel is 30 W. Signal to noise ,i.e., 1670 after 1 scan and a peak width of 5.4 ppm

Moreover, the nutation curve gives information about the electromagnetic field homogeneity inside the coil. A decrease to 70 % was assessed in the measured signal at 450° followed by a decrease to 44 % at 810°. These are standard values in comparison with the literature.

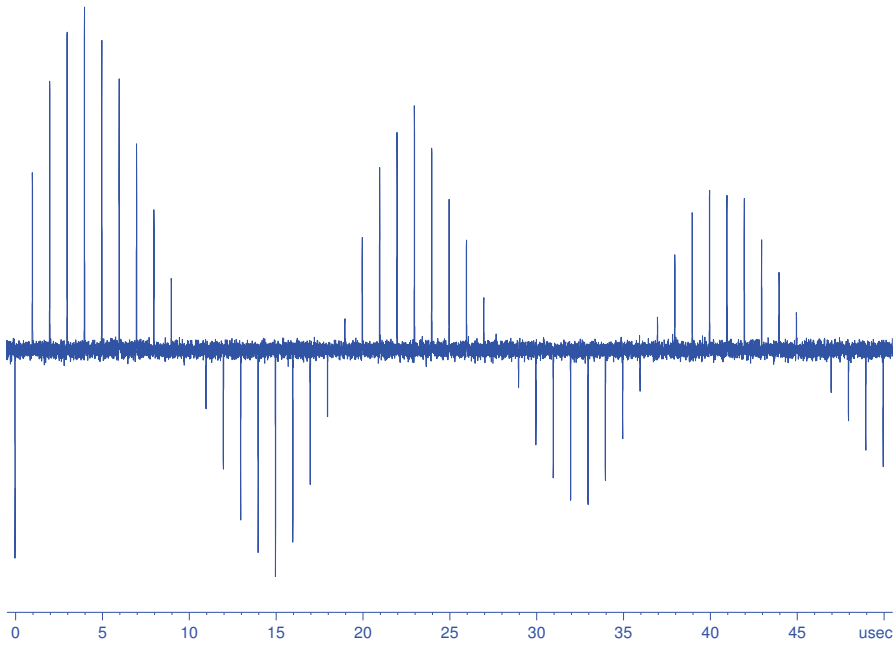

Figure 3.19: Nutation curve for $^{15}NH_4Cl$ to test field homogeneity 70% at 450° and 44% at 810°. The 90° degree pulse is at 5 μs

Finally, this is a recapitulating table of all the values mentioned above (c.f. table 3.2).

	Flat solenoidal coil	Saddle coil
hpdec	Plw1 = 165 W P = 5 µs Plw12 = 30 W	480 W 5,5 µs 270 W
Peak width at half maximum	242 Hz	241Hz
S/N	168	38
homogeneity	At 450° = 70% At 810° = 44 %	42 % 28%
CP	Plw1 = 230 W	150 W
S/N	1672	538

Table 3.2: Spectrometer test for the flat and saddle coils. hpdec power level in W, peak width in Hz, signal to noise, B_1 field homogeneity, CP ^{15}N power level and CP signal to noise

3.9 Comparison between the DNP probe and the e-free probe

The overall performance (S/N and B_1 field homogeneity) of the DNP static probe with a 4 x 4 mm^2 single coil and the e-free probe were compared . The power levels are reported in table 3.3 in dB. It is necessary to reach B_1 field values of 60 and 62.5 KHz in order to perform high resolution PISEMA experiments. These experiments were done by Christopher Aisenbrey using the 400 MHz spectrometer in Strasbourg.

	DNP probe	e-free probe
Coil	4x4 mm^2	4x8 mm^2
NH4Cl ^{1}H 62.5 kHz	6.4 dB	4.5 dB
AcLeu ^{1}H 62.5 kHz	4 dB	"
Rk1/POPC ^{1}H 62.5 kHz	6 dB	"
NH4Cl ^{1}H 60 kHz eff	9.3 dB	7.9 dB
AcLeu ^{1}H 60 kHz eff	6.6 dB	"
Rk1/POPC ^{1}H 60 kHz eff	8.4 dB(estimated)	"
^{15}N 62.5 kHz	6.6 dB	4,5 dB
^{15}N 60 kHz	8.4 dB	5.6 dB

Table 3.3: Comparison of the overall performance of the DNP and the e-free probe. The proton power levels in dB necessary to reach a B_1 field of 60 and 62.5 KHz are reported for both probes

To better compare the two probe the following experiments have been realized:

- Standard CP experiment with ^{15}N labeled NH_4Cl For a B_1 field of 62.5 kHz a proton power level of 6.4 dB and a nitrogen power level of 6.6 dB were necessary. Compared to the e-free biope probe (62.5kHz: ^{1}H - 4.5dB ^{15}N - 4.5 dB) it is about 2 dB smaller. The signal of the DNP probe is about double the signal of the e-free probe. The coil of the e-free probe has about double the size of the coil of the DNP probe.

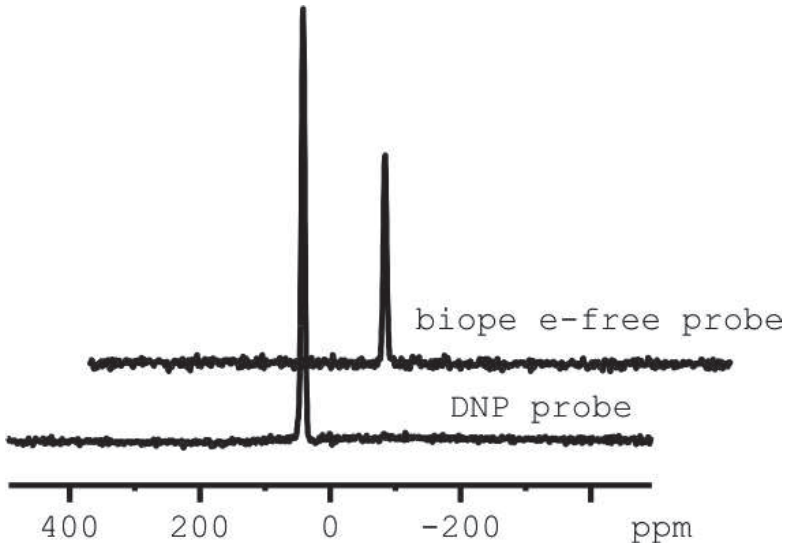

Figure 3.20: Comparison of the DNP probe with the e-free probe. Standard CP experiment on the same NH_4Cl sample using B_1 fields of 63.5 kHz for both. The coil of the e-free probe is about double the size of the coil of the DNP probe.

- ^{1}H nutation experiment

  The ^{1}H nutation experiment consists of a proton nutation pulse off-resonance followed by a regular CP. Ideally the offset of the proton nutation pulse is chosen to obtain the Lee Golburg condition ($i.e., offset = B_1^{eff} cos(57.4°) = B_1^{eff} * \frac{1}{\sqrt{3}}$). The B_1^{eff} can be directly measured. For a 60kHz a B_1^{eff} field of 9.3 dB was necessary on the DNP probe and 7.9 dB on the e-free probe. The widths of the nutation peaks are almost identical for both probes. Hence the ^{1}H B_1 field inhomogeneity is identical for both probes as well.

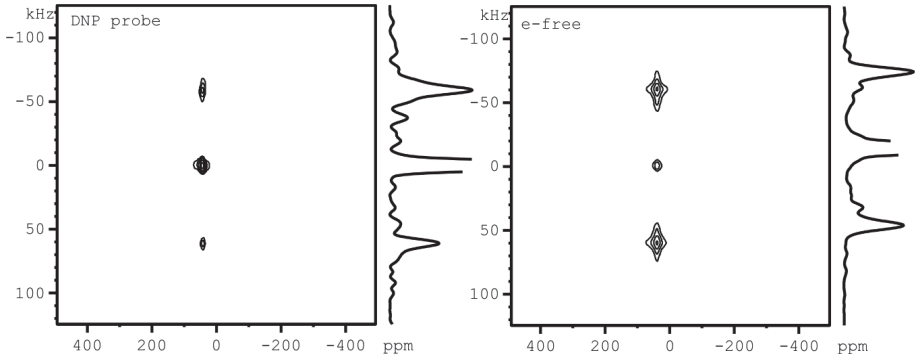

Figure 3.21: ^{1}H nutation experiment with ammonium chloride on the e-free probe and on the DNP probe. The power spectrum and a column are shown.

- ^{15}N nutation experiment

  The ^{15}N nutation experiment consists of a regular CP followed by a nutation pulse on ^{15}N. For a 60 kHz field a power of 7.8 dB was necessary on the DNP static probe and 5.6 dB on the e-free probe. The widths of the nutation peaks are almost identical for both probes. Hence the ^{15}N B_1 field inhomogeneity is identical for both probes.

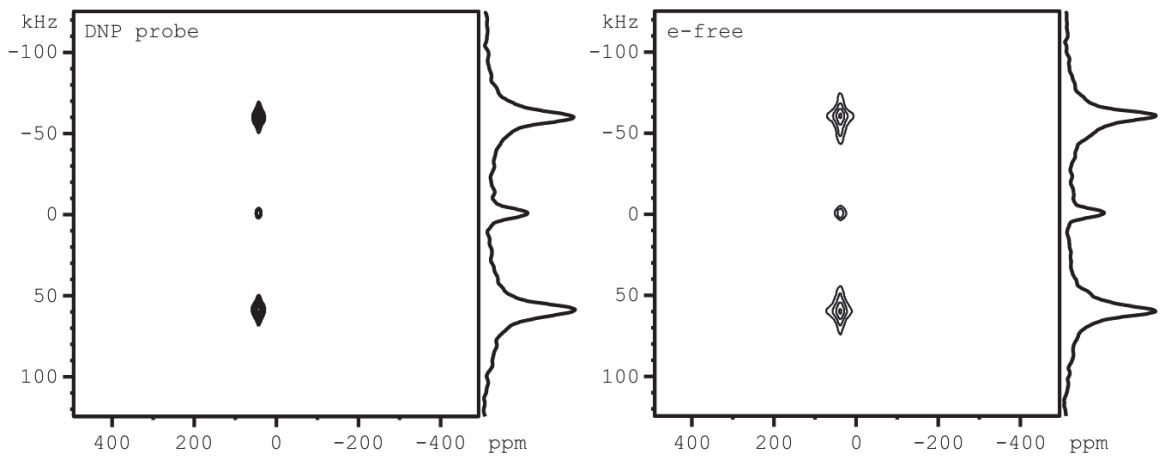

Figure 3.22: ^{15}N nutation experiment with ammonium chloride on the e-free probe and on the DNP probe. The magnitude spectrum and a column are shown

3.10 PISEMA on ^{15}N-AcLeu

For the e-free probe the power levels of NH_4Cl can be used for the measurements of AcLeu. For the DNP probe this was not the case. To maintain 63.5 kHz proton B_1 field a power level of only 4 dB (NH_4Cl 6.4 dB) was necessary. For a B_1^{eff} of 60 kHz a power of 6.6 dB (NH_4Cl 9.3 dB) was used.

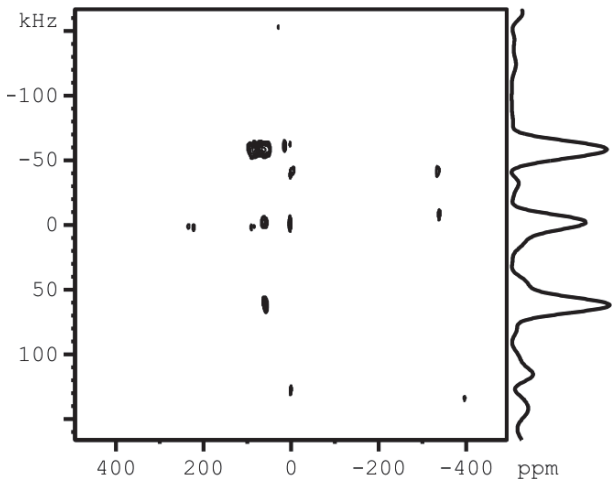

Figure 3.23: ^{1}H nutation experiment with ac-leu on the DNP probe. The power spectrum and a column are shown.

Once the right settings are found, the PISEMA spectrum of Ac-Leu on the DNP probe shows good results with correct splitting values. The sum in the CSA direction shows the correct powder spectrum and the sum in the dipolar splitting dimension shows a dipolar coupling powder pattern.

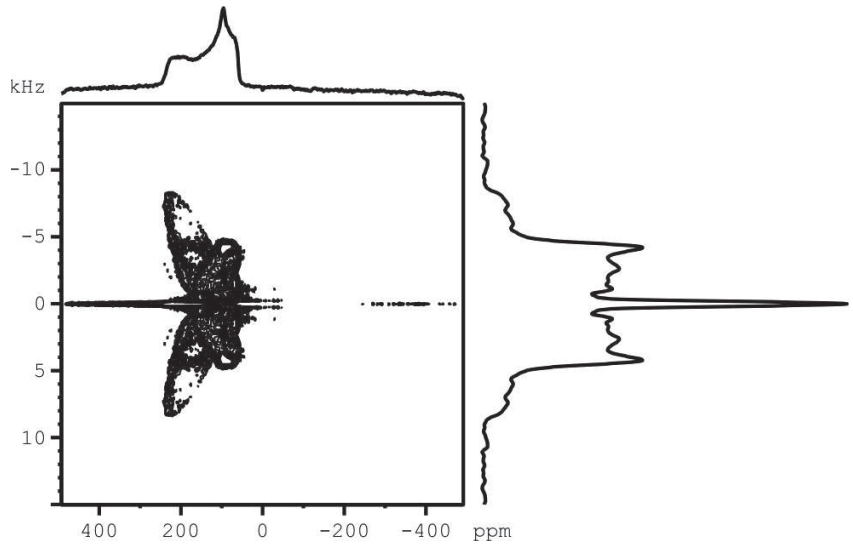

Figure 3.24: PISEMA experiment with ac-leu on the DNP probe made for experimental calibration and test. The 1D spectra are the sum in the two dimensions. The spectrum is not corrected with the scaling factor

3.11 Field simulation for the flat coil

The magnetic field that is generated by a flat coil can be simulated by calculating the value of the field in every point by iteration. This operation takes the whole night (Please see figure 3.25).

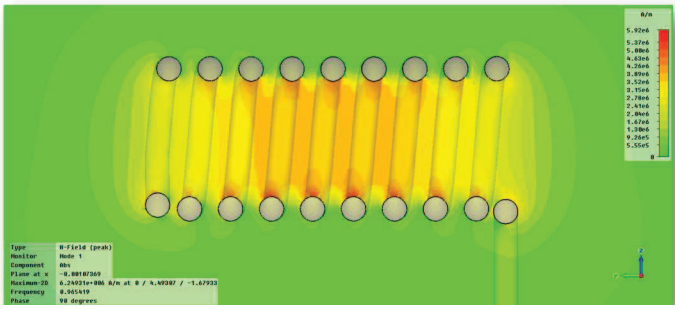

Figure 3.25: B_1 field simulation at 8.9 MHz by Alexander Krahn using CST in the active region of the flat coil with a 3 by 3 mm^2 cross section

Conversion i.e. 1.67 mT/A

This program provides another quality factor that is overestimated to 530 ($\pm$10)

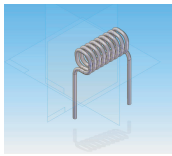

3.12 A 7 mm x 3 mm flat coil for the study of oriented membranes between glass plates

7x3mm^2

Now that probe construction and test was presented, a step by step practical procedure that lead into polypeptides topology determination is reported. The topology of a membrane polypeptide is a description and listing of the segments of the polypeptide chain that form the transmembrane helices and their orientation relative to the membrane [86].

First, the degree of alignment of bilayers can be checked by ^{31}P NMR of the lipid head groups. Note, that addition of salt as well as high bound peptide / protein content can disturb the formation of oriented bilayers [63].

Second, the magnetic spin interactions can be measured: dipolar coupling and chemical shift anisotropy that depend on the sample's orientation. These results are interpreted in terms of inter-atomic distances and Ramachandran angles values [40]. For more details please refer to section 2.13

The results discussed here were obtained with a 3 mm x 7 mm x 11 mm NMR coil. The NMR coil was changed simply because the square flat coil couldn't accommodate the 6 mm x 11 mm glass plate stack. This is true for all the upcoming sections until mentioned otherwise.

In figure 3.26 a proton-decoupled ^{31}P NMR spectrum of a sample of oriented lipid bilayer between glass plates containing a fraction of unoriented bilayers is shown, the bilayer normal is oriented parallel to the static magnetic field B_0.

The contribution of the spectrum at -19 ppm is related to the ratio of unoriented lipids with a bilayer normal perpendicular to the magnetic field and the shoulder at 28 ppm is due to the contribution of the oriented lipids with a bilayer normal parallel to the magnetic field .

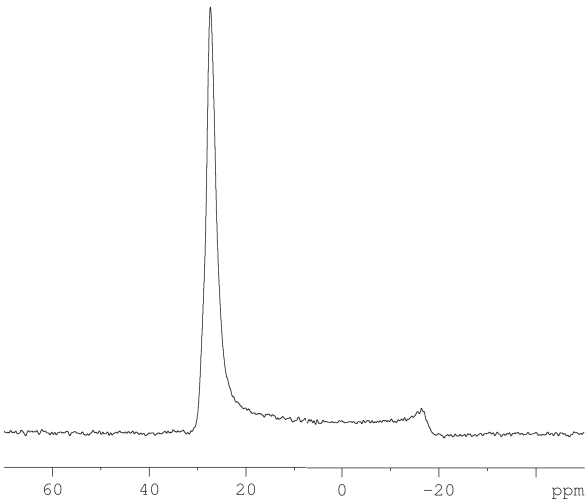

Figure 3.26: ^{31}P POPC spectrum using a Hahn echo experiment. 52 mg of POPC were spread on 15 glass plates at room temperature. The acquisition time is 0.01 s, the first pulse length is 2.5 μs, the second pulse length is 5 μs, phosphorous power level is 7 dB, the proton power is 120 dB, the number of scans 128. The contribution of the spectrum at -19 ppm is related to the ratio of unoriented lipids with a bilayer normal perpendicular to the magnetic field and the shoulder at 28 ppm is due to the contribution of the oriented lipids with a bilayer normal parallel to the magnetic field .

First ^{31}P spectra are shown.

First, a ^{31}P hpdec spectrum of 50mg of POPC is launched. That took 15 minutes (result not shown refer to figure 3.26). The peak at 30 ppm indicates that phosphatidylcholine molecules have their long axis oriented parallel to the magnetic field direction. A minor quantity of phospholipids are oriented perpendicularly to the magnetic field which explains the second peak at -15 ppm.

3.13 Sample support test

Several sample supports were tested for the optimization of DNP results. The sample support orientation and dielectric properties are very important for obtaining highly resolved single peaks and microwave transmission respectively. The sample support is first tested. Several materials are available. The ^{31}P Hahn echo spectra of POPC membranes oriented in between Polyether ether ketone (PEEK), Nylon and Polycarbonate sheets from Goodfellow are shown here. Their orientation properties are compared with those of glass plates of different thicknesses from Marienfeld. When considering the phosphorous spectra, it is clear that the glass plates have the best orientation properties then comes polycarbonate PEEK and finally the nylon. These results can be interpreted by looking at the peak on the right. Its presence indicates the existence of anisotropically oriented bilayers.

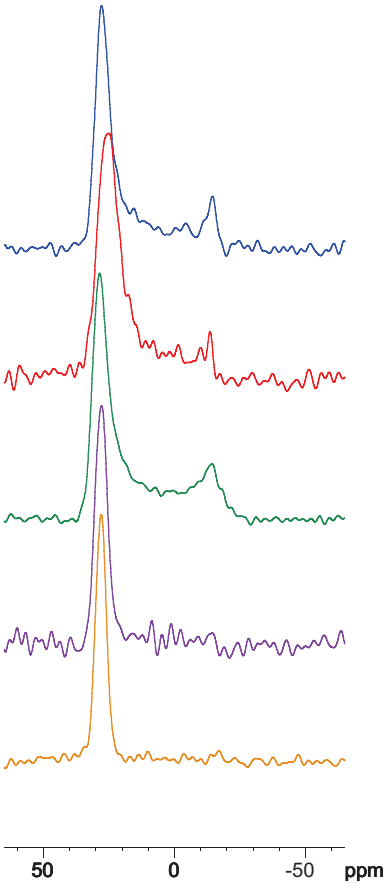

Figure 3.27: ^{31}P Hahn echo spectrum of POPC bilayers to test sample orientation. In orange POPC in between 0.08 mm glass plates, in violet 0.11 mm glass plates, 0.015 mm Nylon in green, 0.02 mm polycarbonate in red and 0.05 mm PEEK in blue

3.14 Polypeptide topology

The first polypeptide that was tested is surfactin. Surfactin is a cyclic lipopeptide from Bacillus subtilis. Its two negatively charged side chains form a polar head opposite to most hydrophobic side chains, accounting for its amphiphilic nature and its strong surfactant properties [90].

First, in order to determine polypeptide topology, the probe in a ^{1}H/^{15}N is used in double mode. The proton-decoupled cross-polarization spectrum of surfactin (7 residues) uniformly labeled with ^{15}N is obtained overnight and has several peaks. It usually indicates the value of the tilt angle of the protein with respect to the lipidic

membrane normal.

The nuclear interactions with the magnetic field are inherently anisotropic and, therefore, dependent on the orientation and conformation of the molecule with respect to the magnetic field direction [92]. This is reflected in the broad NMR line shape of membrane-bound peptides. Consequently signals that arise from different sites often remain unresolved (c.f. section 2.13).

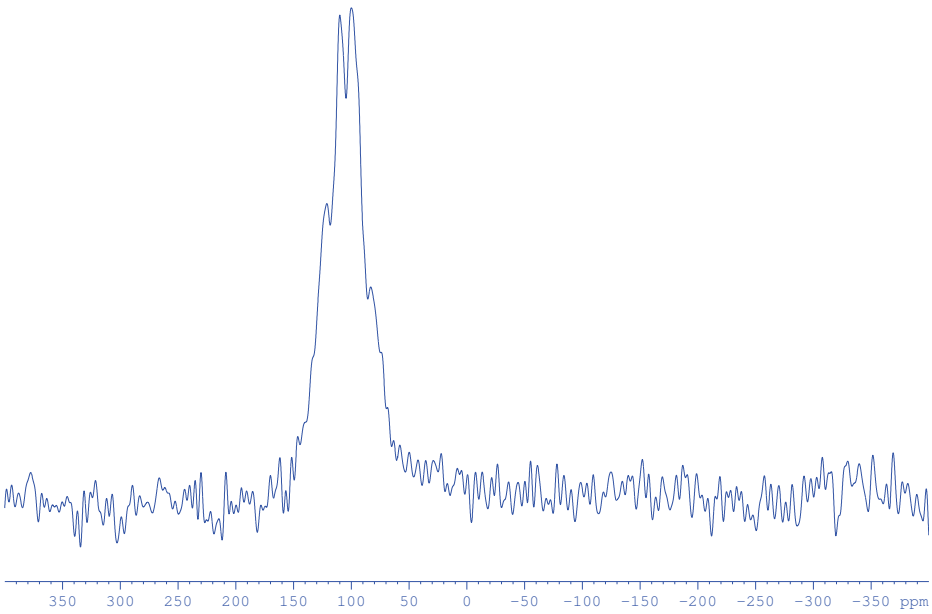

Figure 3.28: Proton-decoupled ^{15}N CP ssNMR spectrum of 1.3 mg of fully labeled surfactin at room temperature. The acquisition time is 0.006 s, the pulse length is 5 μs, contact time 800 μs, nitrogen power level 270 W, decoupling proton power is 200 W, the number of scans 19165. Signal to noise is 16. The nuclear interactions are anisotropic. Therefore the NMR line shape of membrane-bound peptides is broad and signals that arise from different sites often remain unresolved. The resonance peak at 100 ppm indicates that surfactin has an in-plane orientation

These were the first spectra obtained with the DNP solid state NMR probehead.

3.15 T_1 measurements

After the surfactin experiment, no routine hpdec or CP could be acquired at low temperature. First T_1 was first suspected to be too long at these experimental conditions. To begin with, several T_1 measurements were conducted at room temperature and then at low temperature. For measuring T_1, the inversion recovery method was first utilized. Then, the saturation recovery method will be discussed.

Ammonium is a highly symmetric. $^{15}NH_4Cl$ powder, it is utilized as a standard test sample. In the case where ammonium chloride powder is at room temperature a value of T_1 ,i.e., 0.36 seconds is obtained.

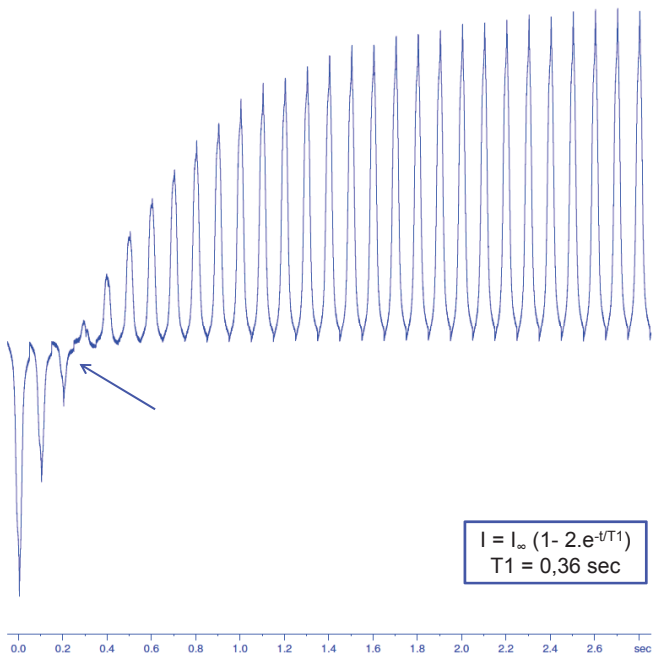

Figure 3.29: Proton T_1 of ammonium chloride at room temperature measured by inversion recovery. By fitting the peak intensity envelope curve to the function $I = I_\infty(1 - 2.e^{-t/T_1})$ a value of $T_1 = 0.36$ is found.

This value is confirmed by the T_1 value measured via CP by saturation recovery at room temperature i.e. 395 ms or 0.4 second cf. figure 3.30.

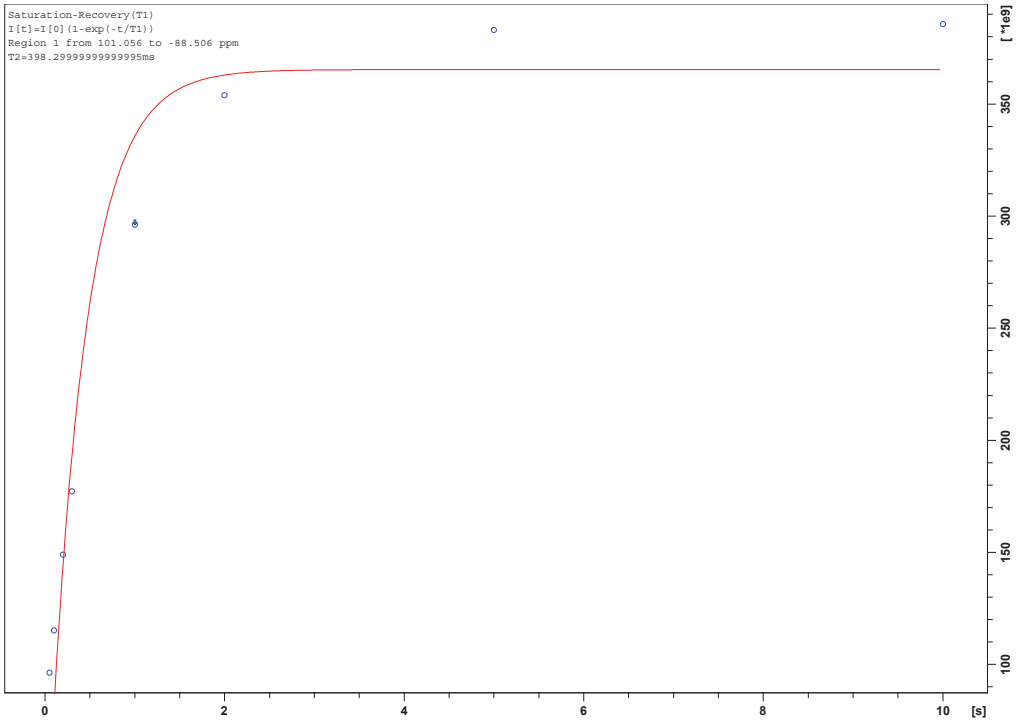

Figure 3.30: Ammonium chloride proton T_1 measurement via CP at room temperature using the saturation recovery. The automatic fit by topspin with the exponential function $I = I_0(1 - 2.e^{-t/T_1})$ gives a value of 0.4 s

For the low temperature measurement (100 K) the spins could not be flipped, i.e., no negative peak could be observed in the nutation curve and therefore the T_1 measurement was made impossible. Please refer to figure C1 in appendix C.

This can be due to the fact that T_1 is too long (in order of days cf. 3.31) [83] or that the B_1 is inhomogeneous or the ^1H peak too wide. Or it is maybe because the inversion recovery pulse sequence relies directly on the inversion of the spins.

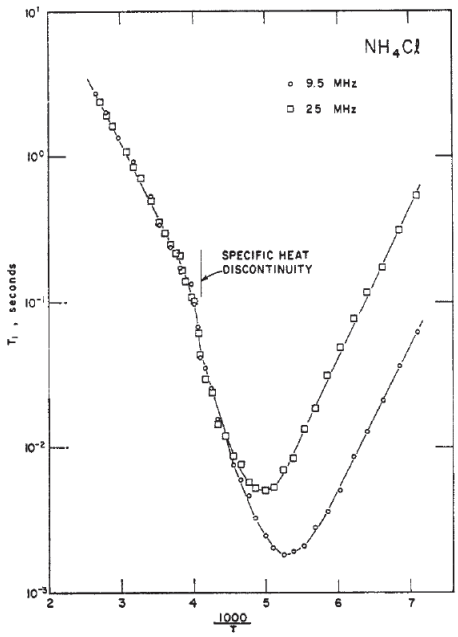

Figure 3.31: Temperature dependence of ^{1}H T_1 in ammonium chloride. The T_1 variation is measured in seconds with respect to the inverse of the temperature T multiplied by 1000. This figure is taken from Snowden et al (1966)

Being sure that ammonium chloride's T_1 is too long at low temperature, another type of sample with a hyperpolarizing agent had to be considered.

Hyperpolarized ammonium chloride has been proven to give good experimental results at low temperature by Hall et al in 1997 [94]. The same sample mixture of frozen glycerol-water solutions that was used for studying arginine and the protein T4 lysozyme by DNP enhanced solid-state magic-angle spinning nuclear magnetic resonance was prepared. Hall et al. obtained signal enhancements up to a factor of 50 in the ^{15}N spectra of the 18.7-kD protein T4-lysozyme, which correspond to a large decrease in signal averaging time or sample size requirements, or both [94]. In this case, 5 mg of ammonium chloride were added to a 60 μl solution of Glycerol-d8/D2O/H2O (60%,20%,20% by weight) and 40 mM of 4 amino-TEMPO.

However and even that it was already proven that this sample had a T_1 in order of seconds at low temperature still no spin flip (no negative peak) could be observed. Seeing that 3 seconds were not enough for spin relaxation, the recycle delay D1 was increased to 3 hours and even then no significant results were found (figure C2 in

appendix C). So, this time, the problem was definitely with the probe and not with the sample.

3.16 B_1 field homogeneity for the 3 mm x 7 mm flat coil and double coil

The spins' magnetization in every part of the sample should experience the same B_1 field therefore, B_1 homogeneity is essential for having a good NMR signal. As a matter of fact one can determine field balancing and homogeneity by comparing the frequency shift of the resonance peak using a network analyzer. In the ideal case the same frequency difference should be observed while touching one of the coil leads with a conducting needle. That wasn't the case for the 3 mm x 7 mm cross section flat coil. Furthermore AWR microwave an rf design software suite was used to prove the results that were observed by hand. AWR is used to design and simulate analog circuits including rf and microwave.

It allows the probe circuit tuning and matching. It also scopes electronic properties such as intensity and voltage. In this case, voltage values simulations at the coil leads showed magnetic field inhomogeneity. It can be seen in figure 3.32 that instead of having the same voltage values at both coil leads, a high voltage value was measured on one lead and a low one at the other. This implies that the field inside the coil is inhomogeneous.

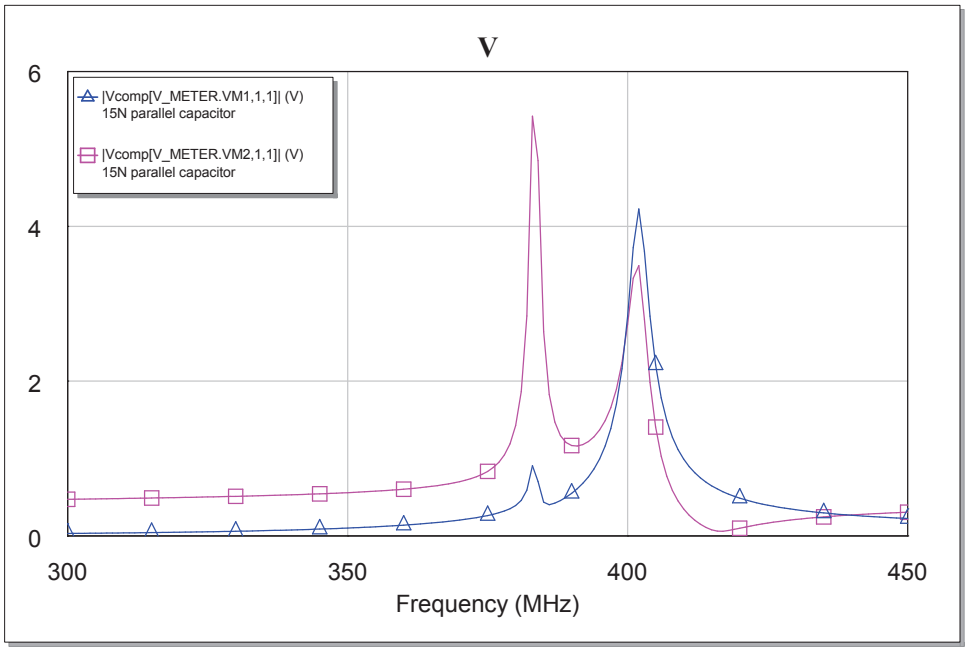

Figure 3.32: Proton voltage simulation using AWR microwave at the flat coil leads with a 7mm x 3mm cross section. The voltage at the right coil lead is in blue. The voltage at the left coil lead is in fuchsia. The voltage is imbalanced at the left coil lead since two voltage maxima instead of one at 400 Mhz.

The spin magnetization were not experiencing the same B_1 field. These results explained why the proton spin magnetization couldn't be flipped in the case of the 7mm x 3 mm cross section flat coil.

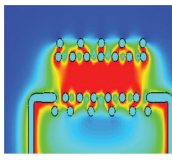

3.17 Double coil configuration

Therefore, a new circuit was designed. In this new design the ^{1}H and ^{15}N circuits were isolated. The ^{1}H and ^{15}N B_1 fields were symmetrized (i.e, balanced) independently. By placing capacitors in series with the coil grounding the proton channel could be tuned and matched at 400 MHz. In this circuit the former X and Y channels were used with inductive matching for ^{1}H and ^{15}N respectively c.f. figure 3.2.

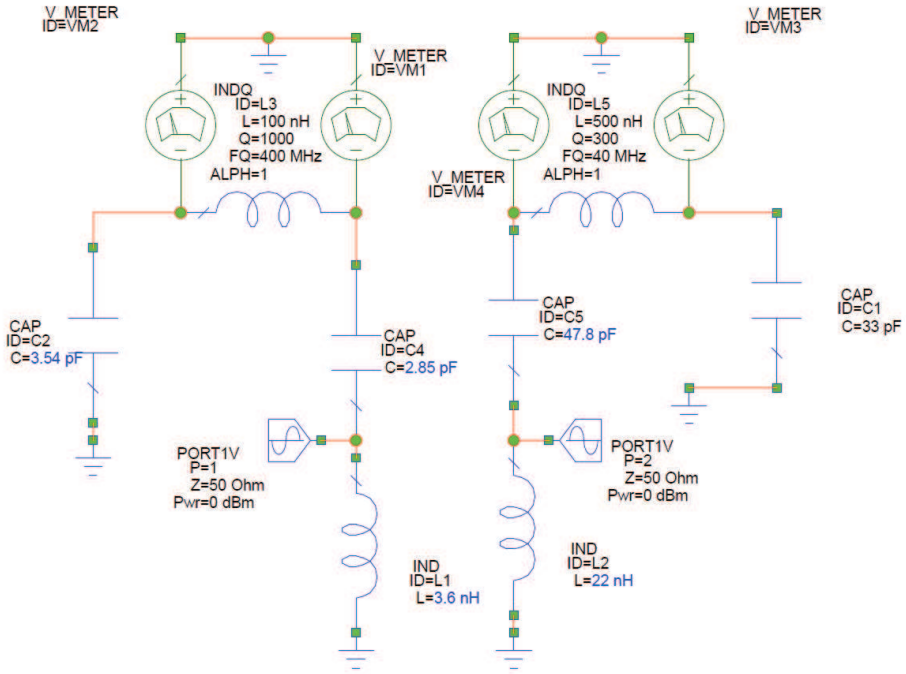

Figure 3.33: Double coil circuit design done with AWR microwave. Port one is for ^{1}H at 400.1 MHz and port 2 is for ^{15}N at 40.5 MHz.

The basic 3D model of the probe with the double coil configuration is shown in figure 3.34. The initial goal is to design a double resonance probe tuned to 400.1 MHz (^{1}H) and 40.5 MHz (^{15}N). This probe will not only accommodate glass stack samples with dimensions up to 3 mm x 6 mm x 11 mm but it will also provide homogeneous field for both ^{1} H and ^{15}N independently. Here is an insight of the probe configuration.

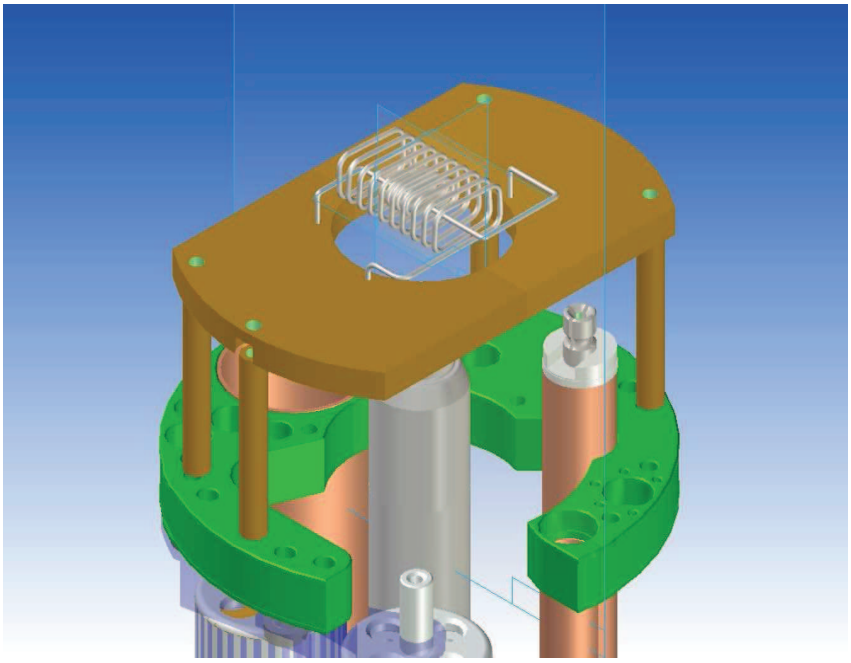

Figure 3.34: Probe top plate design realized with Solid edge. The double coil is shown with the inner coil designed for protons and the outer coil for nitrogen. A vespel coil support in brown is fixed to the top plate to render the assembly more stability. The microwave guide in grey is fixed in the probe center. The lambda half line in copper coating is not used in this double coil design. The top of the teflon capacitors is also shown

In light of the description in the previous part, the preliminary results of the rf pioneer coil configurations are briefly discussed.

Figure 3.35 shows the voltage values at the proton and nitrogen coils leads for the double coil configuration.

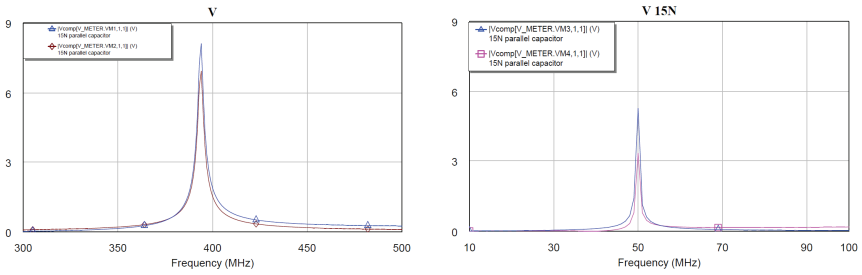

Figure 3.35: Simulation of the voltages at the coil leads using AWR microwave. The voltage at the ^{1}H and ^{15}N coil leads is measured at 400 and 40.5 MHz respectively. The voltage values are equal at both coil leads which indicates that the rf field inside both coils is homogeneous.

Moreover, the rf magnetic field distribution within the double coil configuration was analyzed in an attempt to optimize the magnetic field homogeneity in the active region of the coils. (please refer to figure 3.36 on page 94) .

The field distribution results confirm, that with the configuration used, good rf field homogeneity can be obtained for both coils. The efficiency of the coil configuration is in agreement with initial NMR experiments, where 50 kHz rf amplitude (nutation frequency) for ^{1}H and ^{15}N was achieved with an rf input power of 60W and 400W, respectively [84].

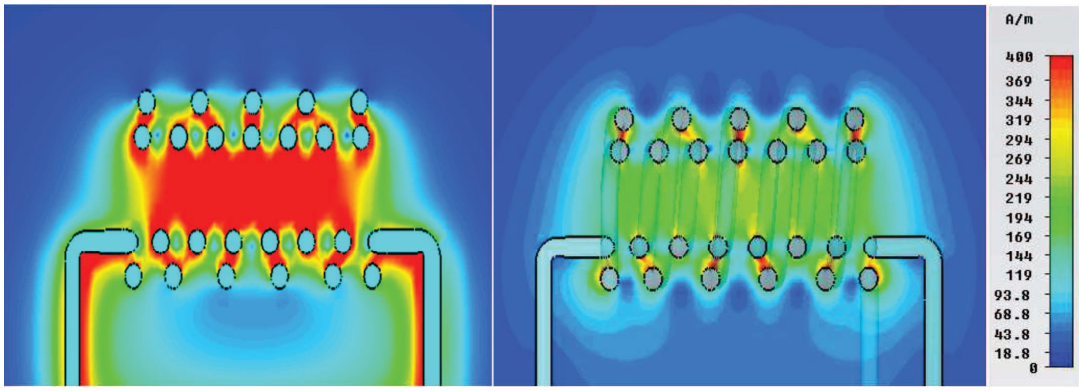

Figure 3.36: Double coil configuration shows a good B_1 field homogeneity. Here the CST Darmstadt (Computer simulation technology) Magnetic field simulations done by Priyanga Bandara is shown. The picture on the left represents the rf magnetic field in the ^{1}H coil at 400 MHz. The picture on the right represents the rf magnetic field in the ^{15}N coil at 40.5 MHz.

Furthermore, the sample must be in the center of the rf coil . In the first setup, experiments were realized at room temperature using ^{15}NH4Cl sample sealed in a plastic bag. This bag will always lie in the coil bottom and is bigger than the sample. Because the proton peak is very wide, signal was acquired on the ^{15}N channel and decoupled on the proton channel. In this case a nutation curve could be recorded. In a second set of experiments the sample was put in a 3.2 mm rotor to make sure the sample was in the center of the coil. Teflon tape around the rotor maintained the sample in the center of the active region of the coil. But still the 180° flip on the proton channel could not be observed. Finally ^{15}NH4Cl sample with 4 amino tempo was tested because it will be used at low temperature. It was wrapped with Teflon tape and slided into the coil center and then everything worked as normal. A nutation curve was acquired and the 50kHz pulse was calibrated at a ^{15}N power of 500W and a ^{1}H decoupling power at 49W c.f. figure 3.38

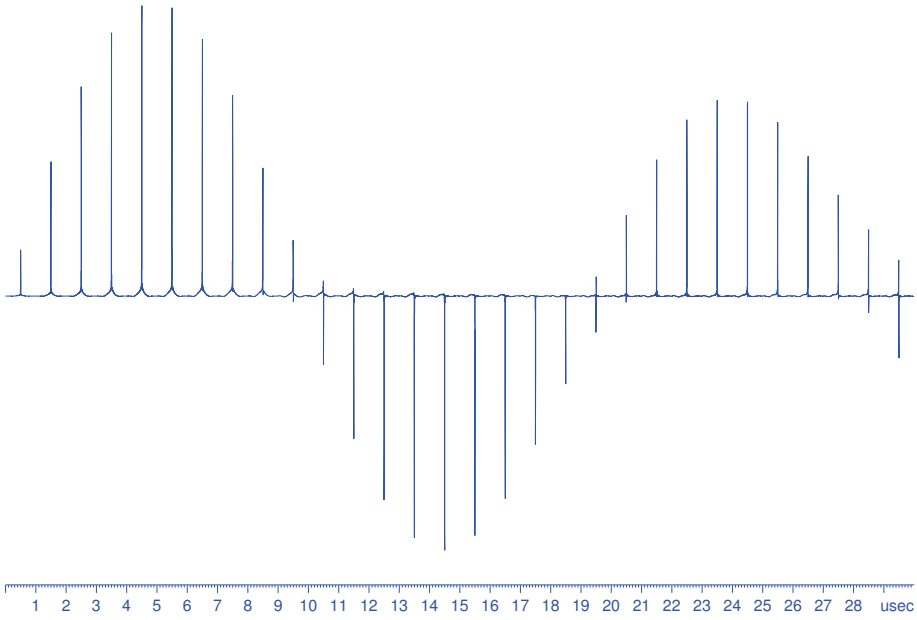

Figure 3.37: Proton pulse calibration. This nutation experiment was realized in order to prove that the field homogeneity in the proton coil was recovered.

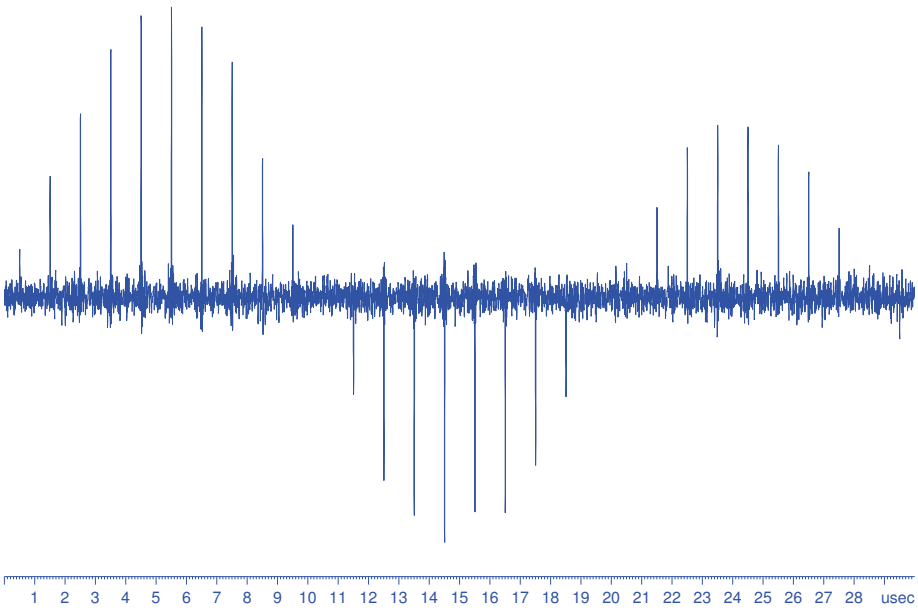

Figure 3.38: ^{15}N pulse calibration

3.18 New strategy for sample study

Now that these issues were clarified, new samples had to be tested. So to go further with the project, a calibrating sample that gives good signal in a short time had to be found. It must have a "sharp" line width at room temperature so that the peak enlargement at low temperature (100 times larger) won't affect the nutation curve. First experiments with hyperpolarized ammonium chloride at low temperature were not successful. That's why a new strategy for the study of static samples at room temperature and low temperature had to be established.

First of all calibrating CP experiment were realized at room temperature.

Knowing that the proton peak width at low temperature couldn't be avoided, experiments were immediately acquired on the ^{15}N channel using a CP pulse sequence. The calibration of the CP experiment was done using the ammonium chloride powder as a standard sample. All the convenient parameters were optimized in order to have the best signal to noise starting with O2: the center of the ^{15}N spectrum of the

sample, spw0 power applied on the ^{1}H channel during the contact time, p3: the ^{1}H 90° pulse duration, pcpd2: the pulse length in the coupling sequence and p15: the contact pulse duration. After the optimization the CP experiment gives maximum signal. Usually amino-acid samples such as glycine and histidine are used for MAS probes.

- ^{1}H spectrum of deuterated glycine

  The first tested sample was glycine. Glycine is the smallest amino acid found in proteins because it has a hydrogen substituent as its side-chain. It usually gives sharp peaks in LT MAS probe. Deuterated glycine was used to limit the proton proton "cross talk". But once again it gave a wide peak.

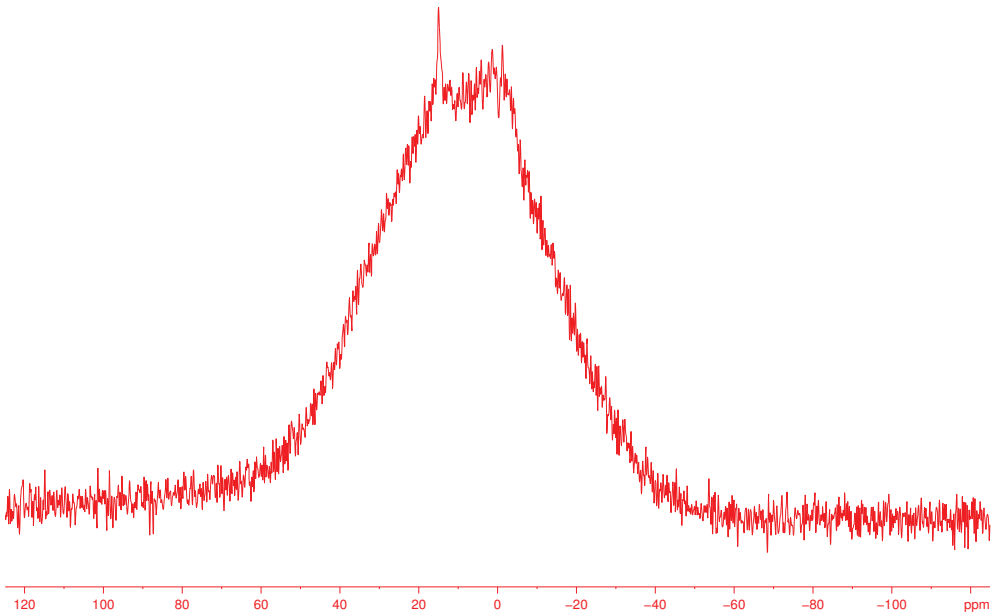

Figure 3.39: ^{1}H one pulse spectrum of glycine 97 % deuterated spectrum in a 3.2 mm rotor at room temperature to test the ^{1}H channel. The pulse length is 5 μs, the proton power level is 50 W. The recycle delay is 30 s, the acquisition time 0.006 s. The peak width is 20 kHz, the number of scans is 1

- Dissolved histidine ^{1}H spectrum assignment

L-histidine is one of the 10 essential amino acids for infants. It plays a key role in production of red and white blood cells. L-Histidine monohydrochloride monohydrate is manufactured by neutralizing L-histidine with hydrochloric acid cf figure 3.40.

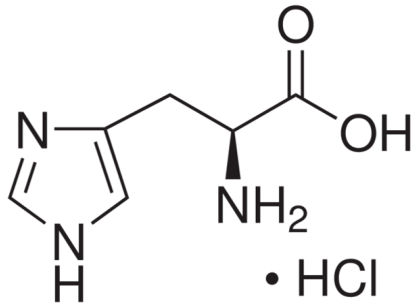

Figure 3.40: Histidine molecule chemical structure

Histidine can be used as a model aminoacid or a standard sample for calibrating CP and PISEMA experiments. Other aminoacids such as proline are routinely used.

A high resolution proton spectrum of histidine shows 5 peaks at 8.688, 7.421, 4.061, 3.383, 3.360 ppm cf figure 3.41 .

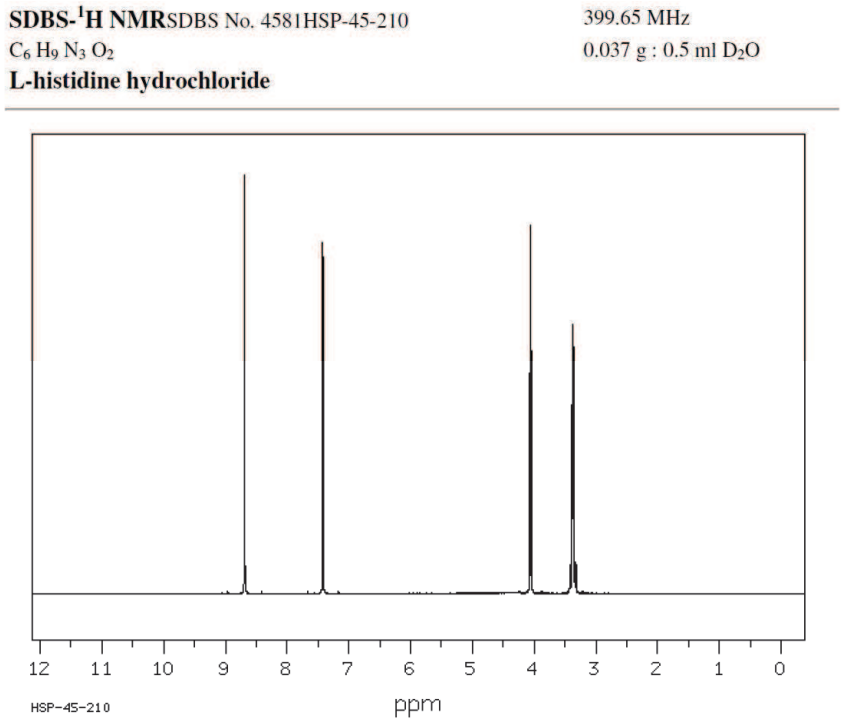

Figure 3.41: Histidine high resolution proton spectrum taken from the Spectral Database for Organic Compounds http://sdbs.db.aist.go.jp/sdbs/cgi-bin/cre$_i$*ndex.cgi*

However with the static probe, only two peaks at 4.7 and 3.3 ppm are distinguished cf. figure 3.42 .

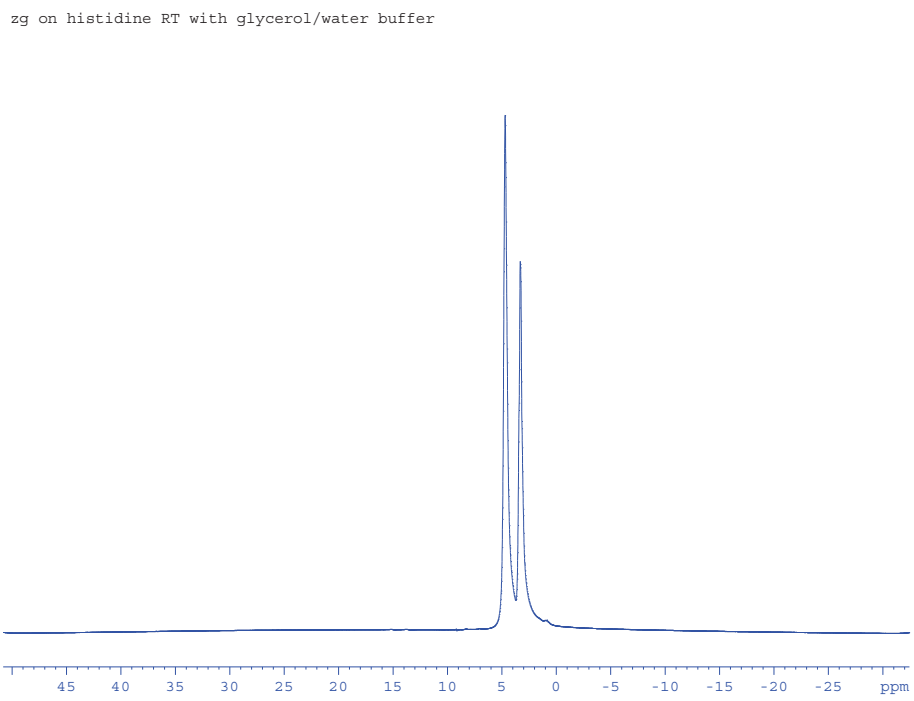

Figure 3.42: ^{1}H one pulse spectrum of 48 mM of histidine in a buffer mixture consisting of 60 glycerol and 40 of water. A 3.2 mm rotor was used as a sample container, it can hold up to 30 μL of solution. The static probe with the double coil was used at room temperature

- Histidine powder ^{15}N CP spectrum at room temperature

  When acquiring the spectrum of histidine, the number of scans is increased. The experiment takes longer than 14h in this case. The signal to noise is 65.

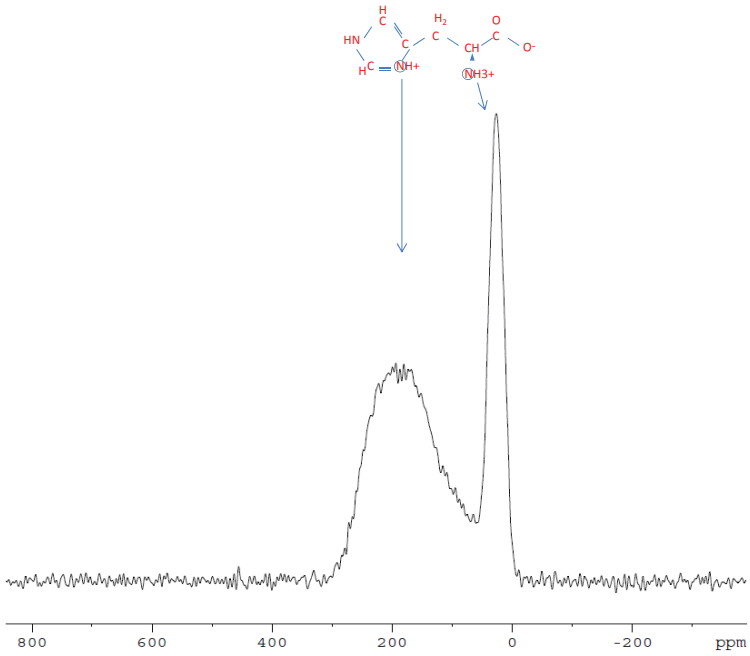

Figure 3.43: ^{15}N CP Histidine in a 2.5 mm rotor spectrum at room temperature, the acquisition time is 0.006 s, the pulse length is 5 μs, contact time 8500 μs, nitrogen power level 500 W, decoupling proton power is 60 W, 1680 scans overnight experiment signal to noise 65, the peak width 1173 Hz

- Histidine powder ^{15}N spectrum at low temperature
  The histidine peak in a static probe is very wide, that is why long acquisition times are necessary. At 130 K, the same parameters as for a room temperature test were applied. And it worked the signal to noise is 11 but it is a good start. But one would better find a calibrating sample at low temperature that gives a signal in a short time in order to calibrate experiments efficiently.

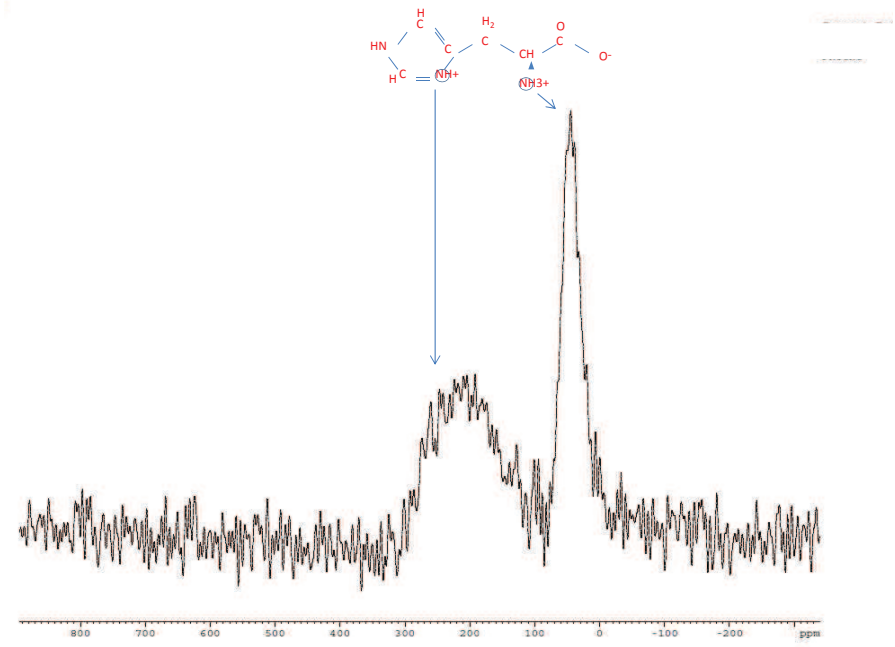

Figure 3.44: ^{15}N Histidine in a 2.5 mm rotor spectrum at 130 K. The acquisition time is 0.006 s, the pulse length is 4 μs, contact time 10000 μs, nitrogen power level 500 W, decoupling proton power is 60 W, number of scans 1680, signal to noise 11. The signal to noise is calculated on the left peak. The peaks interpretation was done by Gerhardt Althoff

4 amino TEMPO and TOTAPOL can be added to histidine to make the T_1 shorter and therefore the acquisition time shorter. The hyperpolarizing agent choice and concentration are discussed in the next sections.

3.19 Radicals' effects on T_1 and probehead performance

Radicals are essential to the performance of dynamic nuclear polarization (DNP) experiments. In the following experiments, the influence of monoradical concentration on the unlabeled histidine proton signal intensity and relaxation (T_1) is investigated. The aim of these experiments is to model histidine behavior after adding 4 amino

TEMPO. Shorter relaxation times are observed when increasing the monoradical concentration. However this process reaches a saturation limit at 60 mM. It is known theoretically that the spin-lattice relaxation time T_1 is shortened due to the paramagnetic centers that are created by the hyperpolarizing agents in vicinity of the nuclei. This phenomenon is referred to as paramagnetic relaxation enhancement PRE. Paramagnetic effects such as relaxation enhancement and paramagnetic shift quench the NMR signal from nuclei in 10 angstrom from the radical center [87]. A drawback of radical adding is line broadening. A process that is observed even at concentrations as low as 10 mM. On the other hand shorter T_1 allows shorter pulse repetition time D1 which compensate for intensity loss.

The 4 amino TEMPO monoradical powder has been transported from the laboratory in Strasbourg in ice and deposit 2 h later at -20°C. The experiences were carried out one month later . The unlabeled DL - histidine is from Sigma. The glycerol from Fulka. Milli-Q water is used. The buffer mixture consists of 60 glycerol and 40 of water containing 48 mM of Histidine. The 3.2 mm rotor used as a sample container can hold 30 μL of solution. Experiences are carried out on a 400 MHz spectrometer supported by an AvanceIII console. The cooling unit uses the liquid nitrogen closed circuit heat exchanger.
Experiments are first conducted at room temperature and then at 120 K. One pulse experiments are conducted in order to acquire proton spectra. A B_1 field of 50 KHz is used. For T_1 measurement, the saturation recovery sequence is used.

A first step is to measure the 4 amino TEMPO EPR signal to make sure that there is no degradation of the radical during transport and storage. Figure 3.46 is the EPR spectra of 4 amino TEMPO at 9 GHz.

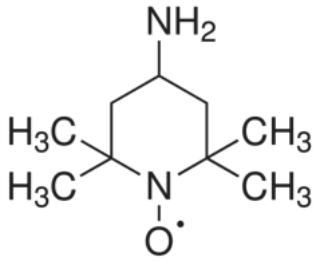

Figure 3.45: 4 amino TEMPO molecule

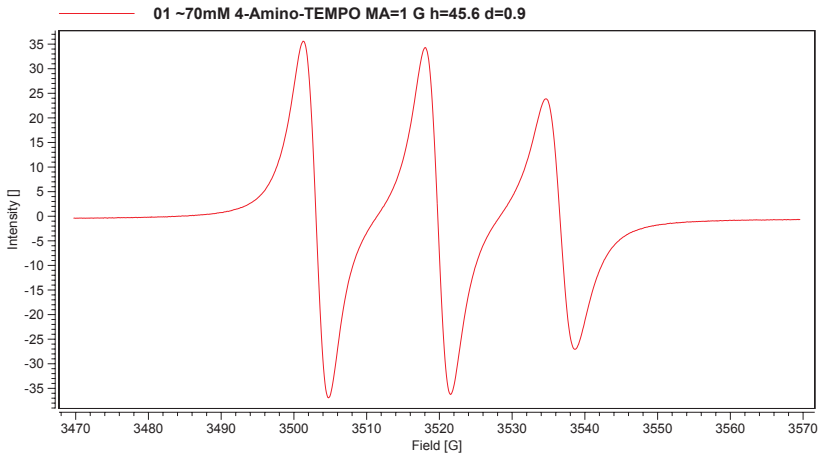

Figure 3.46: 4 amino TEMPO EPR spectrum at 9 GHz. This spectrum has been acquired for spin count to prove radical degradation at -4°C

The following issues will be discussed in this section:

- Measuring T_1 via CP of histidine powder at room temperature by saturation recovery
  In order to avoid wrong parameter settings (namely the recycle delay D1) and to explain why exactly a proper nutation curve couldn't be obtained, T_1 of histidine powder was measured via CP with saturation recovery. For histidine a value of 9.8 sec (error 0.2) was found.

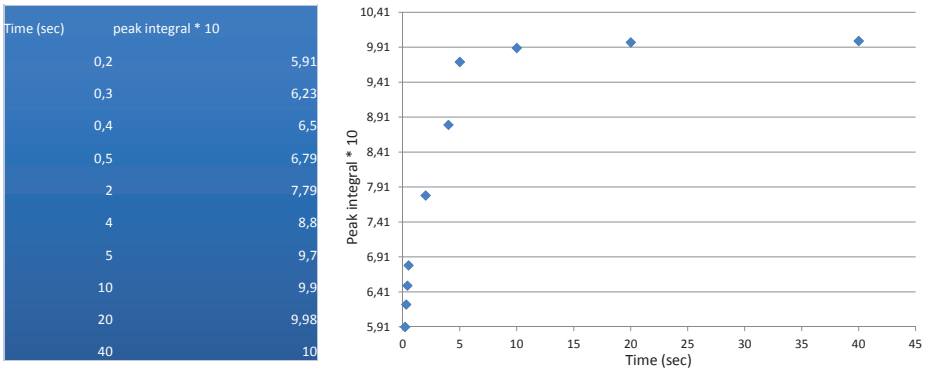

Figure 3.47: Histidine proton T_1 measurement via CP at room temperature using the saturation recovery pulse sequence. The error on T_1 is estimated is 0.2 s

- Hyperpolarized histidine proton T1 measurement

  At room temperature the Histidine proton T_1 is short (131 ms).This value was assessed by direct acquisition since the histidine powder sample was not ^{15}N labeled. It gets longer, i.e., 10 s. at 120 K cf. the following equations [88]:

$$\frac{1}{T_1} = \frac{2}{3} < \Delta\omega^2 > [\frac{\tau_c}{1+\omega^2\tau_c^2} + \frac{4\tau_c}{1+4\omega^2\tau_c^2}] \tag{3.14}$$

$$\tau_c \propto e^{\frac{E}{KT}} \tag{3.15}$$

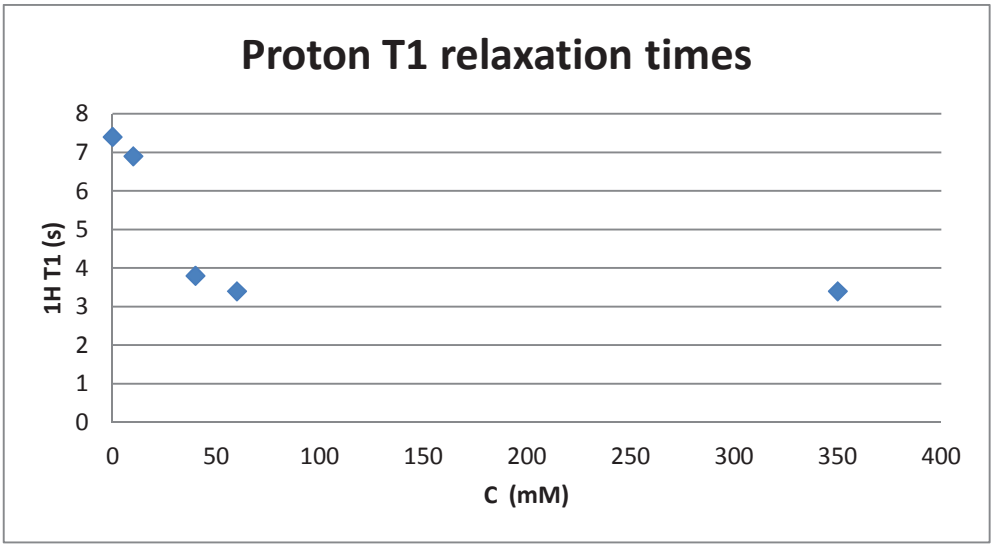

Figure 3.48: Proton T_1 relaxation time measurement by direct acquisition of hyperpolarized histidine evolution with respect of radical concentration in mM. The error on T_1 is estimated is 0.2 s. Similar results were observed by Akbey et al (2012)

At 120 K, the Histidine (dissolved in water and glycerol) proton T_1 measured by direct acquisition is 7.4 seconds without radicals. The shortest value (3.4 s) it can reach was recorded at a radical concentration of 60 mM cf figure 3.48. A shorter proton T_1 means a shorter repetition rate during proton nitrogen cross polarization experiments therefore a bigger signal to noise per unit time. Optimal recycle delay for CP experiments was calculated to be 1.3 x T_1 [87]. In the following paragraphs, the evolution of the relaxation time is analyzed, the signal to noise and the peak width with respect to the 4 amino TEMPO concentration.

- The effect of biradical concentration on probe head performance

  From these measurements, it can be deduced that the addition of 4 amino TEMPO renders the histidine peaks wider: 1.6 ppm for histidine alone then 1.9 ppm with 40 mM of 4 amino TEMPO at room temperature . The peaks are broader at low temperature due to shorter T*2 the spin-spin relaxation

time. Addition of the monoradical affects the probehead performance as well. The signal to noise was measured and compared to the results of Lange et al. [87]. In fact at 120 k the signal to noise is enhanced at 40 mM (672) then it goes down again at 60mM and 350mM cf. figure 3.48. Proportionally the sensitivity goes up from 102 for histidine alone to 251 at 40 mM and then drops again to 62 at 350 mM.

$$k = \frac{\frac{S}{N}}{n_a.\sqrt{T_1.n_S.1.3}} \tag{3.16}$$

The sensitivity k is defined as the S/N per square root of measurement time (taking into account that the optimal recycle delay equals 1.3 times the proton T_1) and sample amount in the rotor. Where n_a is the analyte per rotor in μmol, and n_S is the number of scans.

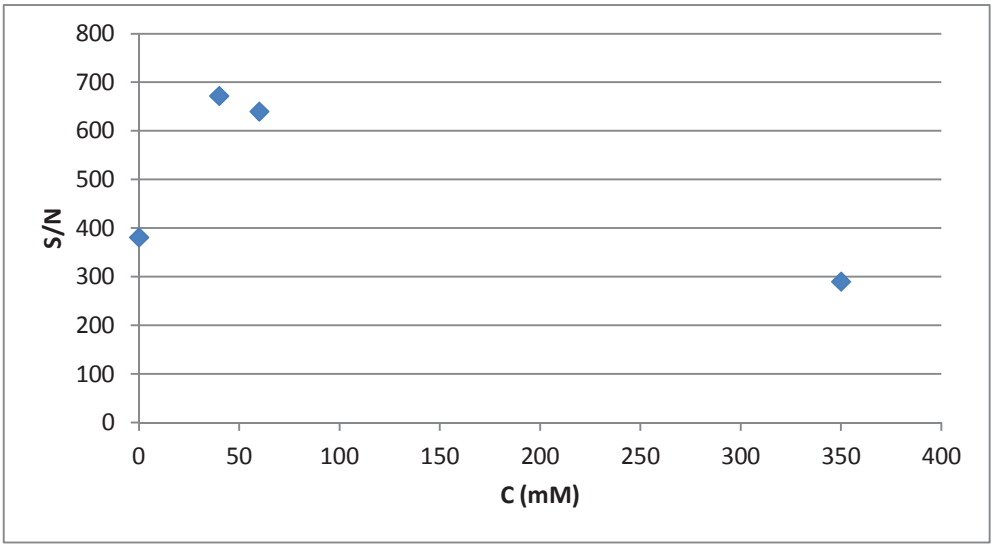

Figure 3.49: Signal to noise of hyperpolarized histidine evolution at low temperature with respect to 4 amino TEMPO concentration in mM

These measurements indicate that biradical concentration should be optimized for having the best sensitivity. A large concentration of radicals allow one to

have a better enhancement but it also reduces the sensitivity. Because radicals screen the detectable nuclei and enlarge the peak widths. On the other hand 4 amino TEMPO (cf. figure 3.45) is not enough to reduce the histidine T_1 to 1 second. To allow fast experiment repetition rate and reasonable PISEMA experiment time (2 hours), T_1 values as short as 1 second are needed. TOTAPOL can also be used. It decreases the proton T_1 in proline from 27.8 seconds to 2.7 seconds with 26 mM of TOTAPOL[87].

3.20 Hyperpolarized $^{15}N H_4Cl$ spectrum characterization

Polarizing agents such as TOTAPOL and 4 amino TEMPO are used to decrease T_1. A mixture of 4 amino TEMPO monoradical at 40 mM with ^{15}NH4Cl dissolved in deuterated water, water and glycerol (20,20,60,v/v/v)[94] sample is prepared. Glycerol freezes at -47 ° C or 226 K [95] and forms glassy samples at liquid nitrogen temperature. The sample phase changes have been monitored. Glassy samples form so that the polarizing agent distributes homogeneously.

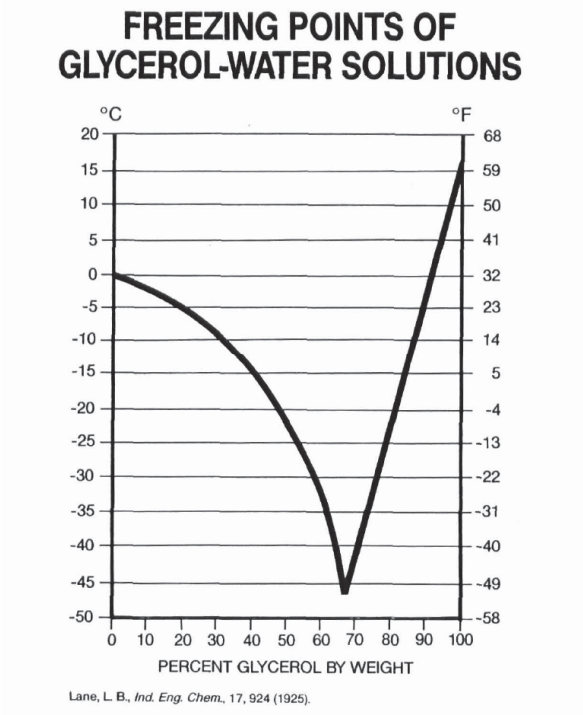

Figure 3.50: Glycerol water freezing point. The freezing temperature is shown both in Celsius and Fahrenheit with respect to the percent of glycerol by weight. Taken from Lane et al (1925)

One of the crucial parameters in NMR is peak width. In the context of the LT DNP ssNMR static probe development, standard samples have been tested to calibrate measurements on membrane polypeptides.

In static NMR, the proton signal is broad because of the heteronuclear coupling between a nitrogen and several protons, the homonuclear dipolar coupling between protons, heteronuclear dipolar decoupling and chemical shift anisotropy. The major complication with ^{1}H NMR is homonuclear dipolar coupling. This is primarily due to the high natural abundance of protons in organic solids. Strongly dipolar coupled proton networks lead to static line broadenings of the order of 50 kHz.

Of course parameter optimization can still be run directly on a membrane sample using a standard CP experiments but it will take days to optimize.

To know why NMR experiments were not working hyperpolarized ^{15}NH4Cl peak width was monitored.

First, the phenomenon was monitored qualitatively with a continuous scan (gs topspin command). Then, the cooling down process was followed step by step from 275 to 135 K. Currently, cooling units are programmed to go down to nitrogen temperatures once at a time. So stabilizing the sample temperature at 230 K for example is difficult. The nitrogen gas flows can be reduced to the minimum so that the temperature change is slow enough that it does not affect the matching and tuning of the probe. A proton peak width of 4461 Hz was recorded at 207 K (c.f. figure 3.51). It was clear that some phase change has occurred since a "broad peak" of approximately 38 KHz was measured at low temperature. Ideally, the peak width shouldn't exceed 2 KHz so that "standard" nutation curves can be obtained while conducting a standard parameter optimization.

The results are shown in figure 3.51. At 178 K the apk phasing function (topspin) was not effective anymore, therefore manual phasing was used. And at 157 K peakw gave aberrant values so the peak width at half maximum was measured manually.

Temperature (°K)	Peak width (Hz)
279	392
270	410
257	427
248	480
229	911
219	1823
207	4461
198	5409
188	7820
178	16595
171	21509
157	31097
152	33034
145	34910
139	35236
135	37846

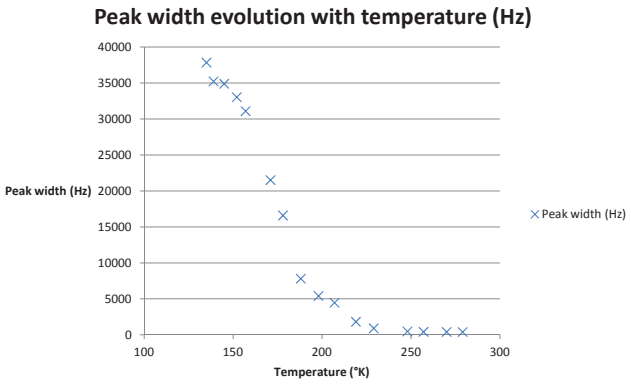

Figure 3.51: The proton peak width of hyperpolarized ^{15}NH4Cl evolution with temperature. The peak width values are reported in Hz and the temperature in K

In the following graph the peaks at 275 K and 135 K are shown. Probe matching and tuning was verified before every measurement.

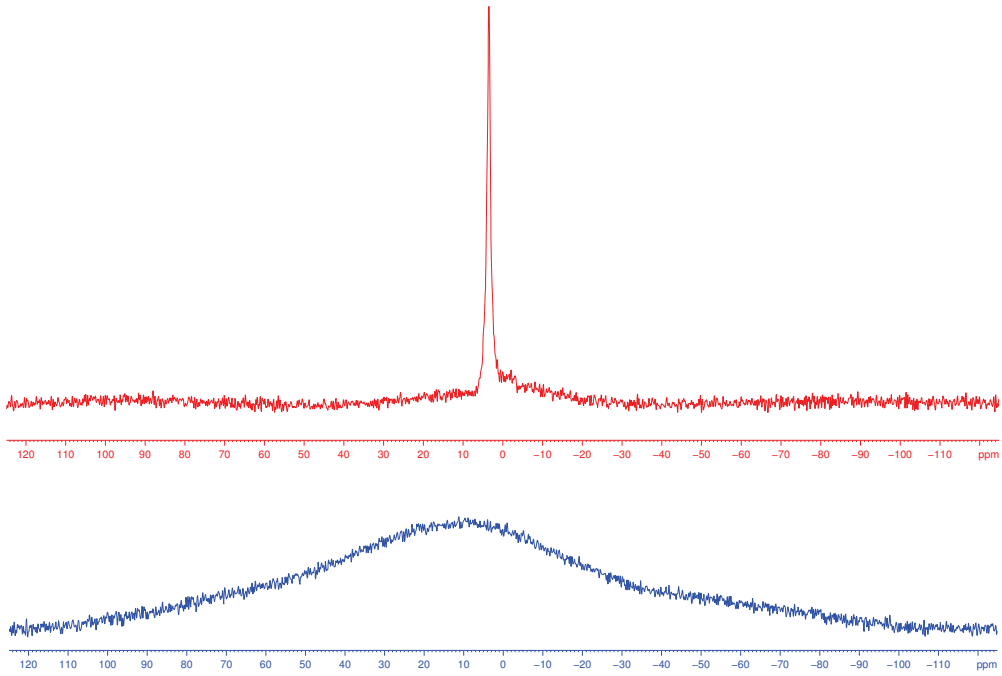

Figure 3.52: Comparison between the direct acquisition proton peaks of hyperpolarized ^{15}NH4Cl at 275 in red and 135 K in blue

- CP experiment on ammonium chloride at 110K

  Next the ammonium chloride spectrum acquisition at low temperature was attempted. For that 6 mg of ammonium chloride powder were dissolved in 60 % of glycerol and 40 % of water with a concentration of 4 amino TEMPO of 60 mM. Here the first ^{15}N CP signal with Ammonium chloride at 110 K is observed. Signal is acquired after 4 scans (recycle delay 30 sec) only. The signal to noise is 14.

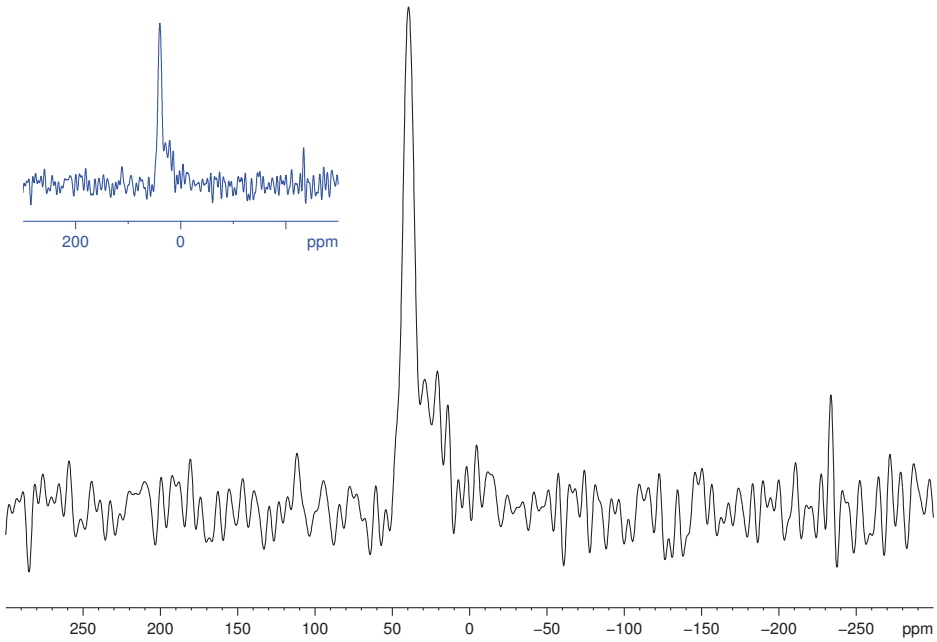

Figure 3.53: Hyperpolarized ammonium chloride ^{15}N CP spectrum at 110 K with the static probe. The pulse length is 3 μs, the nitrogen power level is 500 W, the proton decoupling is at 80 W, the contact time 2000 μs, the number of scans 4, the signal to noise 14 and the peak width 8.4 ppm

- Ammonium chloride T_1 measurement at 110 K

  Finally, the proton T_1 was measured via CP in a preliminary step by saturation recovery. The T_1 value is 3.7 seconds. The 4 amino TEMPO concentration is 60 mM. Now that a suitable calibrating sample was found, oriented samples spectra can be acquired at low temperature.

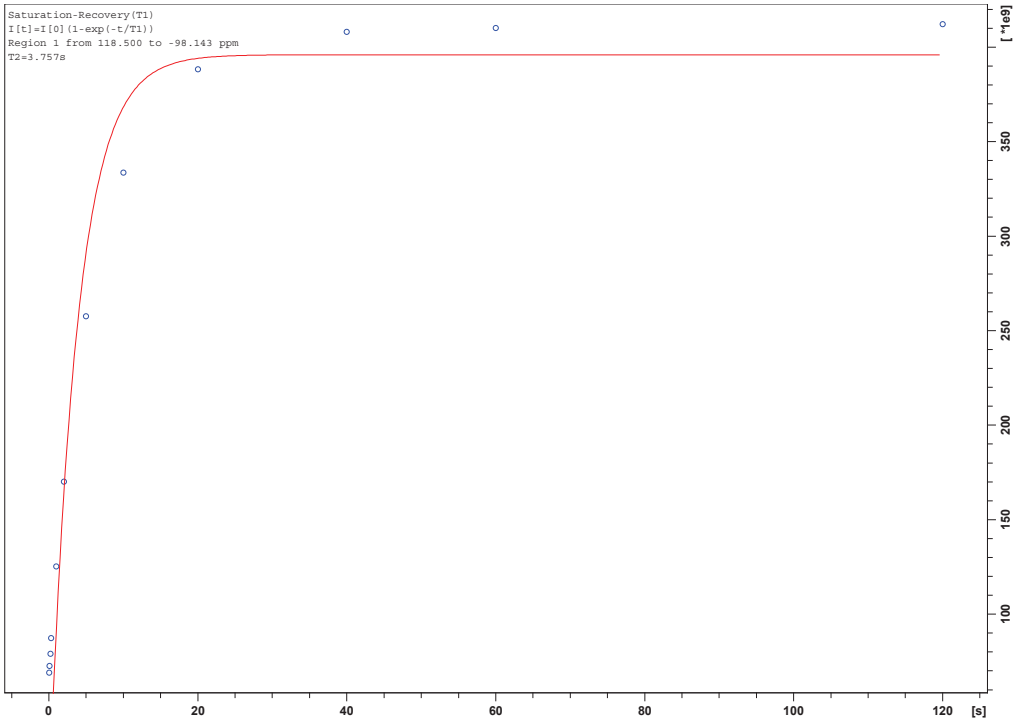

Figure 3.54: Hyperpolarized ammonium chloride T_1 measurement via proton decoupled CP at 110 K 4 scans signal to noise 14 ^{15}N power 500 W decoupling power 81 W. B_1 is set to 50 kHz

3.21 Oriented sample study at low temperature

Now that a calibrating sample that operates at low temperature was found, it is possible to set up an oriented sample experiment at low temperature. In order to confirm that the probe works at room temperature as well as at low temperature a standard polypeptide sample Hϕ19W (also referred to as RK1) was used. It is described in the membrane protein section. 7 mg of Hϕ19W are added to 40 mg of POPC. A peptide to lipid ratio of 1/20 is used throughout the thesis, unless mentioned otherwise. Both powders are dissolved in 150 microliters of TFE and then mixed together. TFE is evaporated with a constant nitrogen gas flow. The mixture is then put in the lyophilizer overnight. The sample is spread on glass plates then are then arranged one over the other and maintained with teflon tape. The sample is then sealed into a plastic bag.

First membrane alignment was checked by acquiring a ^{31}P spectrum for POPC

membrane. It has the shape of a powder pattern spectrum in case of motional averaging around the membrane normal [91]

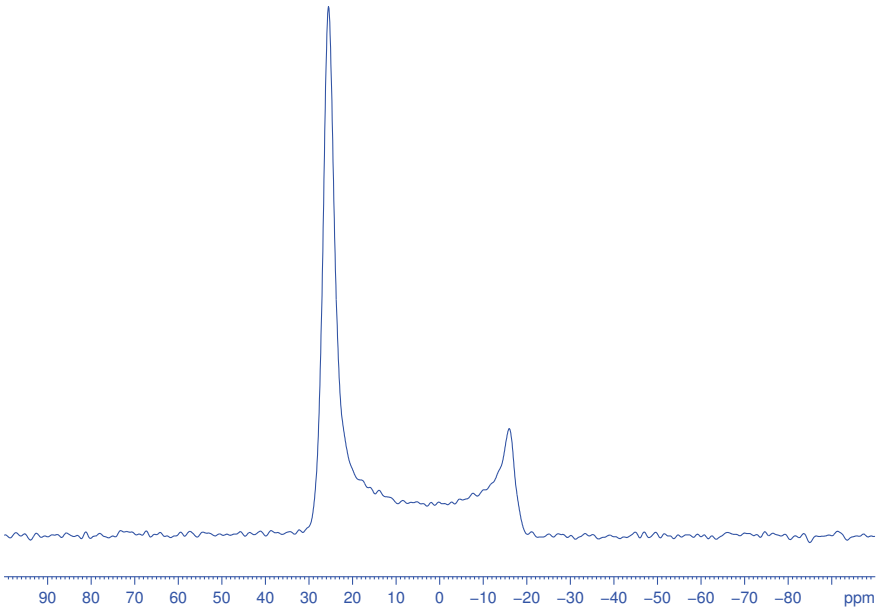

Figure 3.55: Static phosphorous spectrum of 40 mg of POPC oriented sample between glass plates using the one pulse sequence at room temperature. When analyzing the powder pattern, it is clear that most of the lipid sample is oriented parallel to the magnetic field (peak at 28 ppm). The remaining contribution at -19 ppm is due to the unonriented lipids. This is an indication of a partially unordered sample.

Second, a ^{15}N spectrum for 7 mg of Hϕ19W in 40 mg of POPC was acquired to check for polypeptide topology in the oriented membrane. This is also a way to compare the static DNP performance with a E-Free probe that is used in the laboratory.

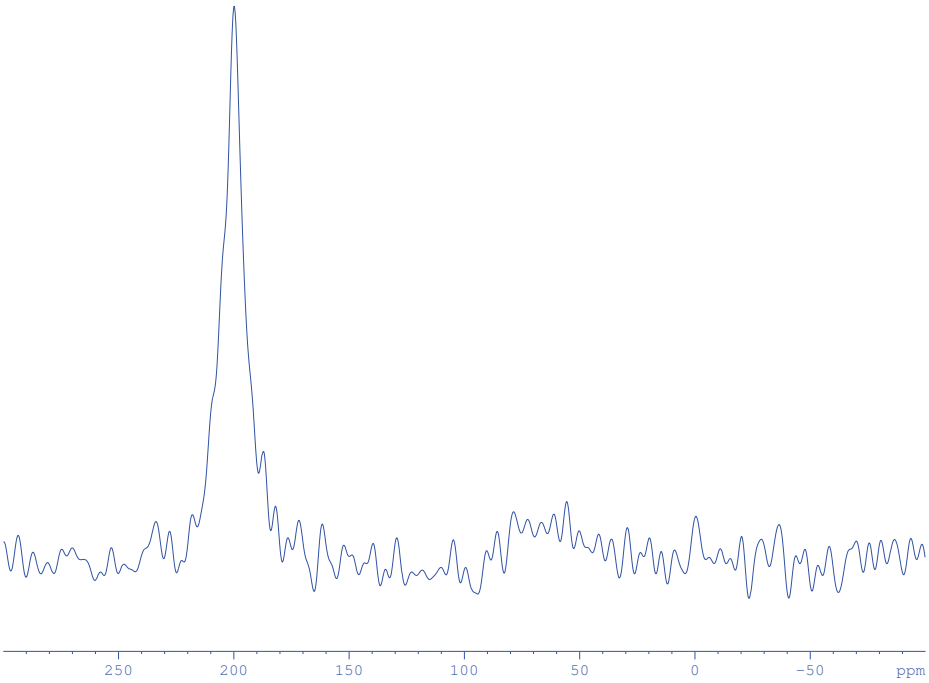

Figure 3.56: ^{15}N CP spectrum of 7 mg of oriented Hϕ19W in 40 mg of POPC between glass plates at room temperature with the E Free probe. The acquisition time is 0.006 s, recycle delay 3 s, the pulse length is 8 μs, contact time 600 μs, nitrogen power level 11.4 dB, decoupling proton power is 10.8 dB, the number of scans 102400. Signal to noise is 24

The sample had dehydrated meanwhile because it was utilized for NMR experiments for a week. That explains the second peak. Hϕ19W is a transmembrane alpha helix (peak at 200 ppm). Nevertheless, the signal to noise ratio is 4 (RG = 2050) after 18432 scans. While it is 24.1 (RG = 4096) after 102400 scans with the E free probe.

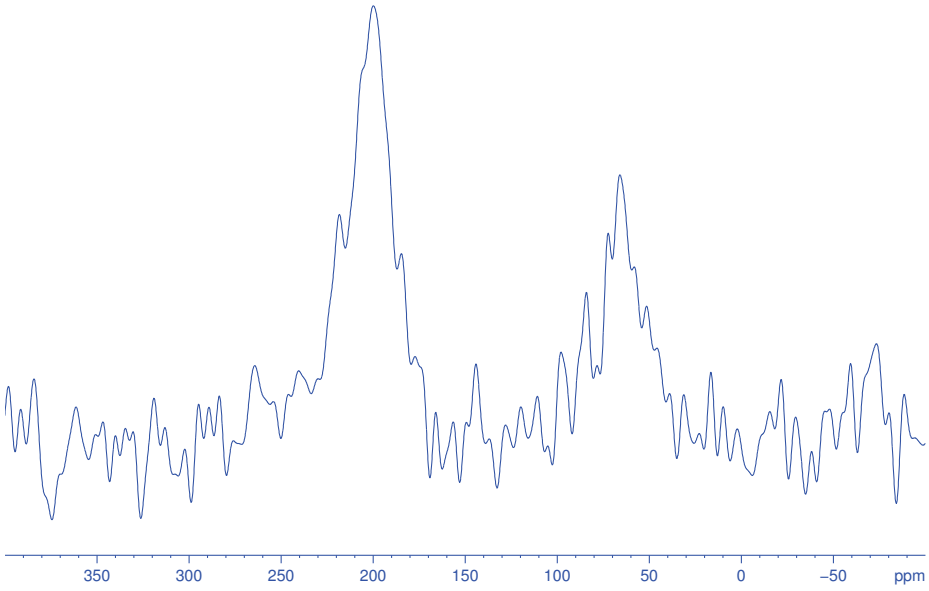

Figure 3.57: ^{15}N CP spectrum of 7 mg Hϕ19W at room temperature with the static probe. The signal to noise is 4 after 18432 scans. The acquisition time is 0.006 s, recycle delay 3 s, the pulse length is 4 μs, contact time 800 μs, nitrogen power level 400 W, decoupling proton power is 60 W. The sample had dehydrated because it was continuously utilized for measurement during a week. That explains the two broad peaks

The CP conditions were properly calibrated on ammonium chloride with 4 amino TEMPO before inserting the peptide sample. At 104 K, the signal to noise is 4.5 (RG = 18) after 2800 scans.

Figure 3.58: ^{15}N CP spectrum of 7 mg of Hϕ19W at 110 K. The signal to noise is 4.5 after 2800 scans. The acquisition time is 0.006 s, recycle delay 20 s, the pulse length is 4 μs, contact time 750 μs, nitrogen power level 400 W, decoupling proton power is 60 W.

A recapitulating table 3.4 is reported.

	Temp (K)	S/N	NS	Is/In (norm S/N)	peakw (Hz)
Rk1 E-free	303	24,1	102400	0,075	1520
Rk1 double flat coil	303	4	18432	0,029	1061
Rk1 double flat coil	104	4,5	2800	0,085	1266

Table 3.4: Result summary: the temperature in K, the signal to noise S/N, the number of scans NS, the normalized signal to noise Is/In and the peak width in Hz are reported

Chapter 4

DNP results

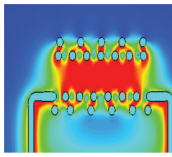

4.1 Material and methods

In this chapter we present first DNP studies on oriented membrane using a 9.4 T NMR magnet at cryo-temperatures and irradiated with 263 GHz microwaves of 7W. The microwaves were generated by a commercially available gyrotron operating at 9.7 T and transmitted into the NMR probe via a corrugated microwaveguide (figure 2.15) . The probe straight waveguide is coupled to the flat coil is shown in figure 3.34. First, DNP experiments were realized on hyperpolarized ammonium chloride. Furthermore, to test the effects of low temperatures and the enhancement by DNP in the context of lipid bilayers, the transmembrane model peptide $h\Phi 17W$ was reconstituted in oriented membranes. The mixtures of peptide, lipid, and biradical were dissolved in 2,2,2-trifluoroethanol, spread onto different sample supports, dried and equilibrated at 93% r.h. of D2O/H2O 90/10, and wrapped to fit the double coil and the single square coil one after the other. The use of partially deuterated "solvent" (lipid and water) channels spin diffusion toward the protonated peptide chain. These samples were investigated by DNP solid-state NMR spectroscopy. ^{15}N signal of the peptide was investigated. CST simulations were realized as a preliminary step before starting the experimental part.

4.2 Microwave CST simulations

A microwave field distribution calculation is made as a preliminary study for previewing accurately the microwave power absorption by the sample in the case of the double coil design. This model includes the microwave propagation into the sample with and without the double coil design. An input power of 1W is used at the microwave port. Several physical phenomena can explain the fringes pattern

observed in the simulations including reflection, diffraction from the NMR coil and the interference of the waves traveling inward and backward. The build up of the straight waveguide is meant to bring the microwave port as close as possible to the sample. The following points will be discussed in this section:

- CST model
- Microwave magnetic field without the double coils
- Microwave magnetic field with the double coils

The 3D model of the double coil and the sample within was designed using solid edge c.f. figure 4.1 . The actual sample consists of a stack of 10 to 25 glass plates and contains 50 mg/ml of sample concentration usually. The file was then saved in a .sat format and used in CST as such. The glass plates' number can be varied and the field distribution can be calculated according to that. Their thickness can be set as a parameter as well. The output from the corrugated waveguide is simulated by a Gaussian beam port which is an accurate description of the experimental observations. This Gaussian beam propagates into space through the double coils and irradiates the sample. The coil acts as a grid causing parts of the microwaves to be transmitted and diffracted, while the other part is reflected. In this model two cases are considered:

- the microwave electric field is parallel to the coil windings
- the microwave electric field is perpendicular to the coil windings

In both cases the observable region was equivalent. Six million mesh cells were used for a total simulation time of 17 hours.

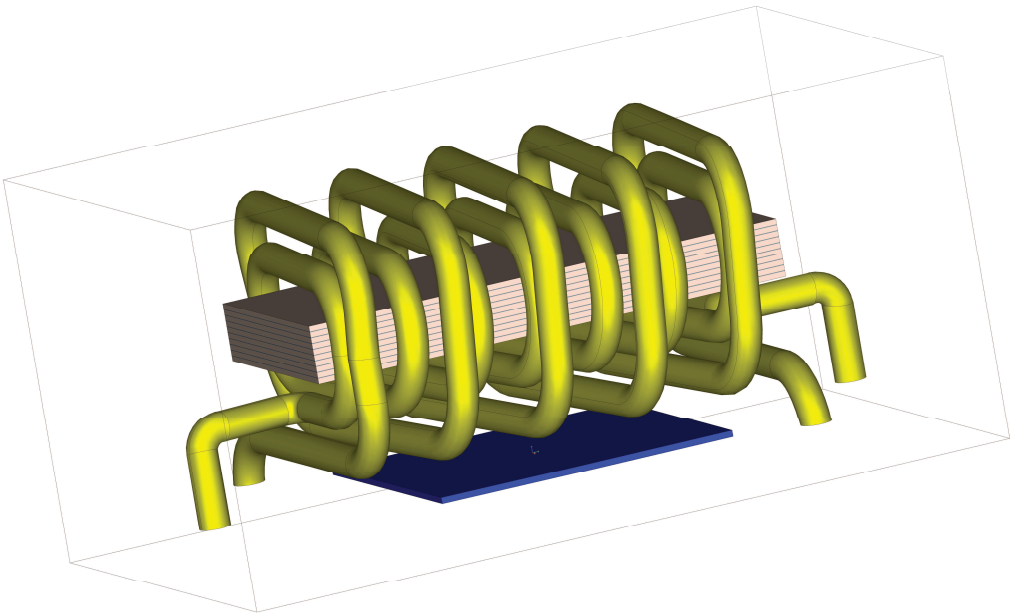

Figure 4.1: The CST model in 3D. The double coils and the glass plates in the center are shown. Nine sample layers were used. The sample thickness was estimated to 0.01 mm. The glass plates dimension was fixed to 5.4 mm by 11 mm and the plates thickness was averaged to 0.12 mm The microwave Gaussian beam is modeled as a blue plane in the bottom

As can be seen in figure 3.34 the waveguide is underneath the coil. A circular hole is left on purpose in the coil support to avoid microwave shielding. The CST transient solver was used. The incoming microwave has a frequency 263 GHz and therefore a wavelength 1.1 mm. The magnetic field without the double coils amplitude is simulated. In figure 4.2 a vertical cut in the [zy] is shown. In an animation,the traveling continuous wave through space and the sample can be seen.

Without the double coils, the field has a maximum intensity in the center of the sample (c.f. figure 4.2) . The interference phenomenon is clearly visible in the structure of the fringes. The glass plates are dielectrics that act as a boundary and reflect some part of the wave while the other part of the wave is refracted. The interference occurs between the microwave incident wave from the waveguide and the reflected wave on the glass plate surfaces. The distance between two maxima in the interference pattern corresponds to the wavelength inside the sample which permits the calculation of a compression factor of 2. This is due to the sample refractive index which is 2 in the case of bilayers. The refractive index of air is 1.

One ought to find the parameter that influence the local maximum. The optimum glass plate thickness can be determined. Moreover the gap between the glass plates is deduced from the bilayers' thickness.

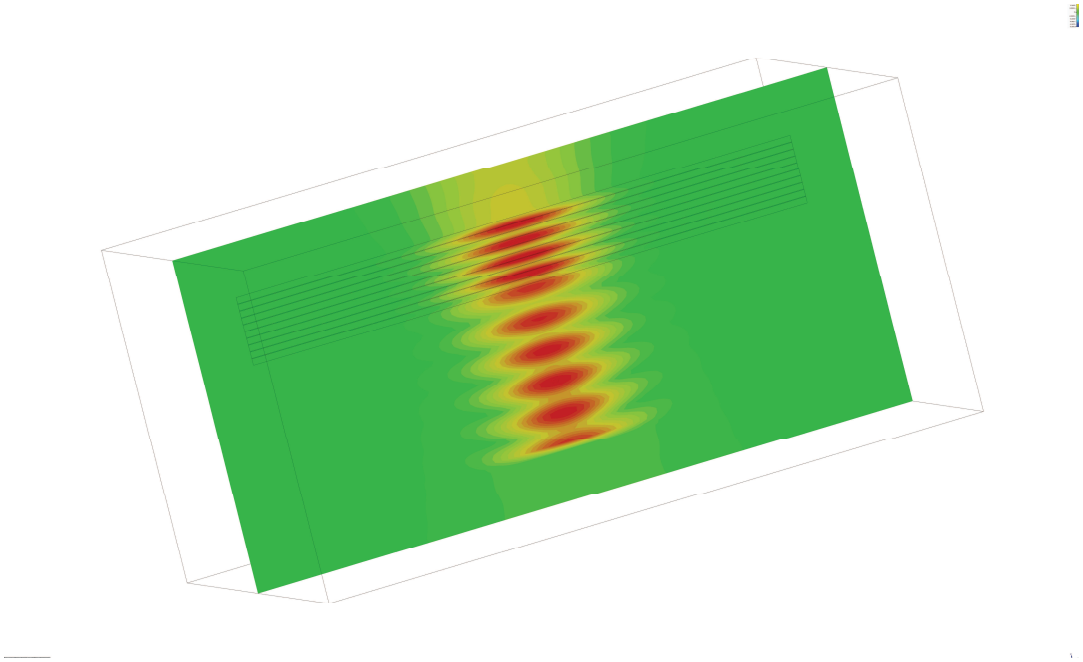

Figure 4.2: Wave compression into the glass plates sample (parallel rectangles on the top). The incoming microwave Gaussian beam from the bottom is compressed in the sample by a factor of 2

The microwave magnetic field with the double coils has been simulated. The magnetic field amplitude is shown in in A/m in figure 4.3 The pitch between the rf coil windings is in the order of the microwave wavelength 1 mm i.e. 263 GHz c.f. figure 4.3. This induces the diffraction phenomenon which is clearly observed as maxima and minima along the z vertical axis. A simulation with a better resolution shows clearly that some areas in the sample are not even irradiated (results not shown). This causes the power loss that will be manifest afterwards in the overall enhancement of the DNP experiments caused by field inhomogeneities.

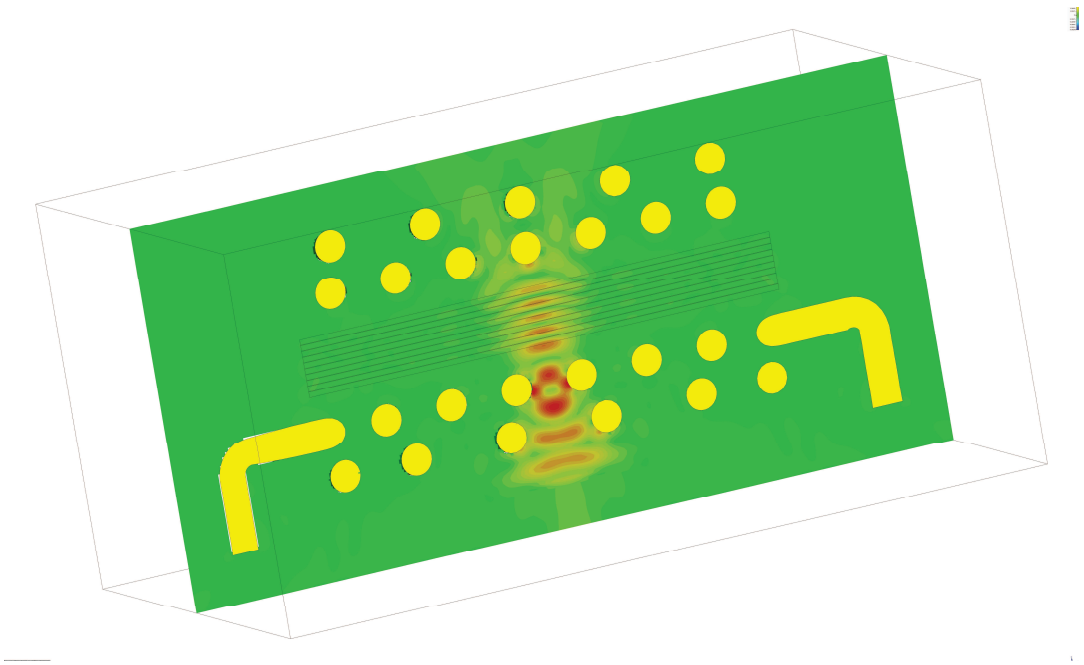

Figure 4.3: Microwave magnetic field magnitude in the sample (rectangles in the center of coils). The pitch between the rf coil windings is in the order of the microwave wavelength 1.1 mm i.e. 263 GHz. This induces the diffraction phenomenon which is clearly observed as maxima and minima along the z vertical axis

Actually, CST simulations provide the electric and magnetic field through the sample. The power generated by the gyrotron can be measured accurately. The microwaves propagate afterwards in an overmoded corrugated waveguide. The Gaussian power output from the waveguide can be mapped by a pyroelectric camera [96]. The diffraction effect of the rf coil is evident in figure 4.3. And the sample area does not always experience the higher microwave field values. The microwave field distribution is used to calculate the DNP enhancement at a given input power. The energy deposit in the sample should be considered in the future as well since the enhancement is inversely dependent on the temperature.

4.3 DNP ^{15}N CP experiments on the MAS DNP probe

In a preliminary step DNP MAS probe was used as a reference. The following results were obtained at the Bruker site in Wissembourg using the 263 GHz DNP spectrometer. Unless mentioned otherwise the DNP CP pulse sequence was utilized.

Both the MAS probe and the static probe are in a double mode.

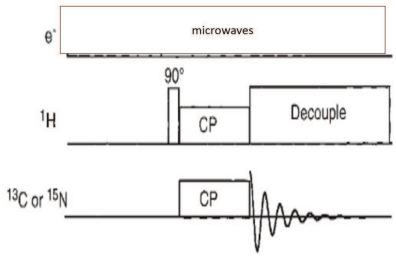

Figure 4.4: The DNP CP pulse sequence. It consist of a CP experiment with constant microwave irradiation at 263 GHz

DNP enhanced spectra of 25 microliters of 1.5 M of ^{15}NH4Cl in deuterated glycerol, D2O and H2O (60%/30%/10%,v/v/v) doped with 20 mM of TOTAPOL (cf. figure 4.5) were measured . An enhancement of 44 was observed with a continuous microwave irradiation.

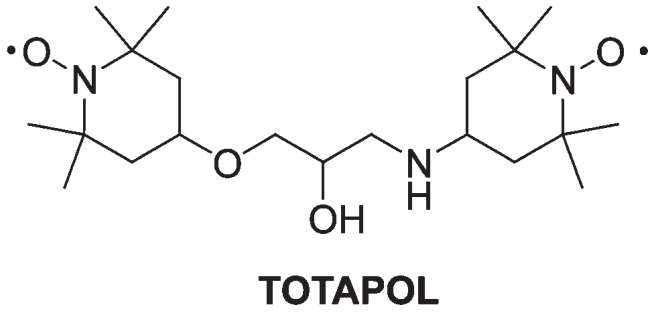

Figure 4.5: Chemical structure of TOTAPOL

The first spectra were recorded with a spinning speed of 5 KHz using an MAS probe at 95 K and 400 MHz c.f. figure 4.6. Here a proton decoupled ^{15}N solid state NMR spectrum of hyperpolarized ^{15}NH4Cl is shown in red and the DNP spectrum is in blue.

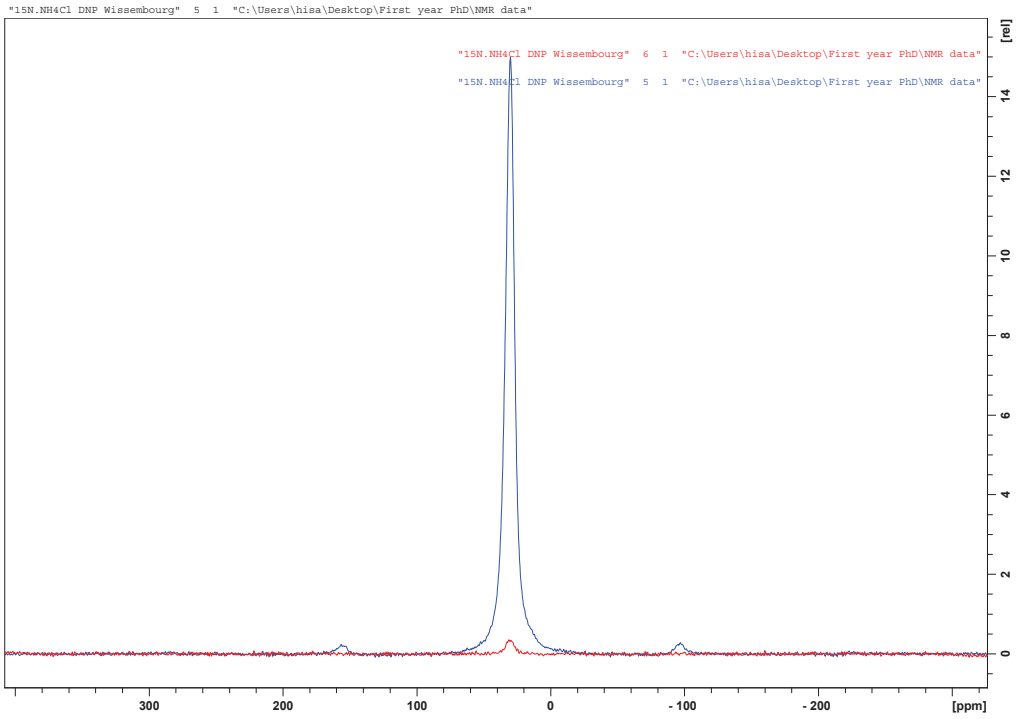

Figure 4.6: ^{15}N CP MAS spectra of 25 microliters of 1.5 M of ^{15}NH4Cl in deuterated glycerol, D2O and H2O (60%/30%/10%,v/v/v) doped with 20 mM TOTAPOL. Here the proton decoupled ^{15}N solid state NMR spectrum is shown in red and the DNP spectrum is in blue with the microwaves on and a collector current of 40 mA. An enhancement of 44 was observed with a continuous microwave irradiation. The spectra were recorded at 5 KHz with an MAS 3.2 mm LT DNP probe at 95 K. The ^{15}N rf field 42 kHz, the proton decoupling 90 kHz Spinal64, the recycle delay D1 is set to 15 s, the number of scans is 16 and the contact time is 1ms.

When the spinning was stopped (the rotor would still spin at 30 Hz) the enhancement went down to 20. The enhancement factor was calculated manually by scaling the two spectra obtained with the microwaves on (blue) and off (red). Two sets of experiments were realized, with 16 scans and 64 scans.

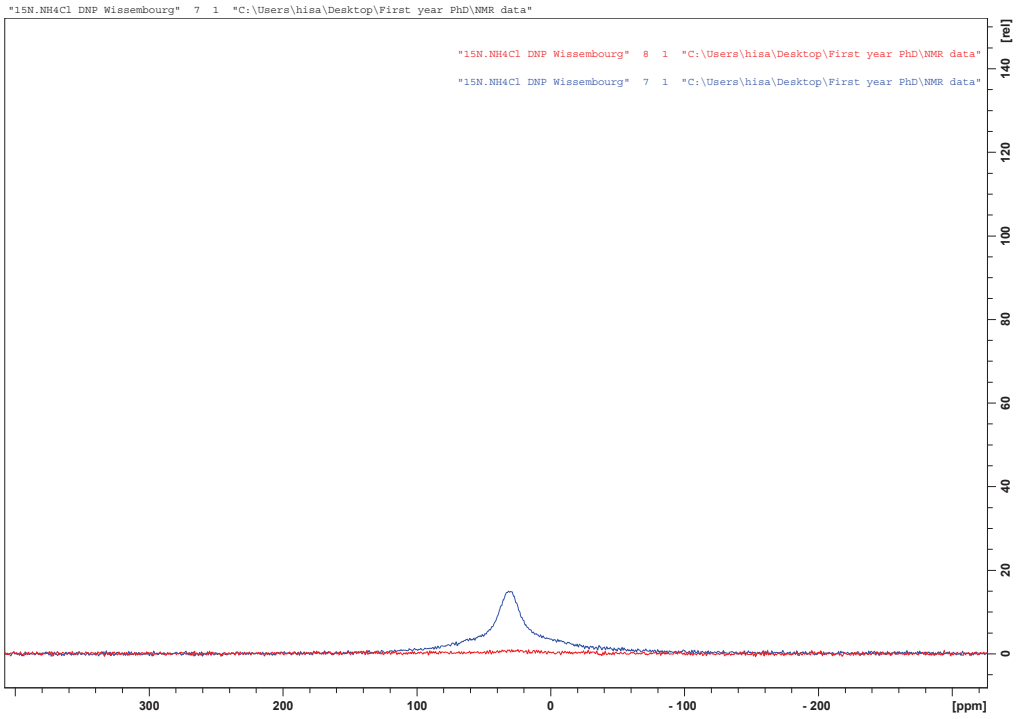

Figure 4.7: ^{15}N CP MAS spectra of hyperpolarized ammonium chloride at a spinning speed of 30 Hz with 16 scans an enhancement of 20 is observed using the MAS probe. The sample consists of 25 microliters of 1.5 M of ^{15}NH4Cl in deuterated glycerol, D2O and H2O (60%/30%/10%,v/v/v) doped with 20 mM TOTAPOL. The ^{15}N rf field 42 kHz, the proton decoupling 90 kHz Spinal64, the recycle delay D1 is set to 15 s and the contact time is 1ms.

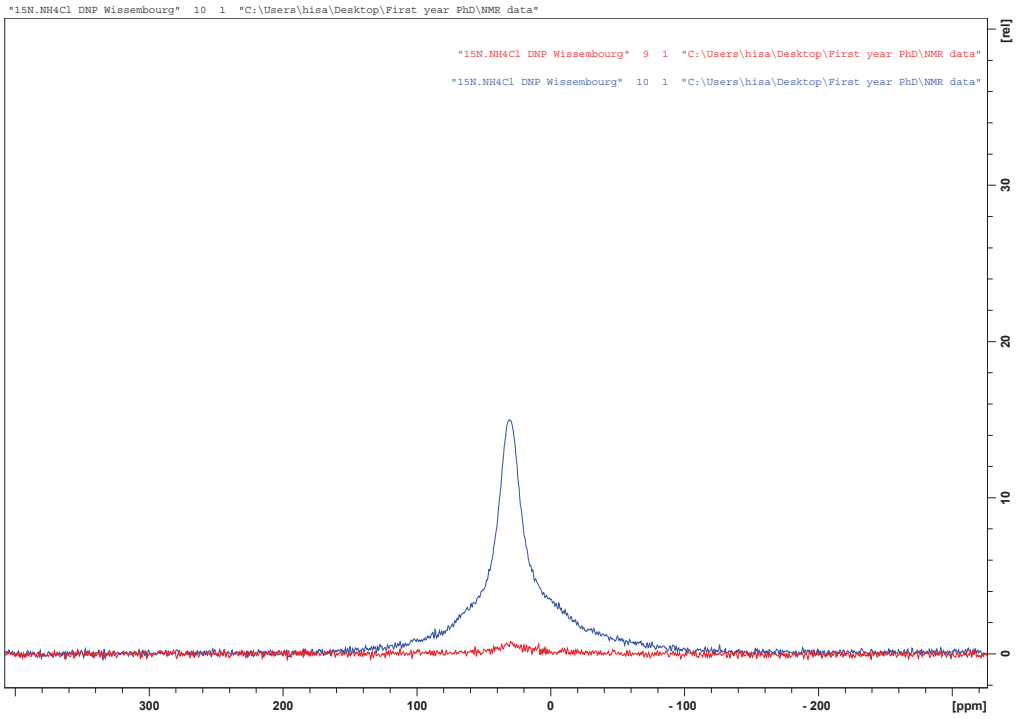

Figure 4.8: Spectra of hyperpolarized ammonium chloride at 30 Hz spinning speed with 64 scans an enhancement of 20 is observed using the MAS probe. The sample consists of 25 microliters of 1.5 M of ^{15}NH4Cl in deuterated glycerol, D2O and H2O (60%/30%/10%,v/v/v) doped with 20 mM TOTAPOL. The ^{15}N rf field 42 kHz, the proton decoupling 90 kHz Spinal64, the recycle delay D1 is set to 15 s and the contact time is 1ms.

4.4 DNP ^{15}N CP experiments on the static DNP probe

After simulating the microwave propagation through the double coil 3D model (CST-Darmstadt), it was time for the first DNP Bio PE probe test with a DNP spectrometer. The same sample was placed in the center of the inner proton coil and centered as much as possible. However, it was not enough in the center and that there was an air bubble in the sapphire rotor. The first enhancement measurement was 13. But after optimizing the CP better, an enhancement of 18 was obtained. The spectra with the microwaves off are in red and the spectra with the microwaves on are in blue. In figures 4.9 and 4.10 the results with 16 scans first and with 64 scans are

shown respectively.

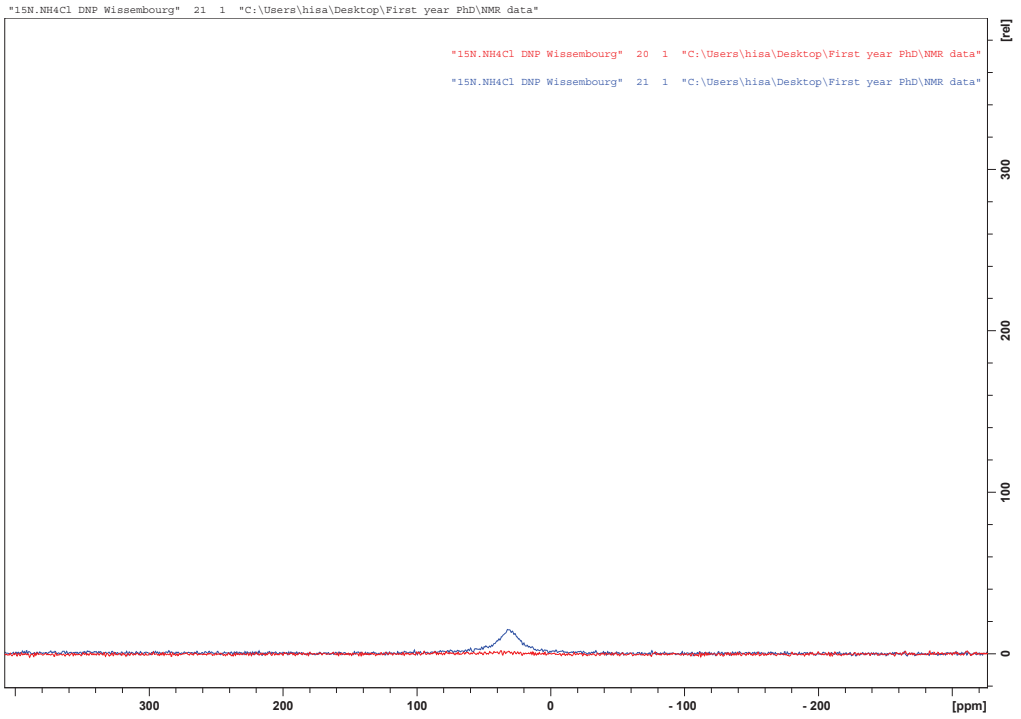

Figure 4.9: ^{15}N CP static spectra with 16 scans of 25 microliters of 1.5 M of $^{15}N H_4Cl$ in deuterated glycerol, D2O and H2O (60%/30%/10%,v/v/v) doped with 20 mM of TOTAPOL. Here the proton decoupled ^{15}N solid state NMR spectrum is shown in red and the DNP spectrum is in blue. An enhancement of 18 was observed with a continuous microwave irradiation. The spectra were recorded with the static probe at 95 K and 400 MHz. The proton decoupling power is 25W and the proton decoupling rf field is at 83 kHz. The nitrogen pulse duration is 4.5 μs and a nitrogen power level is 400W and the nitrogen rf field is at 55 kHz. The contact time p15 of 1.5ms and a recycle delay d1 of 15s are used

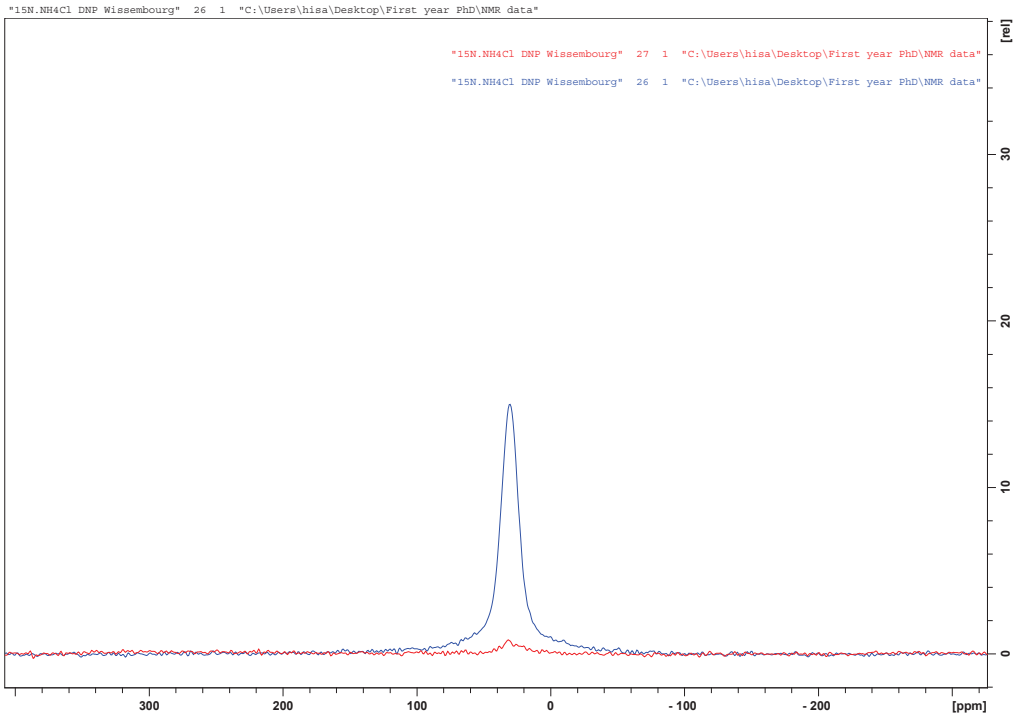

Figure 4.10: ^{15}N CP static spectra with 64 scans of 25 microliters of 1.5 M of ^{15}NH4Cl in deuterated glycerol, D2O and H2O (60%/30%/10%,v/v/v) doped with 20 mM of TOTAPOL. Here the proton decoupled ^{15}N solid state NMR spectrum is shown in red and the DNP spectrum is in blue. An enhancement of 18 was observed with a continuous microwave irradiation and a collector current of 40 mA. The spectra were recorded at 95 K and 400 MHz. The proton decoupling power is 25W and the proton decoupling rf field is at 83 kHz. The nitrogen pulse duration is 4.5 μs and a nitrogen power level is 400W and the nitrogen rf field is at 55 kHz. The contact time p15 of 1.5ms and a recycle delay d1 of 15s are used

The results are summarized in table 4.1. The experimental conditions, the signal to noise ratio, the peak width and the enhancement between the gyrotron off and on mode are shown.

	Spinning (Hz)	Microwaves	scans	Signal to noise	Normalized SNR	Peak width (Hz)	Enhancement
MAS DNP probe	5000	Off	16	8,5	2,1	299	
	5000	On	16	340	85	309	44
	30	Off	16	2,8	0,7	20211	
	30	On	16	37,8	9,4	877	20
	30	Off	64	3,4	0,4	2124	
	30	On	64	78	9,7	885	20
Static DNP probe	no	Off	16	2,2	0,5	26752	
	no	On	16	15,5	3,9	771	13
	no	Off	64	8,1	1	792	
	no	On	64	108	13,5	623	18

Table 4.1: Preliminary results in which the spinning speed frequency in Hz, the microwaves on or off, the number of scans, the signal to noise ratio, the normalized signal to noise ration, the peak width and the enhancement are reported

The proton T_1 of membrane polypeptides was previously measured from proton decoupled ^{13}C CP solid-state NMR measurements under DNP conditions [84] (1.2 sec) and a recycle delay of 3 seconds was used. Therefore the same experimental conditions will be used in the upcoming measurements on polypetides. That will render the experiment much quicker. Further detailed measurements will enable us to measure the spin lattice relaxation time. Thermal magnetization buildup curves should also be measured in a short time. In addition to that a microwave build up curve will also be established.

4.5 Oriented samples on glass plates and PEEK

PGLa is a 21-residue member cationic antimicrobial peptide of the magainin family. It is an α-helical amphiphilic antimicrobial peptide with the following amino acid sequence GMASKAGAIAGKIAKVALKAL amide in DMPC/DMPG bilayers. It is an in plane antimicrobial peptide [97]. It disrupts the cellular lipid bilayer of bacteria, fungi,viruses, and tumor cells. The solid-state NMR measurements using cross polarization DNP on HΦ19W on Glass plates didn't work with the previously

established DNP NMR parameters (collector current at 40 mA). PGLa on PEEK was tested and in this case also no signal could be obtained at all. This is due to the permittivity of PEEK that is similar to the one for glass.

4.6 HΦ19W on HDPE

Finally, High density polyethylene empirically was chosen. It works for samples wrapped in a MAS rotor and give enhancement values as high as 17 for 1 mg of ^{15}N labeled HΦ19W in 6 mg POPC-d31 (5 mol peptide) in the presence of 40 μg bTbK (cf. figure 4.11). For this static DNP experiments 17.8 mg of $H\Phi 19W$ with 100 mg of POPC and 1.65 mg of bTbK are utilized. The peptide to lipid ratio is 1/20. The DNP CP ^{1}H to ^{15}N pulse sequence is used. An enhancement value of 4 is obtained for the $H\Phi 19W$ transmembrane helix which correspond to the peak on the left at 220 ppm. An enhancement of 2 was recorded for the phosphatidyl choline amide group at 50 ppm which is in plane.

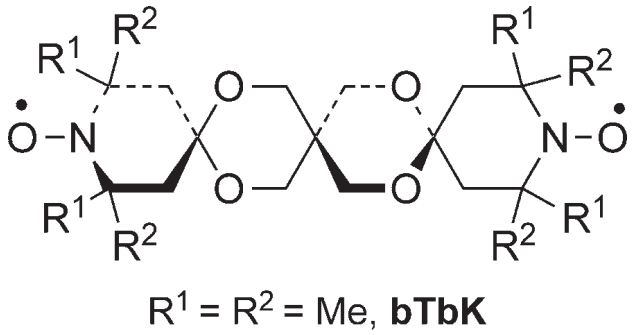

Figure 4.11: chemical structure of bTbk

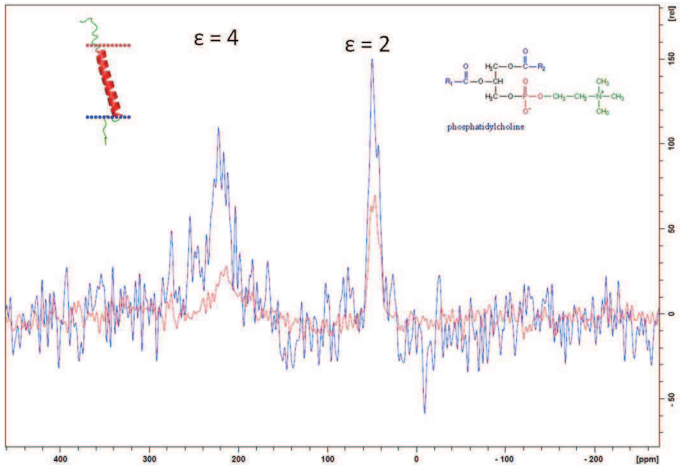

Figure 4.12: ^{15}N DNP CP experiment at 93 K. In blue the $H\Phi 19W$ spectrum with the microwaves on (1024 scans, 20 mA collector current) and in red the normalized spectrum with the microwaves off (10240 scans). A DNP enhancement of 4 on HΦ19W with 20 mM of bTbk on HDPE. The sample consists of 17.8 mg of $H\Phi 19W$ with 100 mg of POPC and 1.65 mg of bTbK. The peptide to lipid ratio is 1/20. The proton decoupling is at 20 W and the nitrogen power level is at 350 W

4.7 PGLa on HDPE

A ^{15}N DNP CP spectrum for PGLa is acquired at 100 K. 5.9 mg of ^{15}N PGLa were added to 78.7 mg DMPC, 25.9 mg DMPG with 20 mM of bTbk. A peptide to lipid ratio of 1/50 is optimal for PGLa samples. The mixture was spread on HDPE and wrapped in a plastic bag.^{15}N static DNP CP experiments were realized at 93 K.

The peptide remains in plane at this low temperature and an enhancement of 2 is observed.

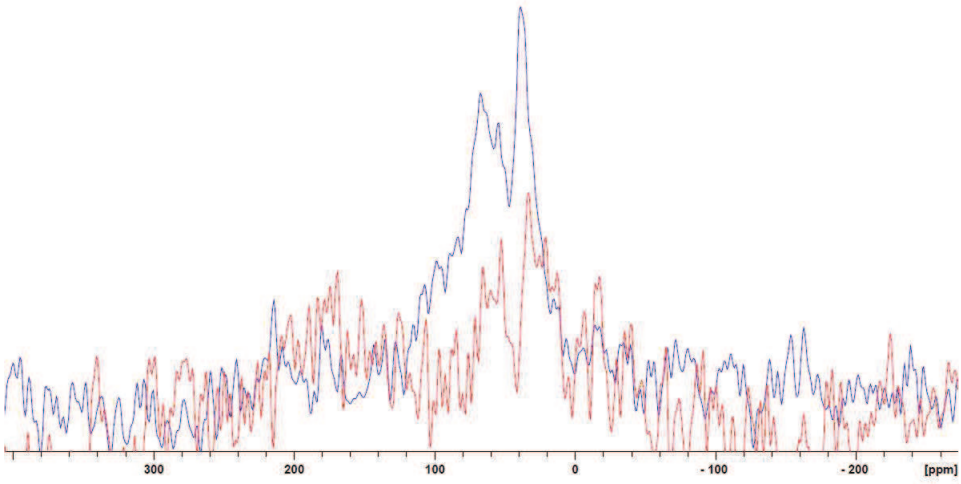

Figure 4.13: ^{15}N static DNP CP of 5.9 mg of ^{15}N PGLa oriented in 78.7 mg DMPC, 25,9 mg DMPG with 20 mM of bTbk on HDPE at 93 K. The peptide to lipid ratio is 1/50. In blue the spectrum with the microwaves on (collector current 20 mA), in red the scaled spectrum with the microwaves off. An enhancement of 2 is obtained. The proton pulse duration is 3 μs and the proton decoupling power is 60 W . The nitrogen power level is 350 W. The contact time p15 of 0.6 ms and a recycle delay d1 of 3 s are used

4.8 HΦ19W with AMUPOL

A new biradical was obtained from the group of Paul Tordo from Marseille. The sample consists of 8.5 mg of HΦ19W, 50 mg of POPC (peptide to lipid ratio 1/20) and 333 micrograms of AMUPol.

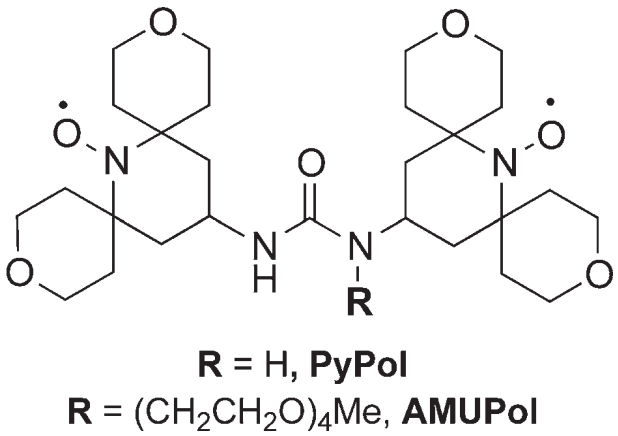

Figure 4.14: Chemical structure of AMUPol

This biradical is supposed to give enhancements as high as 300 in solution. An enhancement of 4.5 was measured in the Bodenhausen DNP facility in Lausanne (results not shown). A signal to noise of 10 was obtained after 50 minutes.

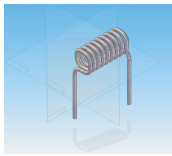

4.9 DNP results with the single square coil

4x4 mm^2

Now that the sample size could be controlled, the initial probe circuit with a single square flat coil with a cross section of 4 x 4 mm^2 was implemented again. 8.5 mg of HΦ19W, 50 mg of POPC (peptide to lipid ratio 1/20) are used in the presence of 333 micrograms of AMUPol. Even if the NMR performance of the probe is 3 times better (signal to noise goes up from 10 to 32), the enhancement value is still the same. A signal to noise of 32 is acquired after 50 minutes of measurement. There is a big advantage, it will cut the experiment time by 16 fold.

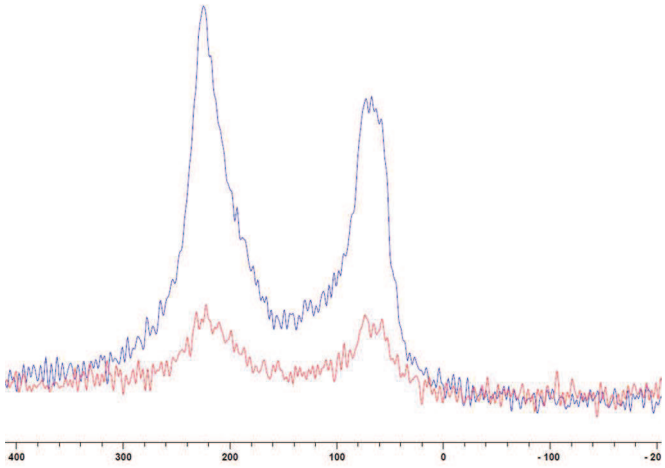

Figure 4.15: ^{15}N DNP CP Hϕ19W on HDPE with a single flat coil at 105 K. The sample consists of 8.5 mg of HΦ19W, 50 mg of POPC (peptide to lipid ratio 1/20) and 333 micrograms of AMUPol. An enhancement value of 4.5 is measured with the microwaves on in blue (collector current 20 mA). The proton decoupling power is 38W, the nitrogen power level 52.4 W, the contact time p15 0.6ms, the recycle delay d1 is 3s and the number of scans is 1024

And finally here is a summary of all the DNP ^{15}N solid-state NMR spectra obtained with the DNP probe presented in table 4.2.

	PROJECT TASKS	Microwaves	collector current	Scans	Signal to noise	Peak Width	Enhancement
NH4Cl	Doubel coil Sample in saphire rotor	off		64	8	2	
		on	40 mA	64	108	1,5	18
	Double coil on Glass plates	off		16	4	25	
		on	40 mA	16	1		
RK1	Double coil Sample on Glass plates (POPE)	off		3250	5,4	30	
		on	40 mA	1400	1,8	32	
		off		1400	2,2	71	
	Double coil on HDPE (POPC)	on	20 mA	1024	7,7	21	4
		on	30 mA	1024	2	21	
		off		**10240**	**9**	**32**	
	Single coil	**on**	**20 mA**	**1024**	**32**	**36**	**4,5**
		off		**1024**	**6**	**48**	
PGLa	Double coil sample on HDPE	off		1384	3	26	
		on	20 mA	12288	8,8	51	2

Table 4.2: DNP results on ^{15}NH4Cl, HΦ19W and PGLa. The collector current, the number of scans, the signal to noise, the peak width and the enhancement value are reported for both the microwave on and off configurations

4.10 HΦ19W in a sapphire rotor

In a last attempt of getting more signal, a HΦ19W sample was inserted in a sapphire rotor. It has been already proven in MAS experiments that sapphire rotors give more signal than zirconia rotors and act as a lens. Moreover, sapphire possesses good microwave transmission properties. As a matter of fact 50 % more signal is obtained using a sapphire rotor with the ammonium chloride sample dissolved in water and glycerol (cf. figure 4.18). The same type of results were expected for oriented samples. The best enhancement factor of 7 was obtained.

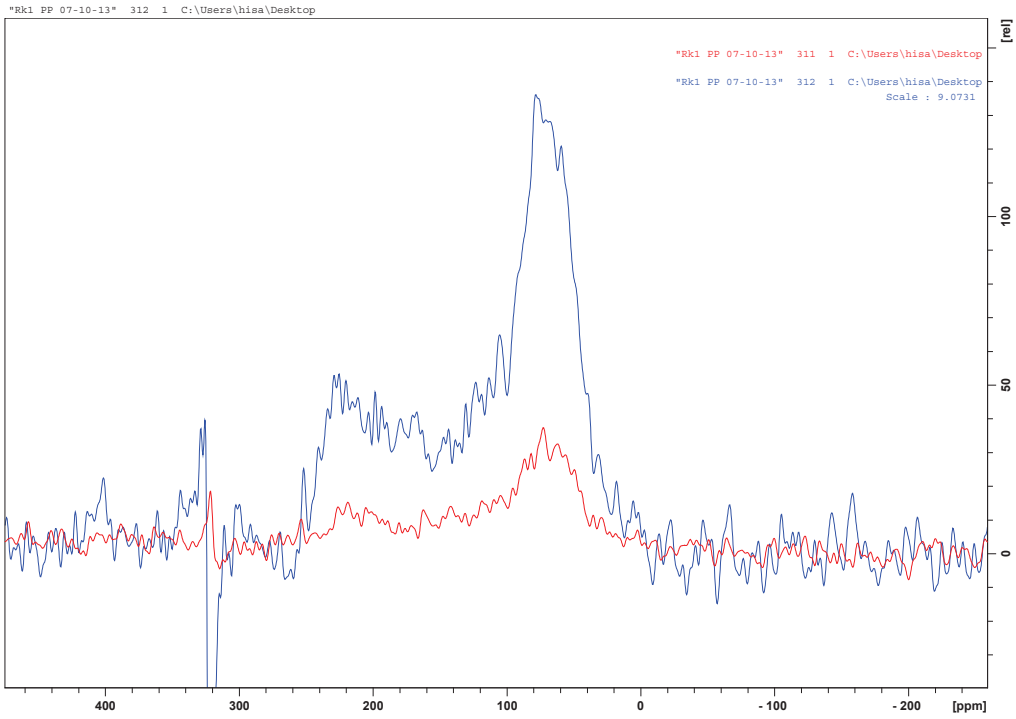

Figure 4.16: 6 labeled HΦ19W in 3.2 sapphire rotor at 90K. Normalized 15N CP with proton decoupling using the DNP static probe with the single coil configuration. The sample consists of 8.5 mg of HΦ19W, 50 mg of POPC (peptide to lipid ratio 1/20) and 333 micrograms of AMUPol. In blue the microwaves are on and the collector current is set to 40 mA . In red 18432 scans with the microwaves off . The blue spectrum was scaled

A Hϕ19W/POPC sample (former oriented sample) in a sapphire rotor shows a maximum enhancement value of 7 at high microwave power (collector current 40 mA). The question that can be asked is why such a low enhancement value? and several reasons can come up: one thing that is known for fact is that the enhancement value for the hyperpolarized samples goes up with the spinning MAS speed [70] (cf. figure 4.17).

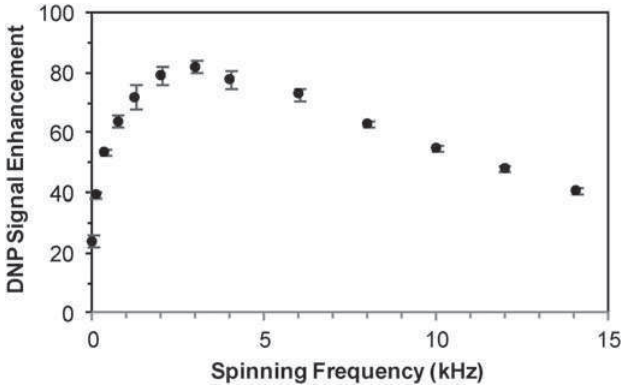

Figure 4.17: Spinning frequency dependence of the ^{1}H DNP signal enhancement of 0.1 M U-^{13}C-^{15}N-proline in glycerol-d8-D2O-H2O (60 : 30 : 10 volume ratio), measured with ^{13}C CPMAS experiment at 97 K. Spectra were measured with and without microwave irradiation at each spinning frequency for calculation of the DNP signal enhancement. 10 s recycle delay, 1 dummy scan, 16 to 64 scans per experiment depending on the spinning frequency. Error bars are indicated on the plot. Taken from Rosay et al 2010

These results have been explained theoretically by Frederic Mentink-Vigier et al [101] Kent R Thurber et al [102]. In parallel, the microwaves operating mode is unknown at the sample level, the sample is always in contact of the coil and the heating may detune the rf coil, the polarization transfer mechanisms are not all operating in the static mode where there is no sample dynamics. Some parts of the sample remain in the shadow and receive no microwave irradiation at all. All of these reasons are possible. While the sample has to remain static, it can be isolated from the coil. Directing a gas flow at it can be a first shot.

4.11 Dependency of the enhancement on the microwave power

For this set of experiments, the $^{15}N H_4Cl$ sample showed for both the zirconium oxide and the sapphire rotors the most enhancement for low microwave power. For higher microwave power the signal got lost (less signal than in the absence of microwaves). This contradicts the previous experiments (enhancement of 18 with a collector current of 40 mA).

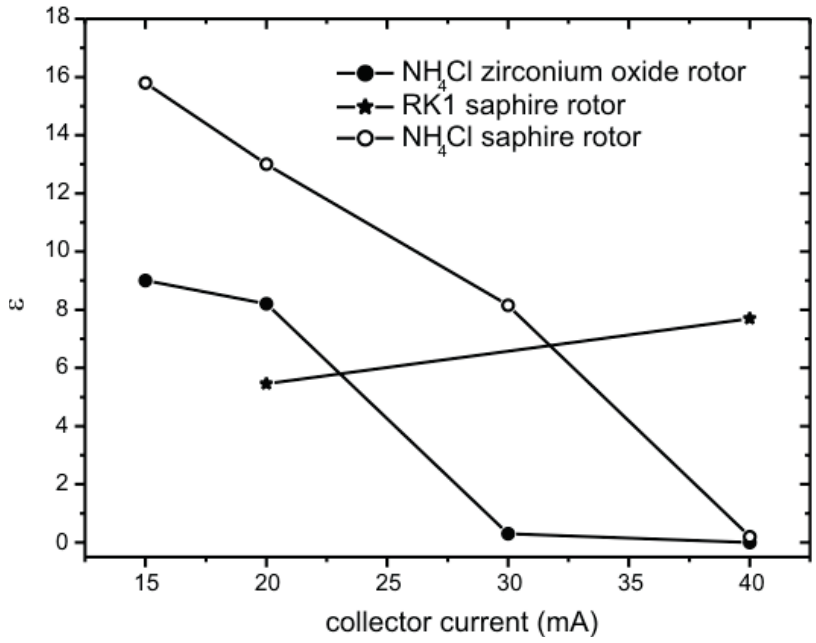

Figure 4.18: Dependency of the enhancement on the collector current (proportional to the microwave power) of 5.6 mg of ^{15}NH4Cl with TOTAPOL and a Hϕ19W sample (with POPC on unoriented polyethylene)

4.12 B_1 field measurements using ^{15}N ammonium chloride

The B_1 field of nitrogen was measured using a CP experiment followed by a ^{15}N nutation peak. The B_1 pulse power curve can be well fitted using a square-root shape $B_1 = \alpha\sqrt{P(Watts)}$

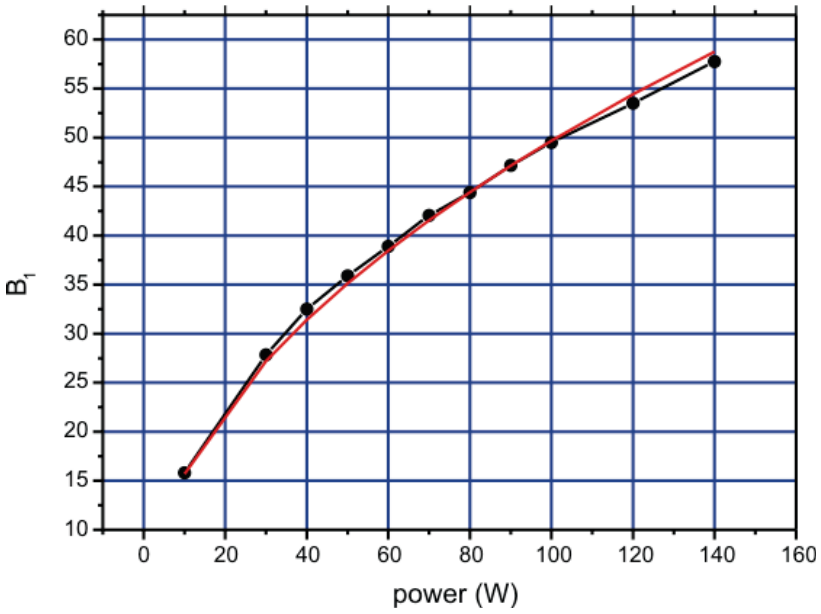

Figure 4.19: ^{15}N B_1 fields measured by nutation (^{1}H-^{15}N CP experiment followed by ^{15}N nutation pulse). The sample consists of 5.6mg of ^{15}NH4Cl with TOTAPOL at 90 K with microwaves at 20 mA collector current. The red line corresponds to a fit with a square-root and a factor 4.97$\pm$ 0.02

Proton nutation experiments were realized using a CP experiment where the first proton pulse was offset by 28.868 kHz and incremented to perform the nutation. The offset corresponds to an B_1^{eff} of 50 kHz at the magic angle with the right power level. The directly measured B_1^{eff} cannot be well fitted with a square root.

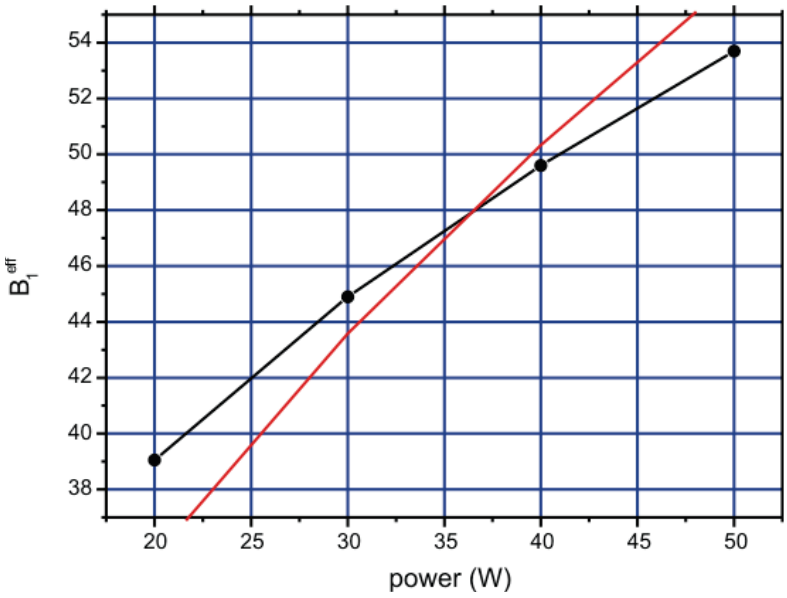

Figure 4.20: ^{1}H B_1^{eff} fields measured by nutation (^{1}H-^{15}N CP experiment using an incremented proton pulse with a frequency offset of 28,868kHz) of 5.6mg of ^{15}N NH_4Cl with TOTAPOL at 90 K with microwaves at 20 mA collector current. The red line corresponds to a fit with a square-root and a factor 8.0$\pm$ 0.2

A back calculation of the B_1 field ($B_1 = \sqrt{B_1^{eff\,2} - 28,868^2}$) leads to a curve which is reasonably well described by a square root behavior.

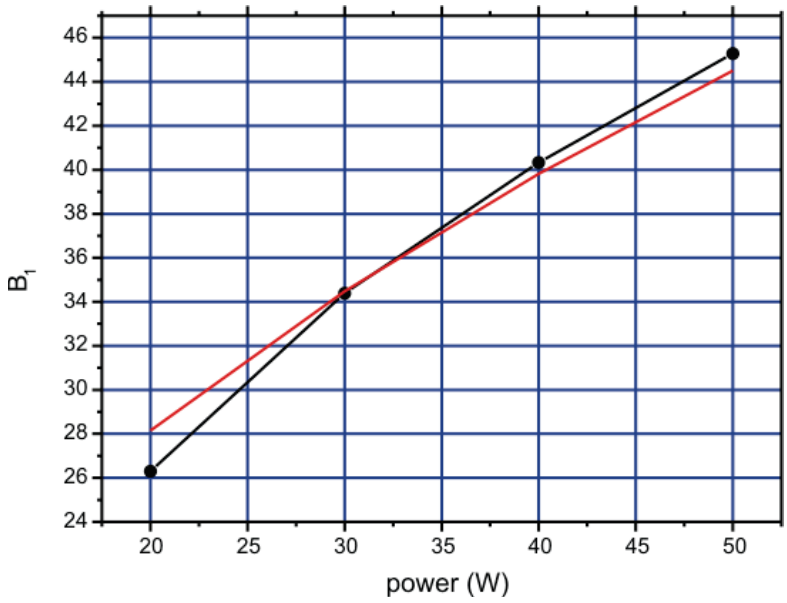

Figure 4.21: ^{1}H B_1 fields measured by nutation (^{1}H-^{15}N CP experiment using an incremented proton pulse with an frequency offset of 28,868 kHz) of 5.6mg of ^{15}N NH_4Cl with TOTAPOL at 90 K with microwaves at 20 mA collector current. The red line corresponds to a fit with a square-root and a factor 6.29±0.10

4.13 PISEMA of HΦ19W incorporated into POPC at room temperature

This thesis chapter could not be closed before attempting a 2D experiment. The proton power levels for the hydrated sample of HΦ19W in POPC changed with respect to ammonium chloride and Ac-Leu. For the 62.5 kHz proton B_1 field a power level 6 dB was now necessary. The proton power necessary to reach a B_1^{eff} of 60 kHz was estimated to 8.4 dB.

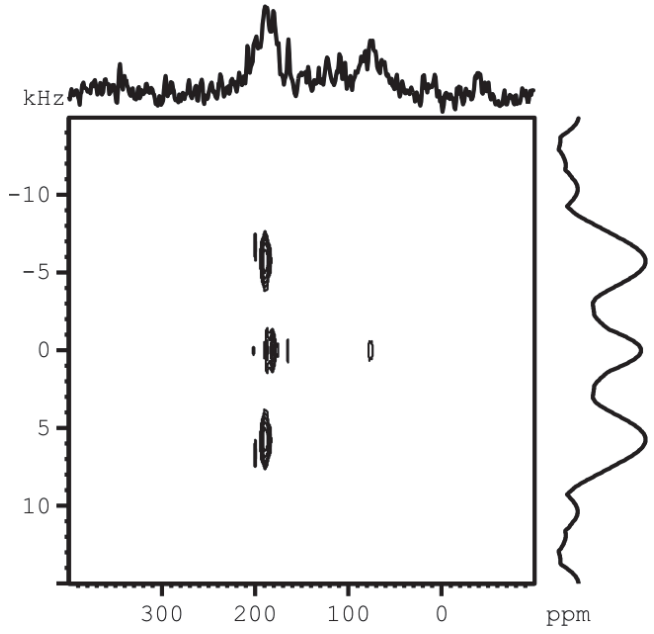

Figure 4.22: PISEMA experiment of HΦ19W in POPC. The f1 dimension consists of only 12 increments. The 1D projections are also shown

Knowing that the NMR coil in the DNP probe has a smaller sample volume, both probes' performances can be considered as equivalent. The proton power levels of the DNP probe were highly dependent on the sample. This is also the case for dry Ac-Leu powder. It made it necessary to readjust proton power levels for each sample. This was not the case for earlier experiments and this can be simply linked to the fact that the NMR coil was deformed when inserting the sample (especially the glass plates).

4.14 DNP PISEMA on HΦ19W at 90 K

A DNP enhancement of 4 results in a gain of 16 in experiment time. Accordingly signal was observed in the first measurement hour. At 90 K the Hϕ19W/POPC sample showed the same power levels as ^{15}NH4Cl. So no need for recalibration. The CP contact time was optimized to 300μs.

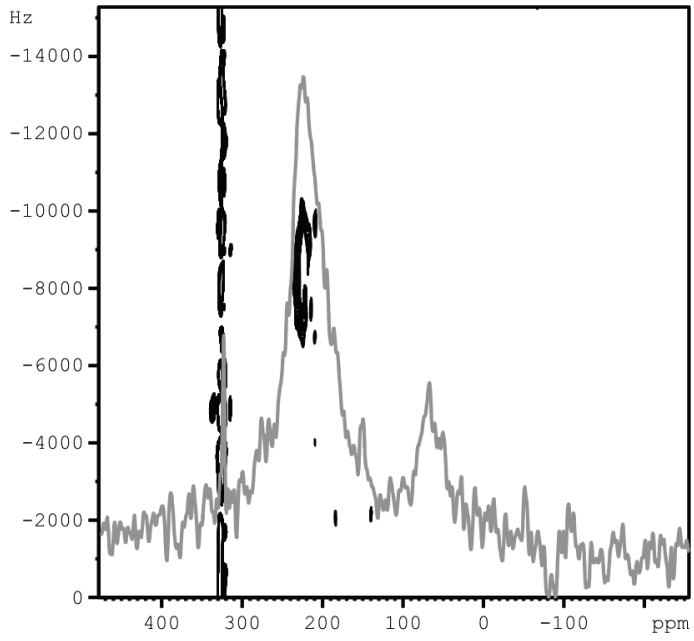

Figure 4.23: DNP PISEMA spectrum of 8.5 mg of HΦ19W incorporated in 50 mg of POPC (peptide to lipid ratio 1/20) and 333 micrograms of AMUPol. Grey: 1D spectrum

The superposition of the PISEMA spectra of HΦ19W at 90 K gives the following results shown in figure 4.24:

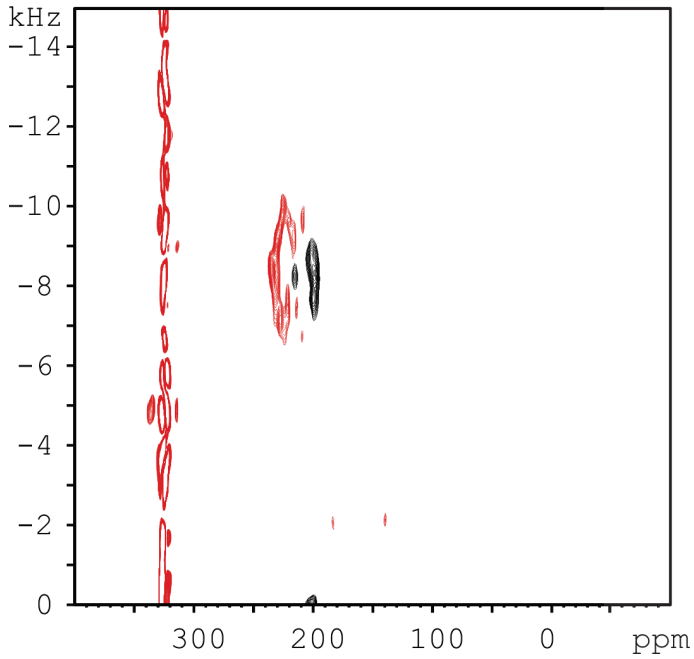

Figure 4.24: Pisema spectrum of 6-labeled HΦ19W incorporated in POPC at 90K (red) and at RT (black). The sample consists of 8.5 mg of HΦ19W, 50 mg of POPC (peptide to lipid ratio 1/20) and 333 micrograms of AMUPol.

The PISEMA spectrum can be reasonably well simulated using an ideal helix. The remaining difference might be explained by variation of the dihedral angles in the real structure. Fitting the data with the simulations gives a tilt angle of 10° with respect to the membrane normal [98] c.f. figure 4.25

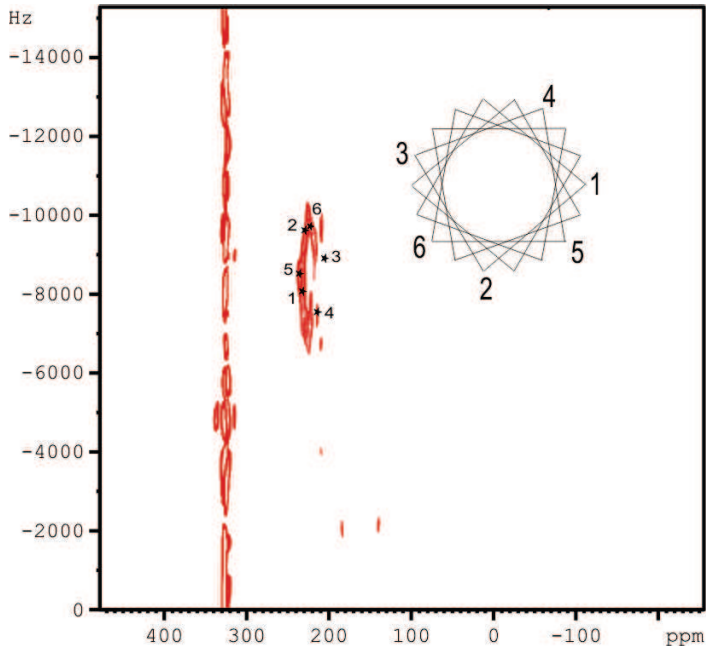

Figure 4.25: Pisema spectrum of Hϕ19W incorporated in POPC at 90 K (red). The sample consists of 8.5 mg of HΦ19W, 50 mg of POPC (peptide to lipid ratio 1/20) and 333 micrograms of AMUPol. And the simulation of an ideal helix (Φ=65°,Ψ = 45°) with a CSA tensor of $\sigma_{11} = 227ppm, \sigma_{22} = 83.5ppm, \sigma_{33} = 70.5ppm$. A tilt of 10° pitch is necessary to adjust the gap between 3 and 4 to the right

Here is how the results can be interpreted:

- The enhancement does not always increase with microwave power
- In this particular case the enhancement of the sapphire rotor cannot be explained by simple magnification of the microwave power. The effect of sapphire is NOT based on an amplification of the signal by sapphire.
- At 90 K the B_1 field doesn't depend on the sample, i.e., power levels from standard can be directly used for sample measurements. This can be explained by the fact that the coil was not distorted during the measurements
- PISEMA at 90 K works well and can be reasonably well simulated. The used peptide (HΦ19W / RK1) shows some motional averaging at room temperature which "destroys" the dispersion in the PISEMA spectrum.

4.15 Conclusion and perspectives

This thesis work describes the development of a DNP/ solid state NMR probehead for the investigation of oriented membranes. DNP has been used to increase the inherently low signal of solid state NMR experiments. This thesis project is focused on the hardware namely probehead development and adaptation to the oriented membrane study. An ultimate coil design has been found to adapt the sample, acquire a good NMR signal and to favor the microwaves transmission. The oriented membrane study started in the early nineties and even if NMR technology is evolving its aims are still the same: studying membrane proteins structure and function to be able to better control drug transfer among other things. Membrane proteins act as a gate control to what can or cannot get into the cell. Endocytosis is one of the most fascinating biological processes going on in the organism. Antimicrobial peptides on the other hand interact with the cell membrane and disrupt it. Consequently, one can think of a direct way of aiming cancerous cells to destroy them selectively. Many cancerous or damaged cells markers are known nowadays. Understanding their structure and function will bring the world of medical research one step forward. Being part of this adventure and collaborating to the buildup of knowledge in these fields is one aspect of this study that should be taken into consideration.

In the beginning, good knowledge of 3D design had to be acquired. This opened up a whole aspect of the study: being able to design and modify parts and seeing them realized afterwards changes the whole view of the high tech world. This engineering skill is essential to anyone who wants to start building up probes or any other piece of hardware. Solid edge 3D model design and construction was the major topic in the first 6 months of the thesis.
The actual probe buildup didn't take that much time. One has to consider every piece of technology nowadays as a mechatronic assembly. Mechatronics is a design process that includes a combination of mechanical engineering, electrical engineering, telecommunications engineering, control engineering and computer engineering. The probe parts range from simple ceramic capacitors to internal transfer units that are assembled independently on different Bruker sites. Assembling these parts in the same frame and probe base required a lot of technical skills and patience. In brief, a probe is an RLC circuit with an NMR coil inducing magnetic field at the resonating frequency of certain nuclei like proton and nitrogen in this case.
Many coils were wound before attaining the last reliable coil design. Only a couple of them were tested. In the first design a 8.8 mm x 4.6 mm x 4.5 mm, 3 turns saddle coil and a 3.7 mm x 3.7 mm x 11.6 mm flat coil were used. All the conducted tests using this probe configuration, including the bench test, high power test and NMR experiments were successful. A bench test refers to the primary tests that are done before the actual spectrometer test. It includes probe tuning and matching.

The high power allows the determination the maximum power that the probe can withstand. This value has to be respected during the spectrometer test to avoid any arching and probe damage. Ammonium chloride powder was used for the NMR experiments. It is highly symmetrical and gives signal very fast. Simple pulse sequences like one pulse and high power decoupling are the most basic NMR pulse sequences and are the basics of all other experiments. Once the 90 ° pulse for the proton and nitrogen were set to 50 KHz CP experiments became a routine procedure. Verifying the B_1 field homogeneity was realized with a nutation experiment and was taken for granted afterwards.

However this square coil design couldn't accommodate the stack of glass plates that is usually used for oriented sample preparation. The new coil with a 7mm x 3 mm cross section was tested with a first model peptide, namely surfactin. This first CP experiment provided a good signal to noise after an overnight experiment. This was not the case for ammonium chloride at room temperature and hyperpolarized ammonium chloride at low temperature. First the T_1 was suspected to be very long and T_1 was measured using saturation recovery and inversion recovery. Reasonable T_1 values were found which couldn't explain why no signal could be obtained. A solution was found while investigating the coil design. Voltage value measurements at the coil leads as well as B_1 field simulations determined that the sample was experiencing an inhomogeneous field.

Therefore a double coil with an independent circuit for proton and nitrogen was realized. The inner coil is for the proton signal acquisition and the outer coil for nitrogen. This double coil generated a good homogeneous field for both nuclei as shown by CST simulations. After several attempts on different samples such as glycine and histidine, an efficient experimental approach was determined. Sample dissolution and freezing are routinely used for this type of experiments. The effect of radical concentration on proton T_1 and probehead performance were assessed among other things. A first CP experiment on HΦ19W was successfully attempted.

Now that all these issues were solved, the first DNP experiments were conducted using hyperpolarized ammonium chloride. A comparison between MAS and static performance was realized. Unfortunately the first attempt of a DNP experiment on an oriented sample with glass plates was not successful using the same conditions as for ammonium chloride. However a quick solution had to be found. A different sample support was suggested. Two different materials were tested: PEEK and HDPE. PEEK showed a similar behavior as for the glass plates. Based on the DNP MAOSS (magic angle oriented sample spinning) results, HDPE was used and an enhancement value of 4 was found. This was a first promising result.

This low enhancement value can be due to the sample's dimensions, the elements aggregation or electron T_1 among other things. Another important element that must be taken into consideration is the irradiated sample volume. The CST

simulations has clearly shown that only 30 % of the sample volume is irradiated. 3.3 mm of the irradiated surface interfere with the incident wave. This fact should add up a correction factor to the overall enhancement factor. Another issue that must be considered in the future is sample composition. Clearly the biradicals don't spread into the whole sample instead they remain in the same place affecting a small percentage of the sample volume. It can be that this phenomenon is less present in the MAS case since the sample dynamics are maintained by continuous spinning. It can be that bTbk does not interact with the membrane or that AMUPol remains in the water phase and doesn't mix with the membrane sample. What can be done is adding glycerol to the sample preparation to promote the formation of a glassy sample. Moreover, smaller biradicals or monoradicals can be utilized to further radical membrane interaction.

Finally, T_1 values have been optimized for MAS sample to facilitate electron nuclei interaction. However these values have to be reconsidered for static samples since the overall dynamics of the oriented membranes are essentially different.

Meanwhile further experimentation made it clear that smaller microwave power had to be maintained in order to reach the ultimate enhancement values. Values of collector current as low as 15 mA showed better enhancement in some circumstances. This is not the case for DNP MAS that clearly show higher enhancement values with the increasing microwave power [70]. Probe detuning is suspected but it is not sure. So it is possible that the high microwave power modifies the sample or the Hartmann Hahn conditions.

The 4 mm x 4 mm coil design was found to give a better NMR signal. Three times more signal was acquired during the same acquisition time. On one hand, this is very interesting to save experiment time. On the other hand, it didn't affect the DNP performance. Moreover it proved that the double coil design didn't interfere with the microwave transmission process.

Finally the HΦ19W on HDPE sample was inserted in a sapphire rotor. The orientation was lost since the support had to be distorted in order to fit in the rotor. Luckily an enhancement of 7 was recorded on the powder spectrum. This proves how much microwave coupling to the sample is important for the enhancement value. Sapphire is clearly transparent to microwaves and prevent more interference and diffraction phenomenons that are destructing the NMR signal in this case.

With this probe configuration PISEMA experiments were conducted at room temperature then at low temperature. The calibration process is time consuming but is fundamental for pulse calibration and the B_1offset value. This 2D experiment was the ultimate goal for the thesis project. It is usually used to measure the alpha helix tilt angle with respect to the membrane normal with better precision. It usually takes four days to accumulate enough signal to noise. With the current signal gain

and thanks to DNP, signal can be distinguished after one hour of acquisition only and after six hours a tilt angle of 10 degrees with respect to the membrane normal was determined.

^{1}H-^{15}N cross polarization experiments, PISEMA and finally DNP experiments with a gyrotron as a microwave source have been successfully realized. With such an NMR probe head the investigation of oriented samples using DNP solid-state NMR will become much more feasible. In particular, it will open the field of oriented solid-state NMR to multidimensional NMR spectroscopy at high-sensitivity.

In the future, the probe design can be improved and the coupling between the sample and the microwaves optimized:

An insert and eject device can be constructed to avoid probe heating every time the sample needs to be changed. Two models are proposed:

To begin with, the main idea of the first model is to bring up the sample from the center. This center sample insert eject model inquires the use of the saddle coil. It would replace the microwave guide in the current LT MAS DNP solid state NMR probehead design. The microwave guide would be placed where the Internal transmission line now is (ITL). The ITL would have to be smaller than 22 mm. It would take the place of the sample transfer line.

Then, the second model respects the existing probehead design. The first idea was to create a pneumatically driven sample insert system which appears to be ineffective at low temperature. So a very simple articulated stick can be designed. It would reach the sample from the side. That adds up a new complication to the process. The sample will have to be identical every time and the trajectory very well established. This problem can be easily solved by using a saddle coil.

A 3D design of the insert eject stick was realized with the help of Martin Armbruster. In brief the sample has to cross the probe frame in a tube held by the previously mentioned stick. This bended sample transfer device is called : "the snake like sample holder". To avoid its collision with the guiding tube's inner surface, the stick's radius was made much smaller than the inner diameter (4 mm and 7 mm respectively). To allow it to be flexible enough the same articulations used in the articulated screw driver were utilized. It consists of two metallic parts with a cube in the middle. So that each part has 180° of rotation liberty. Such parts can have any length. The two parts are linked with an epoxy cylinder. So that one articulation is formed of two cylinders linked by an epoxy rigid part. Each articulation is linked to the other by a cube. The last articulation is linked to the proper sample holder. This sample holder has to be made of polyimide so that it doesn't disturb the field homogeneity. It can be manufactured in the workshop in Rheinstetten (especially in the top half).

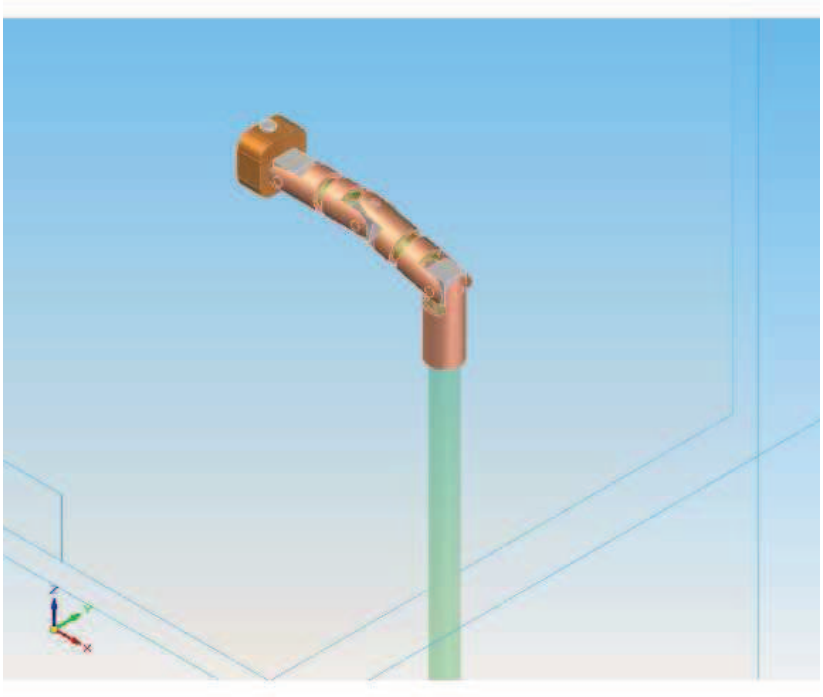

Figure 4.26: Snake model designed using Solid Edge (CAD program from Siemens). An articulated cylindrical stick guides the sample through the sample insert tube to the NMR coil. The sample is held by a sample holder in the last articulation

Lastly, no solution is perfect. It is well known that the solenoidal flat coil is more sensitive. It is usually used for this type of sample. In contrast, a saddle coil is less powerful and sensitive. Both coils were tested with a 400 MHz spectrometer. This will make more applications for the static probehead possible.

The optimization of the coupling between the sample and the microwaves can be achieved by several means listed below. In a next step, several ways are proposed in order to optimize the coupling between the microwaves and the sample:

- radicals directly coupled to the polypeptide sample can be used
- monoradicals which are smaller can be more efficient in static DNP and have to be tested
- Other radicals such as trityl, involving other polarization transfer mechanisms can be utilized
- A sapphire sample support can be manufactured in order to magnify the microwave coupling with the sample.
- For optimizing the wave absorption the glass thickness or material could be changed
- In order to improve to NMR signal it would be a good idea to graft a microresonating circuit on the glass plates. The RC circuit is supposed to have the nitrogen resonating frequency to enhance the nitrogen channel sensitivity. Such a NMR on chip setup is already in use as a miniature NMR biosensor for disease screening.
- Glass plates roughness should also be measured. And the polarization of the output wave is still to be investigated. A compromise has to be found to improve the field homogeneity.
- The microfluidic approach of sample holder was proposed to take advantage of the maximum enhancement in the region attained by the microwaves. Rendering the irradiation more efficient, it will avoid the microwave power to be wasted by limiting the irradiated sample volume
- Optimizing the pitch between the coil winding is also a challenging step for improving the homogeneity
- The sample volume and number of glass plates can be optimized without disregarding the sample volume that must be preserved for having an NMR signal in a reasonable time
- A mirror would be also a good idea, it will focus the incident microwave power on the sample but a major drawback will be more magnetic field inhomogeneity which induces lower enhancement values. This phenomenon can be modeled as a standing wave pattern

This project is one of the several ongoing DNP projects that are aiming to change to world of drug design and disease assessment and therapy. This work was realized in collaboration with the Institute of Chemistry in Strasbourg and Bruker Biospin in

Karlsruhe. It was a three years challenge that started by implementing a flat coil on the existing DNP probe design. This probe can be used for studying biomembrane antimicrobial peptides and improving drug design. If better compatible drugs could be designed millions of people wouldn't have to suffer from side effects. All of this is possible by the study of protein structure and function. And to be able to do that powerful new hardware and contrast agents are needed. Once antimicrobial peptides structure and function are understood, this important data is used by other scientists who iterate the test in order to find the best synthetic sequence with the best antimicrobial activity. Several groups are working on peptide structure and function in the world including Timothy Cross at the University of Florida, Hartmut Oschkinat at the Leibniz-Institute in Berlin, Clemens Glaubitz at the University of Frankfurt and our group Membrane biophysics and NMR in Strasbourg lead by Burkhard Bechinger.

In the field of medicine functional MRI has made considerable advances in the last ten years. If cancer could be assessed without hurting the tissues thousands of prostate patients won't have to endure additional hurtful therapy. By enhancing the MRI signal in factors of 10 000 chances of defeating disease such as cancer can be enhanced. And the acquisition time can be decreased from days to minutes. Hundreds of scientist are working on this around the world: Daniel Vigneron at the University of California San Fransisco in collaboration with Kevin Brindle from the University of Cambridge. To know more about our talented community of researchers , you can visit www.eurohyperperpol.eu and let less time enhance the chances for a better quality of life .

Appendix A

Pulse programming

A pulse program is an ASCII text consisting of a number of lines. Each line may contain one or more pulse program statements which specify actions to be performed by the acquisition hardware and software. The TOPSPIN acquisition commands gs, go, and zg execute the pulse program defined by the acquisition parameter PULPROG which can be set with eda or pulprog. Pulse program execution is a two-step process: After entering gs, go, or zg, the pulse program compiler is invoked which translates the pulse program text into an internal binary form that can be executed.

A.0.1 Depicting the one pulse pulse program

Taken from the Bruker users manuel
;zg
;avance-version (06/11/09)
;1D sequence
    ;$CLASS=HighRes
;$DIM=1D
;$TYPE=
;$SUBTYPE=
;$COMMENT=
    #include Avance.incl
    acqt0=-p1*2/3.1416"
    1 ze
2 30m
d1
p1 ph1
go=2 ph31

30m mc 0 to 2 F0(zd)
exit

ph1=0 2 2 0 1 3 3 1
ph31=0 2 2 0 1 3 3 1

;pl1 : f1 channel - power level for pulse (default)
;p1 : f1 channel - high power pulse
;d1 : relaxation delay; 1-5 * T_1
;NS: 1 * n, total number of scans: NS * TD0

;$Id : zg, v1.102009/07/0216 : 40 : 47berExp$
; symbol before comments.

firstlabel, ze
The statement ze has the following function:

- Reset the scan counter to 0
- Enable the execution of dummy scans.

30m
delay for disk I/O [30 msec]

2 d1
Execute a delay whose duration is given by the acquisition parameter D[1]. This line starts with the label 2, the position where the statement go=2 will loop back to.

p1 ph1
Execute a pulse on frequency channel f1. The pulse length of this pulse is given by the acquisition parameter P[1] . P[1] is normally used for the pulse width of a 90° flip angle

go=2 ph31
Execute 1 data acquisition scan, then loop to the pulse program line with label 2. Repeat this until NS scans have been accumulated.

The phase of the pulse varies according to the current data acquisition scan. For the first scan, p1 will get the phase 0*90 ° , for the second scan 2*90 °, for the third scan 2*90°, for the fourth scan 0*90°, etc. After 8 scans, the list is exhausted. The phase program is cycled so with scan 9 the phase will be set to the first element of the list: 0*90°. Phase cycling is a method of artifact suppression in the spectrum to be acquired. The receiver phase must be cycled accordingly to ensure that coherent signals of subsequent scans are accumulated, not canceled. This is achieved by the receiver phase program ph31 in this example.

The go=label statement executes a delay, the so-called pre-scan delay to avoid pulse feed through before it starts digitizing the NMR signal. During this time the

receiver gate is opened. For AQ_mod = DQD and for any value of AQ_mod In case of an RX22 receiver, the frequency is switched from transmit to receive

30m mc 0 to 2 F0(zd) zd, go=label will omit the dummy scans
The statement zd automatically resets all phase program pointers to the first element

zd can be written behind a delay statement. Such a delay must be at least 10 microsec and its minimum length depends on the number of phase programs. They are then executed during the delay, here it is 30 milliseconds. If they are not specified with a delay their execution will require 3 millisec. The statement zd is normally executed as a part of the mc macro statement.

F0 is a mc clause that is used when a parameter needs to be varied without incrementing the data file pointer.

Appendix B

Pake doublet

The Pake Doublet, as first described by George Pake is a characteristic line shape for crystals and powders. The Pake doublet line shape is induced by dipolar coupling between two spin half nuclei, or from transitions in quadrupolar nuclei such as deuterium. It is the general shape obtained from an orientation dependent doublet.

G.E. Pake utilized it to determine the proton-proton distance in gypsum (CaSO4.2H2O). Likewise one can derive the inter nuclear distance between the hydrogen atoms in water.

In the 1947 paper, fine structure has been measured in the NMR absorption line of protons in crystals. A four component line splitting has been acquired for CaSO4.2H2O. The number of component lines and their spacing was calculated using the dipole-dipole interaction for the proton two system within the water molecule. The dependence of the splitting with the field direction determines the orientation of the line joining protons in the water molecule. This is consistent with the positions of the hydrogen nuclei while considering the chemical bond. A distance of 1.58 A between protons in the water molecule was measured for CaSO4.2H2O [100]. Similarly, hydrated powders show a characteristic fine structure arising from the isotropic distribution of the orientation of the crystallites with respect with the external magnetic field. The "horns" of the Pake doublet correspond to the situation when the principal axis of the coupling interaction is perpendicular to the magnetic field '(i.e. 90 °). The "feet" of the lineshape correspond to the situation when the principal axis of the coupling interaction is parallel to the magnetic field.

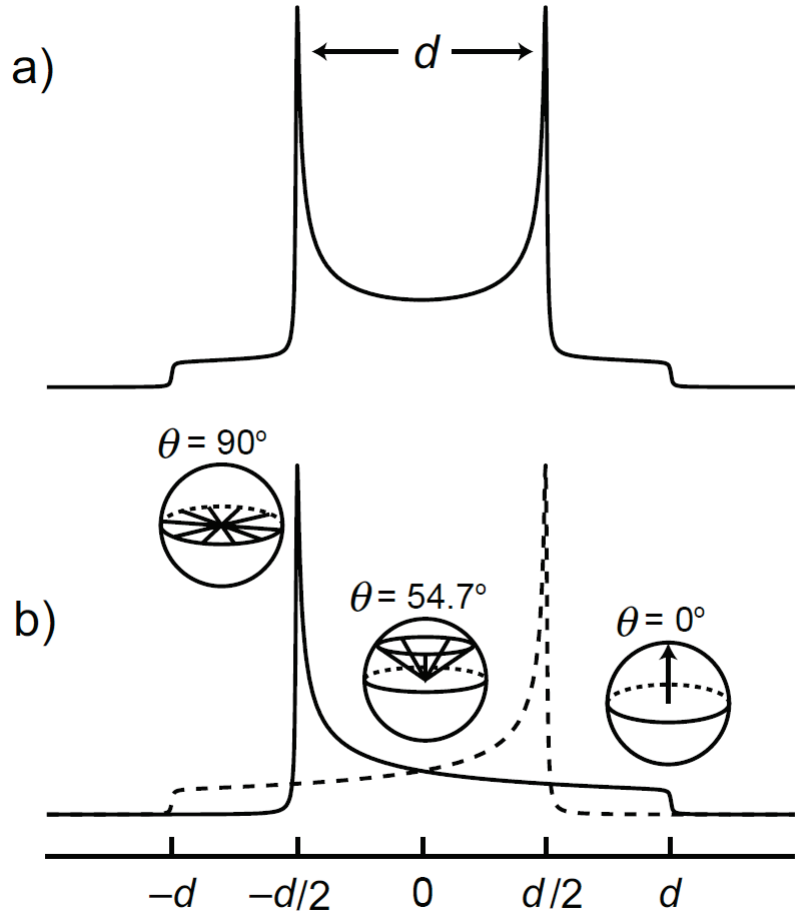

Figure B.1: Pake doublet. Image taken from the university of Hamburg website chemie.uni-hamburg.de

Appendix C

Additional figures

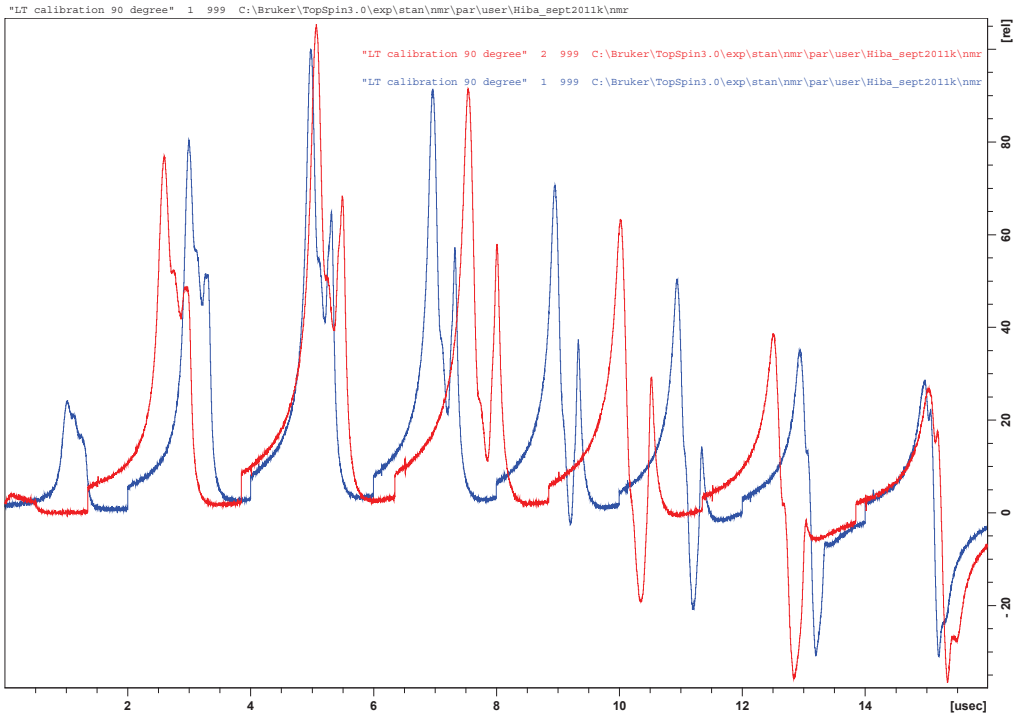

Figure C.1: Nutation curve of ammonium chloride at low temperature

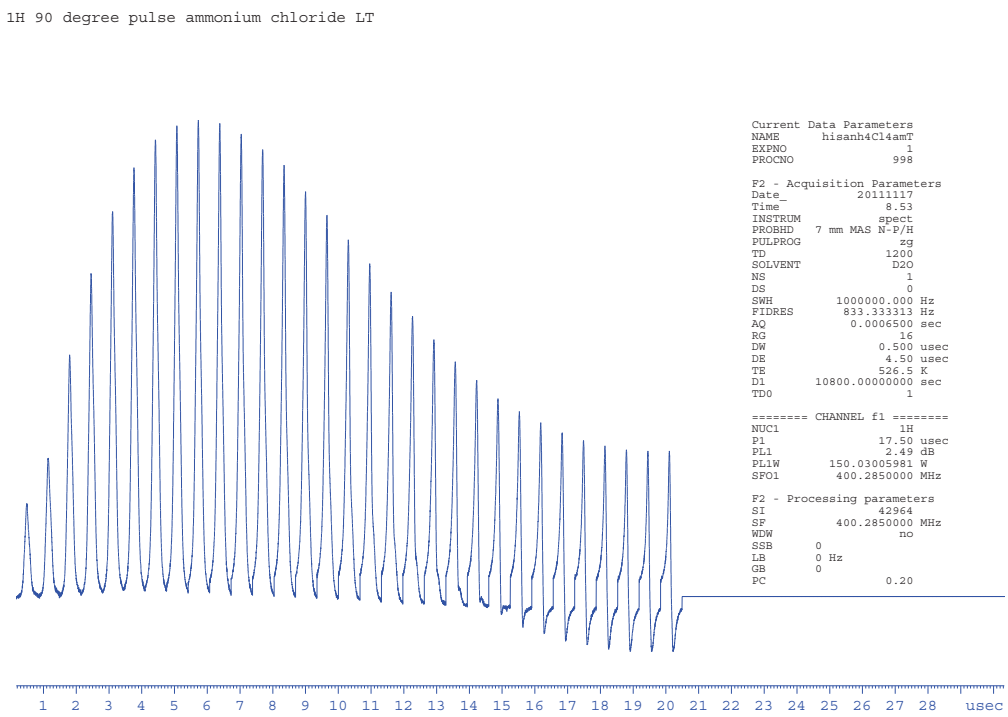

Figure C.2: Nutation curve for hyperpolarized sample

Bibliography

[1] Gennis RB. Biomembranes: Molecular Structure and Function. Springer: New York, 1989.

[2] S.A. Asher and P.S. Pershan Biophys. J. 27, 293 (1973)

[3] Evgeniy S. Salnikov and Burkhard Bechinger. Biophys. J. 100 1473-1480 (2011)

[4] Science. 1993 Sep 10;261(5127):1457-60. High-resolution conformation of gramicidin A in a lipid bilayer by solid-state NMR. Ketchem RR, Hu W, Cross TA.

[5] T. Gullion and J. Schaefer, J. Magn. Reson. 81, 196 (1989).

[6] D. P. Raleigh, M. H. Levitt, and R. G. Griffin, Chem. Phys. Lett. 146, 71 (1988).

[7] S. J. Opella, P. L. Stewart, and K, G. Valentine, Q. Rev. Biophys. 19, 7 (1987).

[8] Bechinger, B., Kim., Y., Chirlian, L.E., Gesell, J., Neumann, J.-M., Montal, M., Tomich, J., Zasloff, M. and Opella, S.J. Orientations of Amphipathic Helical Peptides in Membrane Bilayers Determined by Solid-State NMR Spectroscopy. J. Biomol. NMR 1, 167-173 (1991)

[9] A. A. Nevzorov, M. F. Mesleh and S. J. Opella Magn. Reson. Chem. 42: 162-171 (2004)

[10] Nevzorov AA, Opella SJ. J. Magn. Reson. 2003; 164: 182

[11] T. Prisner, W. Kockenberger Applied Magnetic Resonance Volume 34, Issue 3-4, pp 213-218 August 2008

[12] The dynamic nature of membrane-active peptides from biophysical and structural investigations Burkhard Bechinger. Cell. Mol. Life Sci. 65 3028 - 3039 (2008)

[13] Jimena Fernandez-Carneado, Marcelo J. Kogan, Silvia Pujals,Ernest Giralt Biopolymers (Pept Sci) 76: 196-203, 2004

[14] Bechinger, B. The structure, dynamics and orientation of antimicrobial peptides in membranes by multidimensional solid-state NMR spectroscopy. Biochim. Biophys. Acta(1462):157-183. 1999.

[15] Terence N. Mitchell, Burkhard Costisella.NMR - From Spectra to Structures An Experimental Approach. Springer-Verlag 2007

[16] E. R. Andrew, A. Bradbury, R. G. Eades (1958). Nuclear magnetic resonance spectra from a crystal rotated at high speed. Nature 182 (4650): 1659.

[17] I. J. Lowe (1959). "Free Induction Decays of Rotating Solids". Phys. Rev. Lett 2 (7): 285-287.

[18] M. Mehring, 1983, Principles of High Resolution NMR in Solids, Second Edition, Springer-Verlag, Berlin

[19] K. Schmidt-Rohr and H. W. Spiess, 1994, Multidimensional Solid-state NMR and Polymers, Academic Press, New York.

[20] Lazo, N. D.; Hu, W.; Cross, T. A. J. Magn. Reson. B 1995, 107,43-50.

[21] Scheurer, C.; Skrynnikov, N. R.; Lienin, S. F.; Straus, S. K.; Bruschweiler, R.; Ernst, R. R. J. Am. Chem. Soc. 1999, 121, 4242-4251.

[22] Ramamoorthy, A.; Gierasch, L. M.; Opella, S. J. J. Magn. Reson. B 1996, 110, 102-106.

[23] Le, H. B.; Oldfield, E. J. Biomol. NMR 1994, 4, 341-348.

[24] Dong-Kuk Lee, Yufeng Wei, and A. Ramamoorthy J. Phys. Chem. B , 105, 4752-4762 (2001)

[25] T.A. Cross, Method Enzymol, 289, 672-696 (1997).

[26] Hardware development to increase NMR sensitivity and spectral resolution by novel rf resonators and polarization transfer Alexander Krahn, Bruker Elektronik GmbH (2009)

[27] Greger Oradd and Goran Lindblom MAGNETIC RESONANCE IN CHEMISTRY Magn. Reson. Chem. 2004; 42: 123-131 Lateral diffusion studied by pulsed field gradient NMR on oriented lipid membranes

[28] C. Branden and J. Tooze, 1999, Introduction to Protein Structure, Second Edition, Garland Publishing, New York.

[29] W. Hoffmann, K. Richter, and G. Kreil, 1983, EMBO J., 2, 711-714.

[30] E. Soravia, G. Martini, and M. Zasloff, 1988, FEBS Lett., 228, 337-340.

[31] B. Bechinger, M. Zasloff, and S. J. Opella, 1998, Biophys. J., 74, 981-987.

[32] K. Matsuzaki, Y. Mitani, K. Y. Kada, O. Murase, S. Yoneyama, M. Zasloff, and K. Miyajima, 1998, Biochemistry, 37, 15144-15153.

[33] A. Latal, G. Degovics, R. F. Epand, R. M. Epand, and K. Lohner, 1997, Eur. J. Biochem., 248, 938-946.

[34] Membrane-active host defense peptides - Challenges and perspectives for the development of novel anticancer drugs Sabrina Riedl, Dagmar Zweytick, and Karl Lohner Chem Phys Lipids. Nov 2011; 164(8): 766-781.

[35] R. W. Glaser, C. Sachse, U. H. N. Durr, P. Wadhwani, S. Afonin, E. Strandberg, and A. S. Ulrich, 2005, Biophys. J., 88, 3392-3397.

[36] 950 Plus PepSynthesizer Users' Guide , Millipore Corporation 1992

[37] H. Jakubowski's course on lipid structure, Chemistry Department College of St. Benedict/St. John's University

[38] H. Saito , I. Ando, A. Naito Solid State NMR Spectroscopy for Biopolymers: Principles and Applications. Springer; 2006 edition (2006)

[39] Peter Atkins and Julio de Paula Physical Chemistry, Eighth Edition, Oxford University Press 2006

[40] Les "bicelles" et les "rafts": de nouvelles membranes biomimetique pour l'etude de proteines membranaires par RMN des solides, Universite Bordeaux I ecole doctorales des sciences chimiques, Fabien Aussenac (2002)

[41] E. Fukushima and S. B. W. Roede, Experimental pulse NMR, Addison Wesley publishing company 1981

[42] Abragam, A. Principles of nuclear magnetism. London. Oxford University Press (1961).

[43] Malcolm H. Levitt. Spin Dynamics. John Wiley and Sons, 1. edition, 2001.

[44] R. Griffin, Dipolar recoupling in MAS spectra of biological solids, Nat. Struct. Biol. NMR II Suppl. 5, 508-512 (1998)

[45] Stephen Neidle, Oxford handbook of nucleic acid structure, Oxford university press, New York, 1999.

[46] Evgeniy S. Salnikov and Burkhard Bechinger, Lipid-Controlled Peptide Topology and Interactions in Bilayers: Structural

[47] Insights into the Synergistic Enhancement of the Antimicrobial Activities of PGLa and Magainin 2, Biophysical Journal Volume 100 March 2011 1473-1480 S. J. Opella, NMR and membrane proteins, Nat. Struct. Biol. NMR I Suppl. 4, 845-848 (1997).

[48] Opella, S.J. and Stewart, P.L. Solid-state nuclear magnetic resonance structural studies of proteins. Methods Enzymol. 176, 242-275 (1989);

[49] Hester RK, Ackerman JL, Neff BL, Waugh JS (1976) Separated local field spectra in NMR: determination of structure of solids. Phys Rev Lett 36, 1081-1083.

[50] B. Bechinger, M. Zasloff, and S. J. Opella, Structure and orientation of the antibiotic peptide magainin in membranes by solid-state nuclear magnetic resonance spectroscopy.

Protein Sci. 1993 December; 2(12): 2077-2084.

[51] Opella SJ, Marassi FM, Gesell JJ, Valente AP, Kim Y, Oblatt-Montal M, Montal M.

Structures of the M2 channel-lining segments from nicotinic acetylcholine and NMDA receptors by NMR spectroscopy. Nat Struct Biol. 1999 Apr;6(4):374-9.

[52] C. H. Wu, A. Ramamoorthy, and S. J. Opella, Z Magn. Reson. 109A, 270 (1994)

[53] A. Ramamoorthy and S.J. Opella Solid State Nuclear Magnetic Resonance 4 387-392 (1995)

[54] Sarah D. Cady, Klaus Schmidt-Rohr, Jun Wang, Cinque S. Soto, William F. DeGrado, and Mei Hong Nature. 2010 February 4; 463(7281): 689-692

[55] J. Kummerlen, L.H. Merwin, A. Sebald and H. Keppler, J. Phys. Chem. 96 (1992) 6405.

[56] Thorsten Maly, Galia T. Debelouchina, Vikram S. Bajaj, Kan-Nian Hu, Chan-Gyu Joo, Melody L. Mak-Jurkauskas, Jagadishwar R. Sirigiri, Patrick C. A. van der Wel, Judith Herzfeld, Richard J. Temkin, and Robert G. Griffin J Chem Phys. 2008 February 7; 128(5): 052211. doi:10.1063/1.2833582

[57] Francesca M. Marassi and Stanley J. Opella Journal of Magnetic Resonance 144, 150-155 (2000)

[58] Wu CH, Ramamoorthy A, Opella SJ. J.Magn. Reson. 109: 270. (1994)

[59] Marassi FM, Opella SJ. J. Magn. Reson. 2000; 144: 150.

[60] Marassi, F.M. A simple approach to membrane protein secondary structure and topology based on NMR spectroscopy. Biophys. J. 80: 994-1003. (2001)

[61] Wang J, Denny J, Tian C, Kim S, Mo Y, Kovacs F, Song Z, Nishimura K, Gan Z, Fu R, Quine JR, Cross TA. J. Magn. Reson. 2000; 144: 162.

[62] Marassi FM, Opella SJ. Protein Sci. 2003 Mar;12(3):403-11.

[63] Evgeniy S. SALNIKOV. Etudes structurales de peptides antibiotiques de type peptaibol provoquant des modifications membranaires par spectroscopies RPE pulsee et RMN de l'etat solide.CNRS UMR 7177 Laboratoire de RMN et biophysique des membranes

[64] James N. Shoolery. ANALYTICAL CHEMISTRY, VOL. 65, NO. 17, SEPTEMBER 1,1993 * 733 A

[65] Bruker almanach 2010

[66] Stefan Berger, Siegmar Braun 200 and More NMR Experiments: A Practical Course Weinheim Wiley-VCH Verlag 2004

[67] Melinda J. Duer. Solid state nmr spectroscopy principles and applications. Wiley-Blackwell; 1st edition (2001)

[68] AVANCE III NMR Hardware User Guide

[69] Hahn, E.L. . "Spin echoes". Physical Review 80: 580-594 (1950)

[70] Melanie Rosay, Leo Tometich, Shane Pawsey, Reto Bader, Robert Schauwecker, Monica Blank, Philipp M. Borchard, Stephen R. Cauffman, Kevin L. Felch, Ralph T. Weber, Richard J. Temkin, Robert G. Griffin and Werner E. Maas Solid-state dynamic nuclear polarization at 263 GHz: spectrometer design and experimental results Phys. Chem. Chem. Phys., 2010, 12, 5850-5860

[71] Hu, Kan-Nian et al. Quantum Mechanical Theory of Dynamic Nuclear Polarization in Solid Dielectrics.âĂİThe Journal of Chemical Physics 134.12 (2011): 125105. 2012 American Institute of Physics

[72] Jan H. Ardenkjaer-Larsen, Bjorn Fridlund, Andreas Gram, Georg Hansson, Lennart Hansson, Mathilde H. Lerche, Rolf Servin, Mikkel Thaning, and Klaes Golman Increase in signal-to-noise ratio of >10,000 times in liquid-state NMR September 2, 2003 vol. 100 no. 18, 10158-10163

[73] Changsik Song, Kan-Nian Hu, Chan-Gyu Joo,Timothy M. Swager and Robert G. Griffin TOTAPOL: A Biradical Polarizing Agent for Dynamic Nuclear Polarization Experiments in Aqueous Media. J. AM. CHEM. SOC. 2006, 128, 11385-11390

[74] Carver, Slichter Phys rev 1953, 92,212

[75] V.S. Bajaj et al.Journal of Magnetic Resonance 160 85-90 (2003)

[76] R.A. Wind, M.J. Duijvestijn,C. van der Lugt, A. Manenschijn,J. Vriend,Applications of dynamic nuclear polarization in 13C NMR in solids,Prog. Nucl. Magn. Reson. Spectrosc. 17 (1985) 33-67.

[77] Laszlo Solymar and Ekaterina Shamonina. Waves in Metamaterials (Oxford university press, 2009)

[78] Christian ReiterBreakthrough voltage of capacitors in radio-frequency range Hochschule Karlsruhe- Technik und Wirtschaft 2007

[79] Maier, L.C.; Slater, J. C., "Field Strength Measurements in Resonant Cavities," Journal of Applied Physics , vol.23, no.1, pp.68,77, Jan 1952

[80] Randy Rhea High Frequency Electronics (April 2006)

[81] Andres E, Dimarcq JL. Cationic antimicrobial peptides: from innate immunity study to drug development. Med Mal Infect. 2007 Apr;37(4):194-9. Epub 2007 Feb 15.

[82] C. Aisenbrey, P. Bertani, B. Bechinger, Solid-state NMR investigations of membrane-associated antimicrobial peptides, in Antimicrobial Peptides Humana Press, ed. by A. Guiliani, A.C. Rinaldi (Springer, New York, 2010), pp. 209-233

[83] D. E. Woessner and B. S. Snowden, Jr. ,Temperature-Dependence Studies of Proton and Deuteron Spin-Lattice Relaxation in Ammonium Chloride. J. Phys. Chem., 1967, 71 (4), pp 952-956

[84] E. S. Salnikov, O. Ouari, E. Koers, H. Sarrouj ,T. Franks, et al. Developing DNP/Solid-State NMR Spectroscopy of Oriented Membranes Applied Magnetic Resonance, 2012, Volume 43, Numbers 1-2, Pages 91-106

[85] A. Ramamoorthy, Y. Wei, D. Lee, Annu. Rep. NMR Spectrosc. 52, 1-52 (2004)

[86] Gunnar von Heijne. Membrane-protein topology

Nature Reviews Molecular Cell Biology 7, 909-918 (December 2006)

[87] S.Lange, A. H. Linden, U. Akbey, W. T. Franks, N. M. Loening, B.-J. van Rossum, H. Oschkinat, The effect of biradical concentration on the performance of DNP-MAS-NMR, JMR Volume 216, March 2012, Pages 209-212

[88] E. Fukushima and S. B. W. Roeder, Experimental pulse NMR, Addison-Wesley Publishing Company 1981 pp 146-147

[89] A. Smirnov, T. Smirnova,and P. D. Morse, Very High Frequency Electron Paramagnetic Resonance of 2,2,6,6-Tetramethyl-1-Piperidinyloxy in 1,2-Dipalmitoyl-sn-Glycero-3- Phosphatidylcholine Liposomes: Partitioning and Molecular Dynamics, Biophysical Journal Volume 68 June 1995 2350-2360

[90] Pascale Tsan,Laurent Volpon, Francoise Besson, and Jean-Marc Lancelin Structure and Dynamics of Surfactin Studied by NMR in Micellar Media. J. AM. CHEM. SOC. 2007, 129, 1968-1977

[91] Burkhard Bechinger and Christina Sizun, Alignment and Structural Analysis of Membrane Polypeptides by 15N and 31P Solid-State NMR Spectroscopy. Concepts in Magnetic Resonance Part A, Vol. 18A(2) 130-145 (2003)

[92] Haeberlen U. High Resolution NMR in Solids, Selective Averaging. New York: Academic Press. 1976.

[93] Christina Sizun and Burkhard Bechinger Bilayer Sample for Fast or Slow Magic Angle Oriented Sample Spinning Solid-State NMR Spectroscopy VOL. 124, NO. 7, 2002 9 J. AM. CHEM. SOC.

[94] Hall, et al. Polarization-Enhanced NMR Spectroscopy of Biomolecules in Frozen Solution Science 9 May 1997: 930-932

[95] SDA, Glycerine: an overview, 1990

[96] Emilio A. Nanni, Alexander B. Barnes,Yoh Matsuki, Paul P. Woskov, Bjorn Corzilius,Robert G. Griffin, and Richard J. Temkin,Microwave Field Distribution in a Magic Angle Spinning Dynamic Nuclear Polarization NMR Probe. J Magn Reson. 2011 May; 210(1): 16-23.

[97] Bechinger, B., M. Zasloff, and S. J. Opella. 1998. Structure and dynamics of the antibiotic peptide PGLa in membranes by solution and solid-state nuclear resonance spectroscopy. Biophys. J. 74:981-987

[98] Burkhard Bechinger, Jarbas M. Resende, Christopher Aisenbrey The structural and topological analysis of membrane-associated polypeptides by oriented solid-state NMR spectroscopy: Established concepts and novel developments Biophysical Chemistry Volume 153, Issues 2-3, January 2011, Pages 115-125

[99] Topspin Pulse programming version 2.0 , 2006

[100] G. E. Pake, Nuclear Resonance Absorption in Hydrated Crystals: Fine Structure of the Proton Line, J. Chem. Phys. 16, 327 (1948

[101] Frederic Mentink-Vigier, ÃIJmit Akbey, Yonatan Hovav, Shimon Vega, Hartmut Oschkinat, Akiva Feintuch Fast passage dynamic nuclear polarization on rotating solids Journal of Magnetic Resonance, Vol. 224 , pp. 13-21 (November 2012)

[102] Kent R Thurber, Robert Tycko Theory for cross effect dynamic nuclear polarization under magic-angle spinning in solid state nuclear magnetic resonance: the importance of level crossings. The Journal of Chemical Physics; 137(8):084508 (2012).

Hiba SARROUJ

Sonde DNP/RMN du solide pour l'étude des protéines membranaires

Résumé

Les protéines membranaires en hélices alpha forment le tiers des protéines codées par notre génome. D'autres protéines membranaires sont formées typiquement de feuillets bêta. Leur fonction varie de la formation de pores, la transmission de signaux à l'activité antibiotique. Elles sont aussi capables de transporter de larges cargos comme les protéines ou les acides nucléiques au travers de la membrane. Récemment, les peptides ont émergé comme un moyen prometteur pour le transport de médicaments vers leurs cibles.

Les protéines membranaires peuvent être synthétisées chimiquement ou exprimées et marquées isotopiquement dans les bactéries, isolées, purifiées et reconstituées dans les bicouches lipidiques hydratées. Elles présentent une variété de configurations en interagissant avec ces bicouches lipidiques. Ceci dépend de la composition et de l'épaisseur de ces bicouches. L'orientation des bicouches lipidiques est maintenue mécaniquement en les disposant entre des plaques de verre.

La RMN du solide des échantillons orientés est un des moyens possibles pour accéder à la topologie des peptides associés à des membranes phospholipidiques.

Les échantillons sont difficiles à exprimer dans les bactéries en grande quantités et possèdent une solubilité réduite en dehors des membranes. En outre leur taille est trop importante pour la RMN du liquide et il est difficile de les cristalliser.

Un des inconvénients majeur de la spectroscopie RMN est sa faible sensibilité. Cela résulte du faible moment magnétique nucléaire qui résulte en un décalage Zeeman faible et donc une polarisation réduite. Par ailleurs, l'intensité du signal RMN dépend de plusieurs facteurs comme la quantité d'échantillon la polarisation et le champ magnétique B_0. Et le temps d'acquisition de certaines expériences peut être très long.

Le but de ce projet est d'obtenir plus de signal des protéines membranaires. Dès lors, nous avons développé une cryosonde DNP (dynamic nuclear polarization) / RMN du solide. La DNP est une technique ingénieuse qui est utilisée pour le transfert de polarisation des noyaux hautement polarisés à des noyaux moins polarisés par irradiation microonde. Les microondes vont exister sélectivement les électrons qui transfèreront leur polarisation à l'ensemble des protons voisins, le signal proton peut ainsi être augmenté de 660 fois.

Pour cela la cryosonde DNP RMN du solide qui opère à 100 K et 9,4 T a été utilisée. Une sonde est la pièce mécanique qui maintient l'échantillon dans le centre magnétique de l'aimant du spectromètre. C'est une antenne modulable qui irradie et détecte des champs radiofréquence. La pièce centrale de la sonde est une bobine solénoïdale ou une bobine en forme de selle enveloppant l'échantillon.

La faisabilité de ces expériences DNP a été validée sur une sonde statique. Ces expériences ont été menées sur des échantillons orientés. Une valeur d'augmentation de 7 a été obtenue.